Delft University of Technology

Sensitivity analysis of the first natural frequency of the offshore wind turbines in the Eneco Luchterduinen wind farm

The differences between the identified and modelled first natural frequency of wind turbines with and without scour protection in varying environmental conditions

L.H.P. Middelweerd

TU Delft Delft University of Technology

Offshore Engineering

Eneco Samen gaan we voor duurzaam

December 8, 2017

Sensitivity analysis of the first natural frequency of the offshore wind turbines in the Eneco Luchterduinen wind farm

By

Luuk Middelweerd

Master of Science Thesis

For obtaining the degree of Master of Science in Offshore and Dredging Engineering at Delft University of Technology

Thesis committee:
Prof. dr. A. Metrikine, TU Delft, Chairman of the committee
Ir. P. van der Male, TU Delft, Daily supervisor
Ir. T.C. Raaijmakers, TU Delft, Supervisor
Dr. ir. W.E. de Vries, Eneco, Supervisor
Ir. B. van den Kieboom, Eneco, Daily Supervisor

TU Delft Delft University of Technology

Eneco Samen gaan we voor duurzaam

Abstract

In the Dutch coastal waters more and more wind turbines on monopile foundations are built. An important design parameter is the first natural frequency of the wind turbine. The first natural frequency is dependent on environmental conditions and different soil conditions such as scour. This research gives a better insight into the sensitivities of these influences on the first natural frequencies.

The first objective was to determine the sensitivity of different influences on the first natural frequencies in a full scale test environment. The first natural frequencies of four wind turbines (two protected against scour and two not protected against scour) in the Eneco Luchterduinen wind farm are constantly monitored and the natural frequencies are identified. It was found that only the water level has an identifiable influence on the identified first natural frequency and that the design natural frequencies and identified natural frequencies differ significantly.

After the analysis from the full scale test different influences on the first natural frequency in a numerical computer model are investigated. The computer model predictions confirm that the water level has an identifiable effect and only small effects of backfilling of the scour hole on the first natural frequency are found.

The third objective was to compare the sensitivity of different influences on the first natural frequency obtained from the computer model and from the full scale test. The effects of the water level are comparable. And the effect of backfill of the scour hole was found in the model but not in the full scale test. Therefore no conclusion is made on the effect of backfill nor on the presence of backfill. It was found that in order to mitigate the differences in first natural frequency of the test turbines and the model the soil should be modelled twenty times stiffer.

The main influence on the first natural frequency of the offshore wind turbines in the Eneco Luchterduinen wind farm is the soil stiffness. The only other identifiable influence was the water level. Also in the design of the wind turbine the soil stiffness is underestimated significantly, implying overconservative designs.

Acknowledgements

The past nine months i have been working on this thesis at Eneco. I would like to thank all my colleagues from the offshore operation team and give a special thanks to Wybren de Vries and Bas van den Kieboom for giving me advice and comments during these nine months.

I would also like to thank Pim van der Male, my daily supervisor from the TU Delft for helping me out during the harder parts of my thesis. He did not only supervise my thesis but also spark my interest for offshore wind energy during courses at the TU. I would also like to thank Tim Raaijmakers for giving me advice on scour related questions.

In addition i would like to thank Andrei Metrikine for the discussions we had during progress meetings.

Last but not least i would like to thank my family and everybody in my surroundings who cannot hear another thing about offshore wind turbines and natural frequencies.

Luuk

Contents

List of Figures

List of Tables

List of Abbreviations

Abbreviation	Explanation
LAT	Lowest Astronomical Tide
HAT	Highest Astronomical Tide
MSL	Mean Sea Level
WTG	Wind Turbine Generator
OHVS	Offshore High Voltage Station
FFT	Fast Fourier Transformation
RNA	Rotor Nacelle Assembly
API	American Petroleum Institute
DNV	Det Norske Veritas
MP	MonoPile
TP	Transition Piece
EOM	Equation Of Motion
FRF	Frequency Response Function
OMA	Operational Modal Analysis
MG	Marine Growth
RPM	Rounds Per Minute
LSCF	Least Squares Complex Frequency
NLS	Non-Linear Least Squares

1 | Introduction

1.1 Introduction

Due to the ever growing energy demand more electrical energy has to be generated. The conventional ways of producing electrical energy are often not renewable. The last few years the public opinion on polluting power plants have changed dramatically. Also it has become more clear that the driver for the warming up of the earth and change of climate is mankind itself. Therefore large electricity producing companies are encouraged to produce electricity in a sustainable way. Another important driver for the energy transition is that the reserves of non-renewable energy resources are not endless. The expected reserves for extraction of coal, crude oil and natural gas are: 109, 53 and 54 years[17]. These reserves for extraction are calculated on the energy consumption of today and do not take into account the expected large rise in energy consumption. Next to the environmental hazards of the use of fossil fuels for the production of electrical energy production renewable energy resources are not dependent on the stability of a country or a government. Therefore a transition to renewable energy resources could make countries energy independent.

In the 2015 United Nations Climate Change Conference new rules and regulations were issued. Also goals for renewable electrical energy production were set. Based on these international goals the Dutch government did set its own goals. These goals state that in 2020 14% of the produced electricity has to be from renewable sources and in 2023 16% of the produced electricity. Nowadays only 5.8% of the total electricity production is from renewable resources[18].
This means an enormous step is needed in the production of renewable electrical energy. There are a few conventional ways of producing renewable electrical energy. One of the ways to produce renewable electrical energy is by the use of wind. The energy from the wind is converted to electrical energy by the use of a wind turbine. The first wind turbine that produced electrical energy was installed in Denmark at the end of the nineteenth century. The first large wind turbine was installed in 1940 in the USA, this wind turbine had a capacity of 1 megawatt. From this moment the development of wind turbines was dependent on the price of fossil fuels. When the price of fossil fuels was low there was no development on the field of wind energy converters. But for instance during the 1970's oil crisis the concept of a wind farm was introduced.

In the Netherlands the largest part of the renewable electricity production is from wind energy. Figure 1.1.

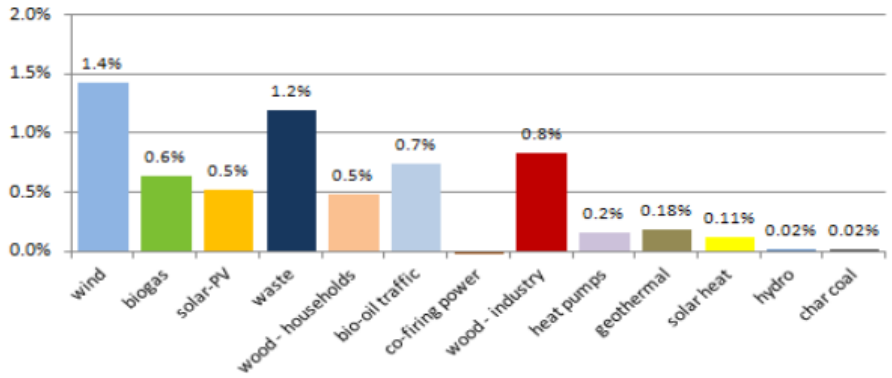

Figure 1.1: *The distribution of renawable electricity production in the Netherlands, May 2016[1]*

The largest part of this electricity production is from onshore wind. And a small part from offshore wind. In order to meet the government goals one of the options is to build large wind turbines. This can be done offshore and onshore. However building larger wind turbines onshore have some downsides. It is not possible to build large farms onshore because of the lack of space in the Netherlands. Another

problem with large onshore wind turbines is that they may have to be placed in urban environments and therefore may cause problems with the local communities. The other option is to build large offshore windfarms. These offshore wind turbines do not have the same problems as onshore wind turbines. Offshore there is enough space to build large wind farms and there are fewer placement restrictions. Also the technical energy potential for offshore wind is large in the Netherlands. The technical energy potential for offshore wind is 1000 TWh[19]. This relates to sites no further than 50 km from shore and with maximum depths of 50 m. The Dutch government set the goal of 3.1% electricity production from offshore wind in the year 2023[18].

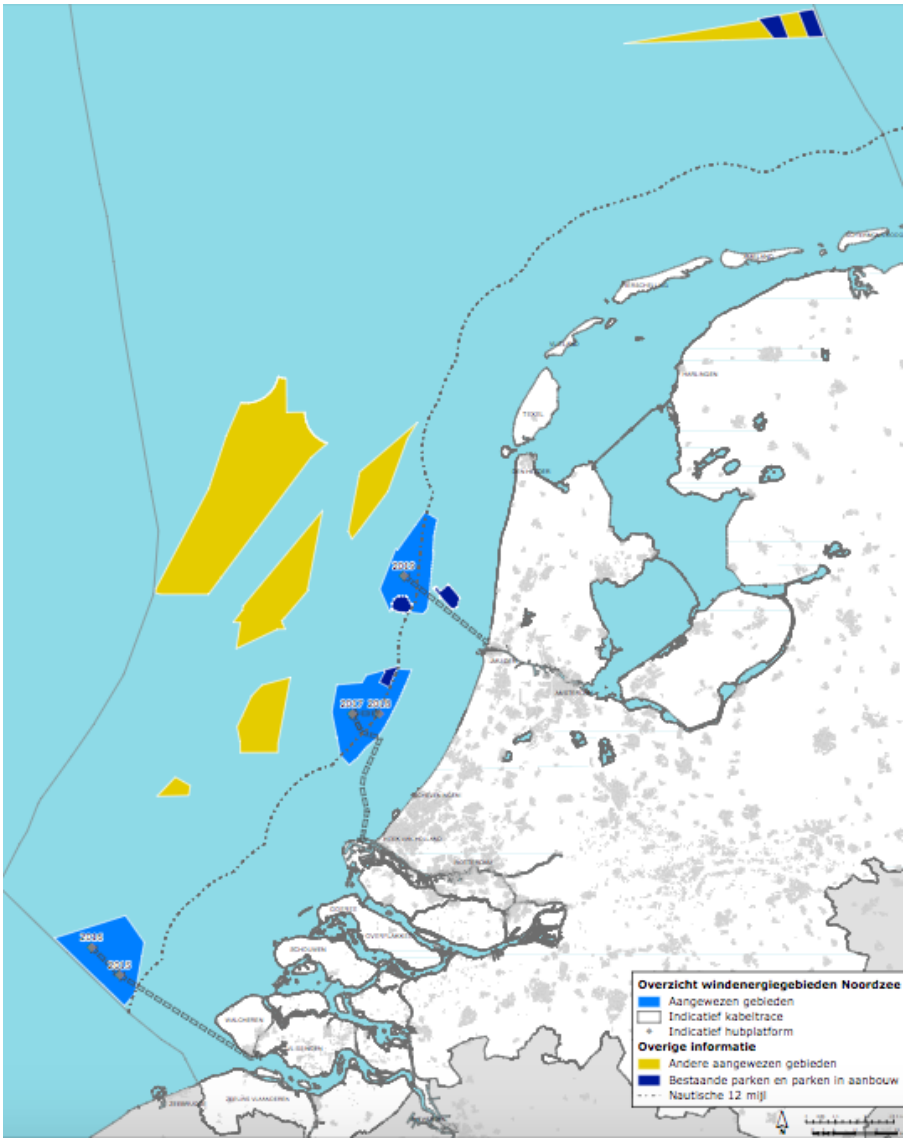

Figure 1.2: *Map of existing and upcoming offshore wind farms [2]*

In Figure 1.2 The existing wind farms can be found as dark blue and the upcoming farms as light blue. In the coming five years each year two sites with a potential of 350 MW are tendered.

During the tender phase of an project the production cost of energy is estimated. This production cost of the electrical energy is expressed as the levelized cost of energy (LCoE). The levelized cost of energy is the main driver for every energy project. The levelized cost of energy is the net present value of the unit cost over the lifetime of a generating asset.

$$LCoE = \frac{\text{sum of costs over the lifetime}}{\text{sum of electricity produced over the lifetime}} \tag{1.1}$$

The levelized cost of energy is used to determine if a project is worth to undertake. Also with the

LCoE a project can be compared to other projects. The lifetime of a project is usually the design lifetime. Energy producing companies want the levelized costs of energy to be as low as possible in order to make the profit of an project as high as possible. A high profit ensures that the financiers of a project are confident in a project and are willing to finance future projects.

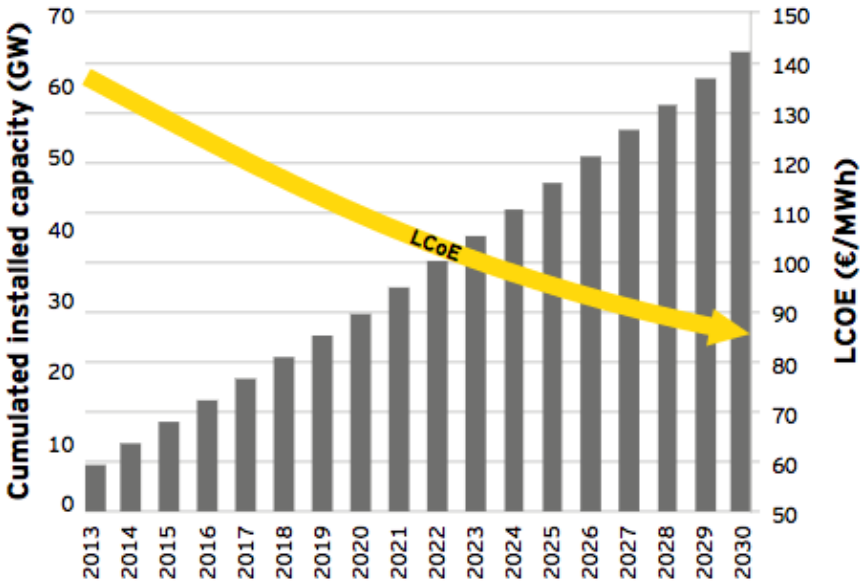

Figure 1.3: *Expectation levelized cost of energy [3]*

In Figure 1.3 the expected levelized cost of energy for offshore wind energy in the Dutch coastal waters can be found for the upcoming years. A large reduction can be found from upscaling the projects and wind turbines. But cost reduction can also be achieved in technical improvement of the wind turbines. An option to achieve this cost reduction is to make improvements to the foundation design. Since about 16% of the total cost of a wind turbine is from the foundation [20]. Also an offshore wind farm consist of many wind turbines and therefore a reduction of costs in the foundation of the wind turbine would have a large effect on the total costs of an offshore wind project.

Another option to reduce the costs of the foundation is to stop using scour protection. This could also be a large cost reduction since the scour protection is needed for every installed monopile. At the moment there is limited information about scour around monopiles available. Most information about scour is from bridge structures in steady current. In offshore conditions there are different scour mechanism. These combined wave and wind scour combinations might lead to a less deep scour hole. And therefore the use of scour protection might be unnecessary.

1.2 Problem description

In this research the Eneco Luchterduinen offshore wind farm is considered. All the wind turbines in this wind farm have a monopile foundation. Other design options are available for support structures[4] of the wind turbines but at the moment in the Dutch coastal waters only the monopile foundation is used. During the design of these monopile foundations there are many factors that need to be taken into account and DNV codes [21] give strict guidelines to make sure that the wind turbines will endure the total design lifetime. One of the most important design restrictions is the natural frequency of the wind turbine. The natural frequencies of the wind turbines may not coincide with any excitation frequency. Some of these excitation's are the wave induced loads an the self-induced loads. The self-induced loads are present in many frequency spectra but the 1P and 3P region are the most important ones[4]. In the 1P region there is an excitation due mass to imbalances of the rotor. Therefore the excitations in the 1P region have the same frequency as the rotor frequency. The 3P region is associated with the

blade passing frequency. Each time a blade passes the tower the shadowing effect of the wind induces a load. Therefore the frequency of the excitations in the 3P region are three times the rotor frequency.

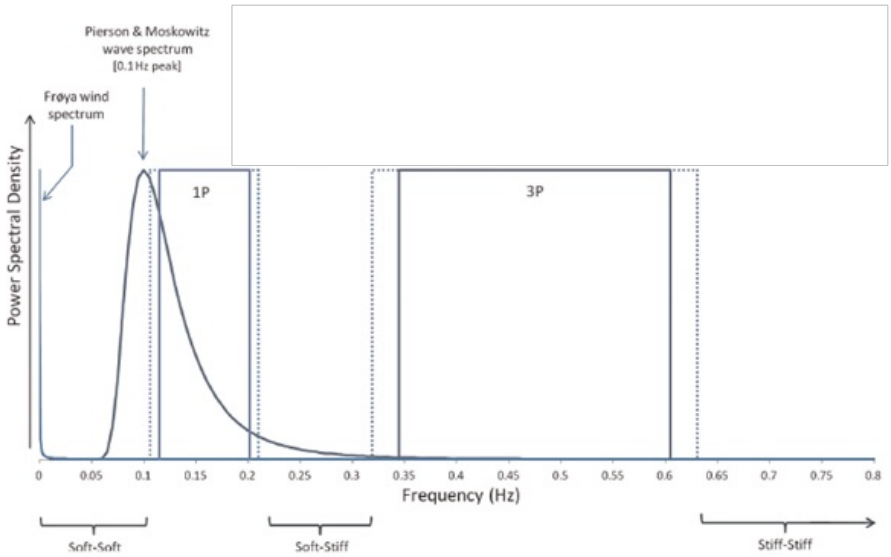

Figure 1.4: *Design approach for offshore wind turbines [4]*

In Figure 1.4 the frequency spectra of these excitations can be found. The first natural frequencies of the wind turbine may not coincide with these excitation frequencies in order to avoid the occurrence of resonance. Based on this principle three classical design approaches are defined:

- Soft-soft design: the wind turbine first natural frequency is less than the 1P frequency range.
- Soft-stiff design: the wind turbine first natural frequency is between the 1P and 3P frequency range.
- Stiff-stiff design: the wind turbine first natural frequency is higher than the 3P frequency range.

These regions can also be found in Figure 1.4, it is easy to observe these regions do not coincide with excitation frequencies from the wind turbine itself. In the Eneco Luchterduinen wind farm a design in the soft-stiff region is chosen.

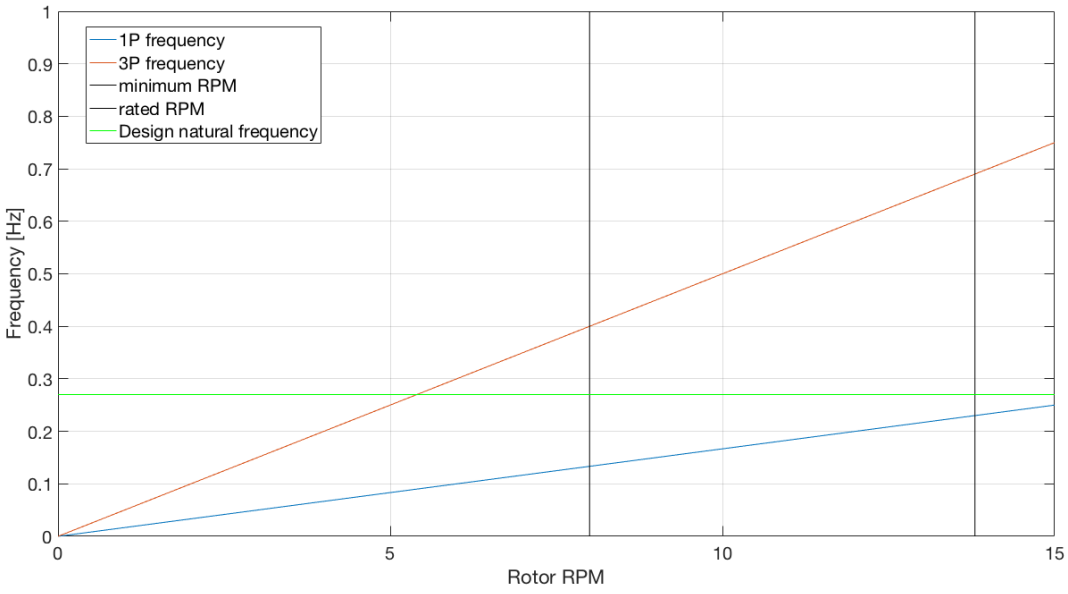

Figure 1.5: *Sparse Campbell diagram for the Eneco Luchterduinen wind turbines*

For a soft-stiff design a Campbell diagram is used as is shown in Figure 1.5. The two vertical black lines indicate the operation window, the blue line is the 1P frequency and the red green line is the 3P frequency. The green line is the average design first natural frequency.

In the Eneco Luchterduinen wind farm four wind turbines are under constant monitoring. And two of these wind turbines are not protected against scour. Many aspects of the wind turbines are monitored. One of the things that are monitored are the bending accelerations, with these accelerations the first bending natural frequency of the wind turbines can be identified. There are many factors varying the first natural frequencies of an offshore wind turbine, for example the water level, the wind speed, the wave height and the scour depth. And the sensitivity for some of these factors on the first natural frequency is not well known. A better understanding on the influence these factors do have on the first natural frequencies of the wind turbines will lead to more accurate computer models and eventually might lead to a more cost effective design.

In earlier studies was found that the first natural frequency of an offshore wind turbine is varying constantly[22]. For example at the Belwind wind farm in Belgium it was found that with higher water levels lower first natural frequencies were identified. Also the first natural frequencies of the wind turbines varied with the same frequency as the water level did. From earlier research a small effect of the wave heights was found on the first natural frequency of offshore wind turbines[22]. The Belwind wind farm is also situated in the North Sea and therefore is a good reference. In this research the effects of different wave heights and water levels on the first natural frequency are also investigated.

Two of the wind turbines that are outfitted with measurement equipment are not protected against scour and scour holes are present around these wind turbines. The effect of scour on the first natural frequency is found in earlier research. There is found that the first natural frequency of a wind turbine with no scour hole drops approximately 8% for a fully developed scour hole[23]. The decrease in natural frequency was found at four different offshore wind farm locations, where wind turbines are placed on monopile foundations in sandy soils. The decrease in first natural frequency is due to the lack of lateral soil stiffness inside the scour hole. Also the absence of sand in the scour does effect the soil stiffness of under-laying layers. The overburden pressure on these layers is reduced and subsequently the soil stiffness of these layers is lower.

In earlier studies was also found that the design first natural frequencies are significantly lower than the identified first natural frequencies [24], [25]. Deviations of 2 to 13% between the design first natural frequency and the identified first natural frequency were found [25]. This increase in first natural frequency is subscribed to the effect of pore pressure build up and to the inappropriate use of p-y curves for large diameter piles [24], [25].

1.3 Objective of the thesis

The objective of this thesis is to get a better insight into the sensitivities of different influences on the first natural frequency of the wind turbines in the Eneco Luchterduinen wind farm.
In order to reach this objective three different steps are made. First the identified first natural frequencies of the monitored turbines are evaluated (Chapter 3), then the natural frequencies obtained from a computer model are evaluated (Chapter 4) and finally the observations from the identified and the modelled natural frequency are compared (Chapter 5).

- *Research questions*
  - What is the sensitivity of different influences on the identified first natural frequency from measurements
  - What is the sensitivity of different influences on the first natural frequency from a model

– How should the differences between identified natural frequencies and modeled natural frequencies be mitigated

2 | Eneco Luchterduinen

This study will focus on wind turbines in the Eneco Luchterduinen wind farm. This wind farm is located in the Dutch coastal waters, figure 2.1.

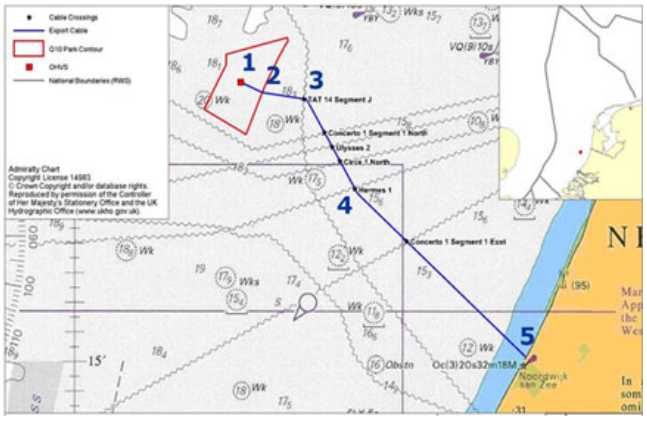

Figure 2.1: *Location Eneco Luchterduinen*

The wind farm is located 23 kilometers from the coast of Zandvoort. This location does not interfere with shipping routes, oil and gas activities and military exercise areas. An important note is that on most days the wind farm is invisible from the Dutch mainland. This is important in order to maintain the support of the Dutch residents.

2.1 Wind farm

The Luchterduinen wind farm consist of 43 wind turbines. The installed turbines are Vestas turbines. The turbine model is "V112-3.0 MW Offshore". These turbines have a rated power of 3.0 MW. The rated power of the entire wind farm is 129 MW, which is enough to supply 150,000 households with renewable electrical energy.

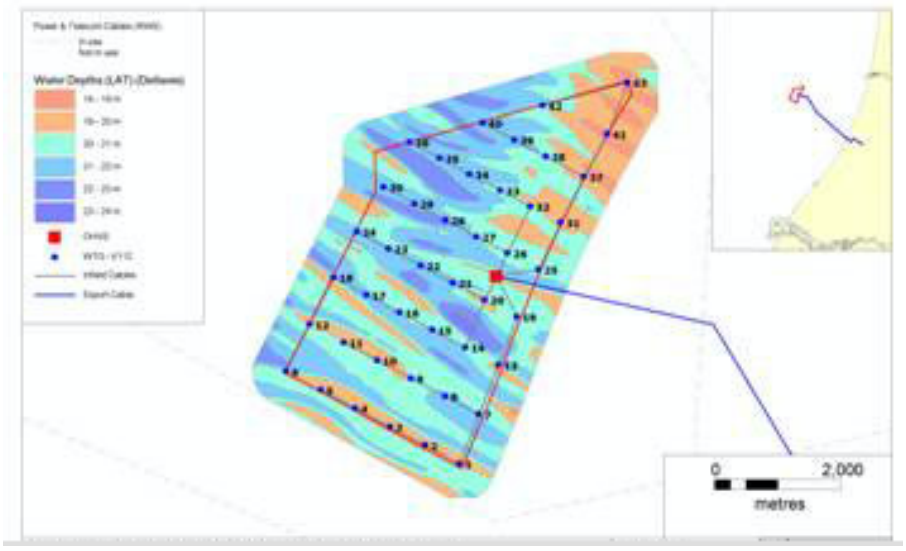

Figure 2.2: *Wind layout and connection*

In Figure 2.2 the layout of the wind farm can be found. The Windturbines are connected to the grid in strings. All these strings are connected to the offshore high voltage station. From this high voltage station the electrical energy is transported to the Dutch coast near Sassenheim.

2.2 Turbine description

As discussed in section 2.1 43 Vestas "V112-3.0 MW Offshore" wind turbines are installed. The specifics of the turbine are:

Rotor diameter	
Hub height	
Number of blades	
Rotor mass	
Nacelle mass	
Nominal rotor speed	
Cut in wind speed	
Rated wind speed	
Cut out wind speed	

Table 2.1: *Turbine specifics*

The diameter of the tower is not constant. On the the top the diameter is 3.31 m and on the bottom 4.50 m.

2.3 Foundation

The foundation of the turbines is a monopile foundation. In this design there is no transition piece. The turbine tower is directly bolted to the monopile. Therefore the top of the monopile also has a diameter of 4.50 m and the bottom of the monopile has a diameter of 5.0 m. The monopiles rise 17.30 from the lowest average tide. All monopiles have anodes for corrosion protection. The secondary steel (boat landing, ladder) of the monopile is installed before installation of the monopile. Since every location in the wind farm has different soil and water depth conditions the length of the monopiles differ per location. Also the penetration depth into the soil differs per location.

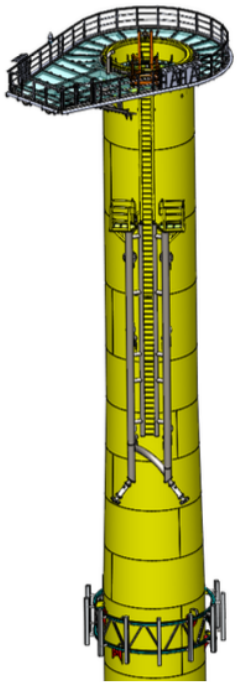

Figure 2.3: *Overview of the top section of the monopile*

2.4 Environmental conditions

In this section The environmental conditions at the offshore wind farm location Eneco Luchterduinen are discussed. Prior to the installment of the wind farm extensive environmental studies were executed. The depth, wind, wave and current conditions will be discussed.

2.4.1 Bathymetry

The water depths at the wind farm location range between 23m and 18m at lowest average tide.

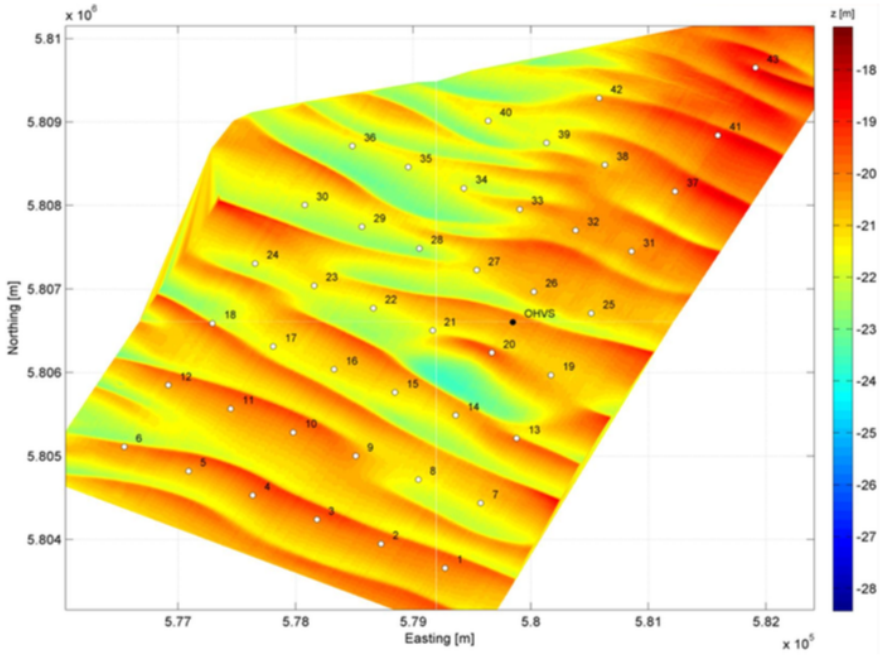

Figure 2.4: *Bathymetry at wind farm location*

In Figure 2.4 the bathymetry at the wind farm location can be found. From Figure 2.4 can be observed that sand waves are present at the wind farm location. These sand waves are important for the design process. The sand waves move during the life time of the wind farm therefore the movement of the seabed must be taken in to account when determining the penetration depth of the monopiles.

	Minimum	**Average**	**Maximum**
Wavelength	194 m	542 m	906 m
Wave height	0.4 m	1.6 m	3.0 m
Migration rate	-3.7 m/year	3.1 m/year	15.2 m/year

Table 2.2: *Sand wave properties*

In Figure 2.4 can be found that almost all wind turbines are placed on top of the sand waves. Since the total sand wave migration over the life time of the wind farm is significantly shorter than the typical sand waves at the wind farm location, the influence of these sandwaves is expected to be limited. The movement of these sandwaves can be found in Table 2.2, from these movements the change in seabed level at each monopile location can be determined. A monotonically decrease or increase in seabed level can be expected for the vast majority of the wind turbines. The largest seabed change can be found around turbine 28 and turbine 20. Near turbine 28 a increase in seabed level of 1.3 m can be expected and near turbine 20 a decrease of 2.1 m. These changes can effect the lateral soil stiffness at the monopile locations. A change in lateral soil stiffness can also cause a change in the first natural frequency of the wind turbines.
The long term mean sea level is expected to rise by around 2.5 mm/year the rising rate will increase with 0.3mm/year, therefore a sea level rise of 0.21 m is expected after 30 years. A change in sea level

also has an effect on the dynamics of the wind turbines. A higher sea level means more contained mass and a change in the natural frequency of the wind turbine.

Water level	Elevation	Elevation with sea level rise
Highest astronomical tide	2.10 m	2.31 m
Mean sea level	0.90 m	1.11 m
Lowest astronomical tide	0.00 m	0.00 m

Table 2.3: *Water levels*

All the elevations in Table 2.3 are with respect to the lowest astronomical tide. Also the extreme water levels have to be considered. These can be found in Table 2.4.

	Return period years			
	1	10	50	100
High water level	3.00 m	3.40 m	3.60 m	3.70 m
Low water level	-2.10 m	-2.30 m	-2.50 m	-2.50 m
High water level with sea level rise	3.21 m	3.61 m	3.81 m	3.91 m

Table 2.4: *Extreme water levels*

The water levels found in Table 2.3 and Table 2.4 are of importance because they influence the dynamics of the wind turbine. An higher water level results in higher contained mass and therefore a change in the first natural frequency of the wind turbines. More elaborate information about the water depths and sand waves can be found in Design part C [26] and the Morphology study [27].

2.4.2 Wind

Extreme wind conditions are modelled for the location of the wind farm. The wind speeds are determined for a reference height of 10 m and extrapolated for the hub height. Extreme wind conditions are modelled for 1, 2, 5, 10, 50 and 100 year return periods.

$$U(z) = U_0 \left(1 + C * ln\left(\frac{z}{10}\right)\right) \tag{2.1}$$

Where C,

$$C = 5.73 * 10^{-2} (1 + 0.15U_0)^{0.5} \tag{2.2}$$

and U_0 is the 1 hour mean wind speed at height $z = 10$.

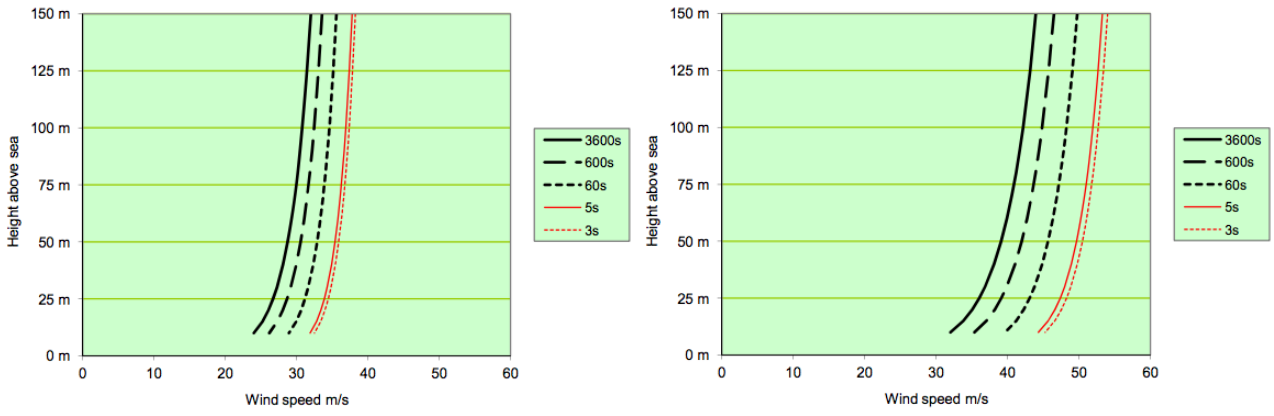

(a) *1 year extreme wind speed* ***(b)*** *50 year extreme wind speed*

Figure 2.5: *Extreme wind speed for different heights*

The average wind speed at the wind farm location is $9.5m/s$ this is at hub height. In Figure 2.6 the occurrence of different wind speed directions can be found in the form of a wind rose.

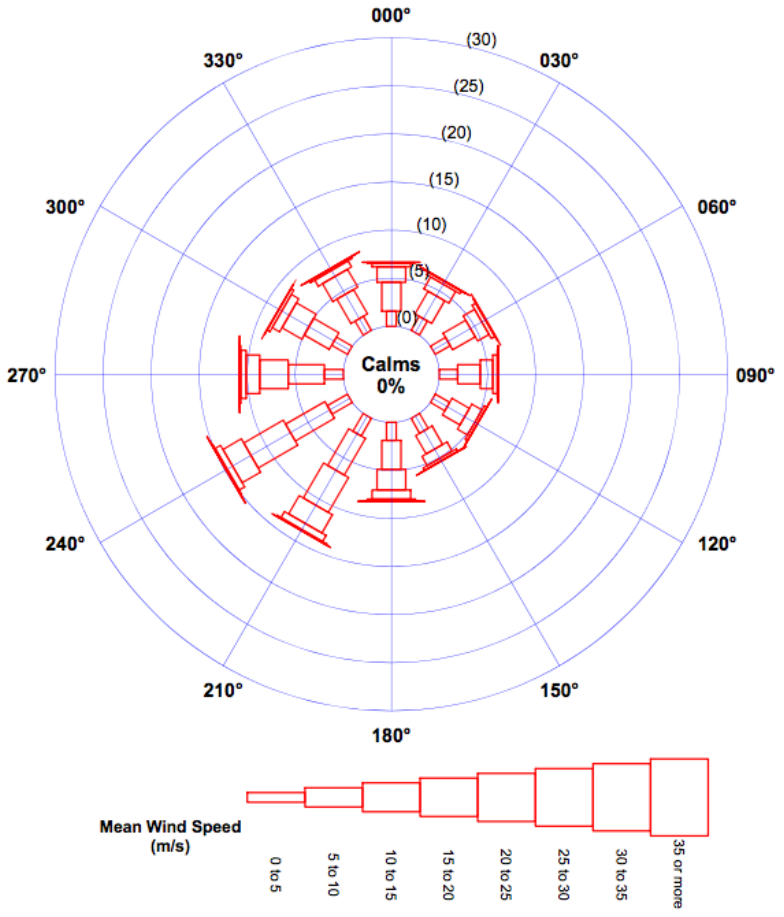

Figure 2.6: *Wind rose with mean windspeeds*

More elaborate information about the extreme, average wind speeds and calculation methods can be found in the metocean report [28].

2.4.3 Wave

Extreme and average wave conditions are modelled for the wind farm also the wave period is modelled. In Table 2.5 the extreme 1, 2, 5, 10, 50 and 100 year wave conditions can be found. These high waves can influence the dynamics of the wind turbines. The high waves might also be a driver for the backfilling of the scour hole.

	Return period years					
	1	2	5	10	50	100
$H_s[m]$	5.7	6.1	6.6	7.0	7.8	8.2
$T_z[s]$	7.7	8.0	8.0	8.6	9.1	9.3
$T_p[s]$	11.4	11.8	12.3	12.7	13.4	13.7
$H_{max}[m]$	10.8	11.2	12.4	13.1	13.7	15.4

Table 2.5: *Extreme wave heights and periods*

In Figure 2.7 a histogram can be found this histogram represents the waves occurring in 1 year. The red box shows the waves that occur most frequently. These are waves with a maximum wave height of 2.5 m and a zero crossing period between 3 and 6 seconds.

SNEXT 3km model Gpt S3005146, 52.4196°N, 4.1425°E, msl constant depth 20 m. Any reject data infilled by NEXTRA 15578 52.45°N 3.86°E																		Numbers
			Mean zero-upcrossing period Tz (s)															
	Hs (m)		0 to <1	1 to <2	2 to <3	3 to <4	4 to <5	5 to <6	6 to <7	7 to <8	8 to <9	9 to <10	10 to <11	11 to <12	12 to <13	13 to <14	14 to <15	Total
9.0	-	9.5	-	-	-	-	-	-	-	-	-	-	-	-	-	-	-	-
8.5	-	9.0	-	-	-	-	-	-	-	-	-	-	-	-	-	-	-	-
8.0	-	8.5	-	-	-	-	-	-	-	-	-	-	-	-	-	-	-	-
7.5	-	8.0	-	-	-	-	-	-	-	-	-	-	-	-	-	-	-	-
7.0	-	7.5	-	-	-	-	-	-	-	-	2	-	-	-	-	-	-	2
6.5	-	7.0	-	-	-	-	-	-	-	-	2	-	-	-	-	-	-	2
6.0	-	6.5	-	-	-	-	-	-	-	3	7	-	-	-	-	-	-	10
5.5	-	6.0	-	-	-	-	-	-	-	9	4	-	-	-	-	-	-	13
5.0	-	5.5	-	-	-	-	-	-	4	27	-	-	-	-	-	-	-	31
4.5	-	5.0	-	-	-	-	-	-	56	19	-	-	-	-	-	-	-	75
4.0	-	4.5	-	-	-	-	-	-	152	10	-	-	-	-	-	-	-	162
3.5	-	4.0	-	-	-	-	-	84	356	-	-	-	-	-	-	-	-	440
3.0	-	3.5	-	-	-	-	-	835	149	-	-	-	-	-	-	-	-	984
2.5	-	3.0	-	-	-	-	3	1,878	15	-	-	-	-	-	-	-	-	1,896
2.0	-	2.5	-	-	-	-	1,058	2,317	2	-	-	-	-	-	-	-	-	3,377
1.5	-	2.0	-	-	-	88	5,536	767	-	-	-	-	-	-	-	-	-	6,391
1.0	-	1.5	-	-	-	1,074	10,806	473	1	-	-	-	-	-	-	-	-	12,354
0.5	-	1.0	-	-	-	10,040	7,869	900	9	-	-	-	-	-	-	-	-	18,818
0.0	-	0.5	456	261	118	9,350	3,128	447	79	30	7	2	3	2	2	-	-	13,885
	Total		456	261	118	20,552	28,400	7,701	823	98	22	2	3	2	2	-	-	58,440

Figure 2.7: *Wave histogram for 1 year*

Important for the modelling of the natural frequency is the wave period or wave frequency this may not coincide with the natural frequency of the wind turbine. In Figure 2.8a the frequency spectrum for the 1 year waves can be found. In Figure 2.8b the wave direction can be found.

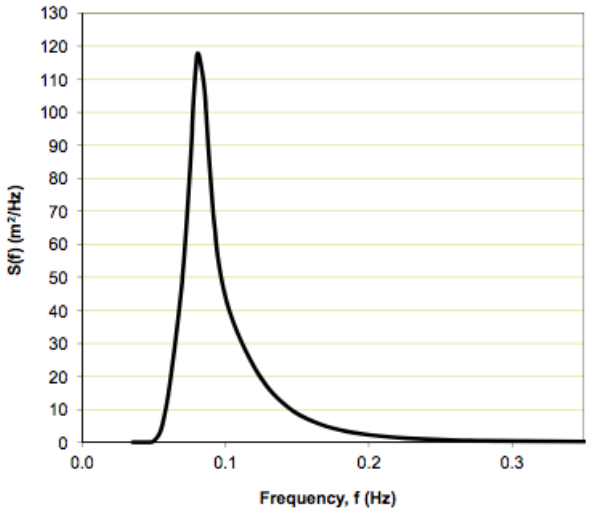

(a) *Frequency spectrum waves*

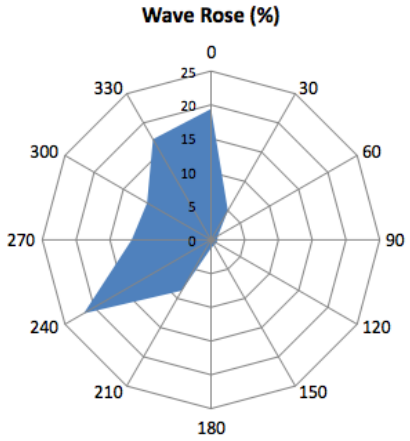

(b) *Wave rose*

Figure 2.8: *Wave conditions*

More elaborate information about the extreme, average waves and calculation methods can be found in the metocean report [28].

2.4.4 Current

Currents are also important when considering a monopile foundation. They are an important hydrodynamical load and can be a driver for scour like waves. Currents are also important because they affect the kinematics of the waves. When waves and current have opposite direction the waves become larger and when the waves and current have the same direction the waves become smaller.

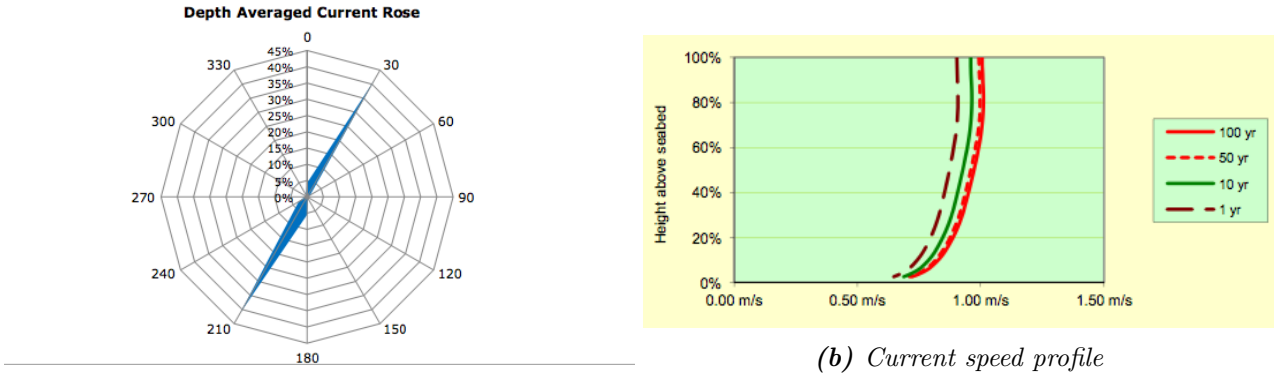

(a) Current rose

(b) Current speed profile

Figure 2.9: *Current conditions*

In Figure 2.9a can be seen that the current is highly directional. This is due to the tidal currents. These tidal currents are always in the same direction. In Figure 2.9b the current velocity can be found. The velocity is maximal at sea level and minimal at the seabed. The profile is created by the 1/10 power law. It is assumed that the current velocity is uniform for the first 30%.

More elaborate information about current velocities, directions and calculation methods can be found in the metocean report [28].

2.5 Monitored Turbines

In the Eneco Luchterduinen offshore wind farm four wind turbines are developed for extensive monitoring. These four wind turbines differ in design, two of these four wind turbines have a monopile foundation with scour protection and two monopiles are designed without scour protection. The wind turbines without scour protection are built in order to get a better understanding of the effect of scour on the dynamic behaviour of an offshore wind turbine.

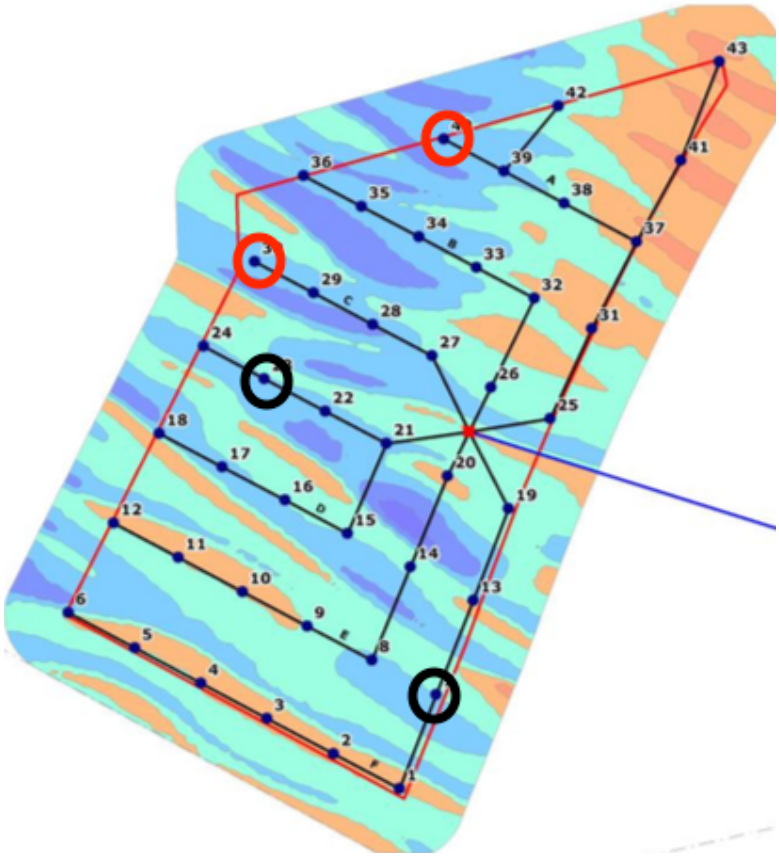

Figure 2.10: *Locations monitored turbines*

In Figure 2.10 the wind turbines that are monitored can be found. The turbines in the black circles have a monopile foundation design with scour protection, turbine number 7 and 23. The wind turbines in the red circles have a monopile design without scour protection, turbine number 30 and 42.

Turbine number	*Water depth (wrt. LAT) [m]*	*Pile mass [t]*	*Penetration depth [m]*	*Pile length [m]*
WTG 7	21.0	445.79		63.46
WTG 23	21.1	449.39		64.16
WTG 30	21.5	600.59		73.43
WTG 42	20.6	610.79		74.93

Table 2.6: *Pile penetration and weights for monopile positions*

In Table 2.6 the penetration depths and weights of the monopile foundations at the monitored locations can be found. It is obvious that the monopiles without scour protection have a larger penetration depth and thus a larger mass. The big difference in penetration depth between monopiles 30 and 42 is due to different soil conditions. It is measured that the soil at the location of monopile 42 is less stiff. All the monitored wind turbines are built in similar water depths and just before a through in the sand waves. Therefore the influence of the sand waves is the same at each monitored wind turbine. Also the water levels at each wind turbine is approximately the same. This is done in order to have similar effects of the water level at each wind turbine. On the monopile foundations the tower of the wind turbine is placed at all different locations the same tower is placed.

2.5.1 Scour & Design scour protection

Two of the Monitored turbines in the Eneco Luchterduinen are not protected against scour and two of the monitored turbines are protected against scour. Scour is the hydrodynamic removal of sediment around the monopile foundation of a wind turbine. The removal of sediment can effect the soil properties around the wind turbines. This effect can be mitigated by the use of scour protection.

A more elaborate discussion about scour mechanisms, the consequences of scour and scour protection can be found in Appendix A.

The scour protection at the monopiles of the Eneco Luchterduinen offshore wind farm consist of two layers, a filter layer and a rock armour layer.
First the filter layer is installed, the installation of the filter layer is done before the monopile is in place. In other words the monopile has to be hammered through the filter layer. In order to prevent winnowing of the filter layer the filter layer has minimum thickness of 0.3 m. Since the monopile needs to be hammered through the filter the gravel of the filter layer may not be too large. At the Eneco Luchterduinen wind farm the filter layer consist of 1-3" inch gravel. The installation of this 0.3 m thick filter layer is executed whit a fall pipe vessel. A fall pipe vessel is used in order to get maximum accuracy. Because there are still inaccuracies when using a fall pipe and since the filter layer needs to be 0.3 m thick on every place an installation thickness of 0.5 m is used.
After the monopile is hammered through the filter the rock armour layer is installed. The rock armour layer also consists of different layers. These different layers are needed to create maximum stability. The stability is created by the interlocking effect of the different rock sizes. In case of the scour protection present at the Eneco Luchterduinen wind farm a three layer scour protection is installed. This scour protection should survive 50 year storm conditions and the rock armour layer consist of rocks with a of grading 10/200 kg.

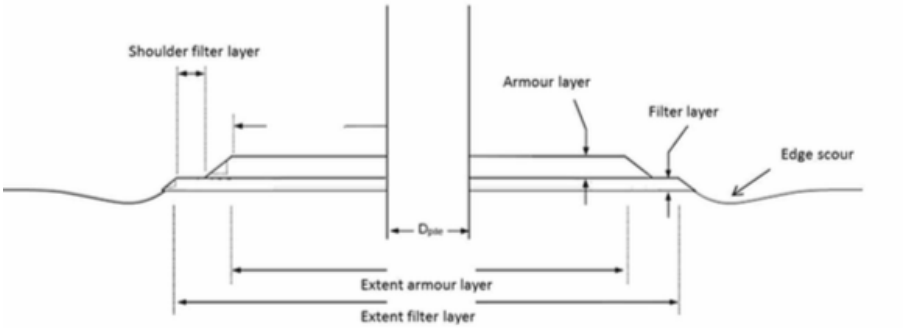

Figure 2.11: *Schematic overview of the installed scour protection*

The extent of the scour protection should be large enough in order to eliminate the effect of edge scour on the monopile. From model tests it is concluded that the area of the filter layer should be 4.7 times the pile diameter. And the rock armour layer should be three times the pile diameter. Since the monopiles are installed when the filter layer is already in place the accuracy of the placement of the monopile should be taken into account. Therefore the size of the filter layer is 27.4 m and the rock armour is 18.2 m.

For the monopiles without scour protection local scour is expected. This scour is due to the immediate effect of the monopiles. The scour holes are expected to develop to a fully developed scour depth of $1.3 * (D + 2 * MG)$, where D is the pile diameter and MG is the thickness of marine growth around the monopile. The scour angle is expected to be 10 degrees.

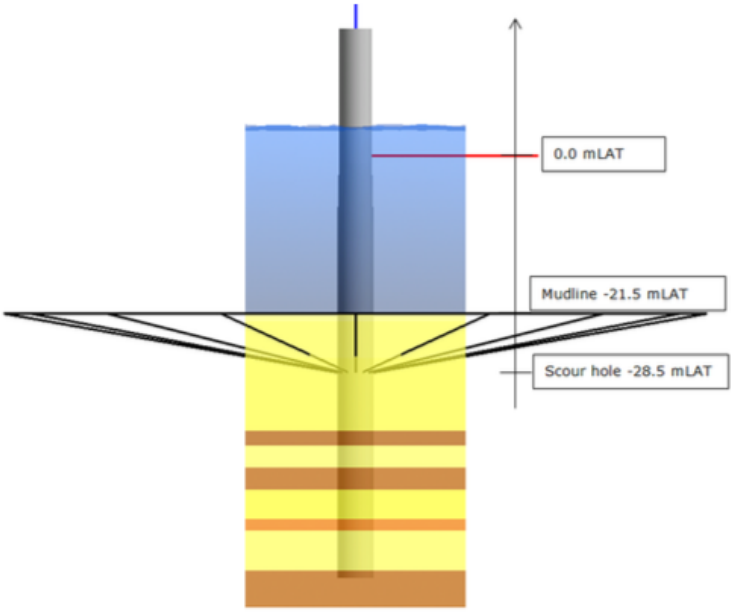

Figure 2.12: *Expected scour hole around monopile 30*

2.5.2 Design natural frequency

In the previous sections the design of the wind turbines in the Eneco Luchterduinen wind farm is discussed. An important design parameter is the design natural frequency. In order to calculate the design natural frequency a computer model is used. The tower and monopile are modelled as an 1D Euler-Bernoulli model from this computer model the mass and stiffness matrices are obtained. There are different options to model the pile soil interaction [4]. In the computer model used by the designers a Winkler spring model is used. The stiffness of these springs is determined from the p-y curves. Since the p-y curve is non linear the stiffness of the springs is taken as the slope of the p-y curve. A more elaborate explanation about the use of p-y curves can be found in the DNV codes [21].

The mass matrix of the monopiles consists of the structural members, the appurtenances and the additional mass.
Structural members:

- Mass of the turbine tower
- Mass of the monopile

Appurtenances:

- Weight of the tower equipment
- Weight of tower flanges as lumped masses
- Weight of the rotor nacelle assembly
- Weight of the boatlanding and acces ladders as uniform distributed mass
- Weight of the external platform as lumped mass
- Weight of the resting platform as lumped mass
- Weight of the internal platform as lumped mass

Additional mass

- Weight of the sacrificial anodes as lumped mass

- Added mass
- Contained mass
- Mass of the allowable corrosion

With the mass and stiffness matrix of the system the first natural frequency can be calculated. With the following equations,

$$0 = M\ddot{x} + Kx \tag{2.3}$$

In Equations 2.3 the undamped equation of motion for the monopile can be found. Where M is the mass matrix and K is the stiffness matrix. A solution to this equation of motion could be a harmonic motion, Equation 2.4.

$$x(t) = \Phi sin(\omega t) \tag{2.4}$$

In Equation 2.4 Φ is the amplitude and ω is angular frequency of the harmonic motion.

$$0 = \left(K - \omega^2 M\right)\Phi \tag{2.5}$$

Equation 2.5 is obtained when combining Equation 2.3 and 2.4. In order to avoid the trivial solution $\Phi = 0$ is disregarded. There for $K - \omega^2 M$ must be 0. This can be done by finding the eigen values, Equation 2.6.

$$0 = det\left(K - \omega^2 M\right) \tag{2.6}$$

By solving this eigenvalue problem the angular eigenfrequencies (natural frequencies) can be obtained. These angular frequencies are converted to the time domain with Equation 2.7. The eigenvalues are the angular natural frequencies. By inserting the obtained angular natural frequencies the mode shape Φ for each angular frequency can be obtained.

$$f = \omega \frac{1}{2\pi} \tag{2.7}$$

In total the natural frequencies are calculated for 12 different soil scenarios.

- *Flexible scenario* –> This scenario will provide lower bound frequencies across the site. In this scenario full development of the sand waves is present, maximum corrosion, the maximum high tide and for the positions without scour protection a fully developed scour hole.
- *Fatigue scenario* –> This scenario represents the average natural frequency. In this scenario there is full development of the sand waves, half corrosion, the water level is at mean sea level and for the positions without scour protection a fully developed scour hole.
- *Stiff scenario* –> This scenario will provide the upper bound frequencies across the site. In this scenario there is no development of sand waves, no corrosion, the water level is at lowest astronomical tide and for the positions without scour protection there is no scour hole present.

When evaluating these three scenarios four different soil conditions are used. The upper and lower bounds of the soil and the drained and undrained soil scenarios. Combining these there are a total of 12 scenarios. These 12 scenarios will have 12 different stiffness matrices.
The design natural frequencies can be found in Table 2.7 the first natural frequencies for the soft, median and stiff region. The soft region represents the softest region from the 12 tested regions. This is when the soil is at lower bound and undrained. The stiffest region is when the soil is at the upper bound and drained.

Turbine number	Natural frequency [Hz]		
	Soft	Median	Stiff
WTG 7	0.271	0.273	0.278
WTG 23	0.272	0.273	0.278
WTG 30	0.263	0.264	0.289
WTG 42	0.266	0.267	0.291

Table 2.7: *Design natural frequencies*

These design natural frequencies should be inside the frequency range by the wind turbine manufacturer, in this case Vestas. Comparing the design natural frequencies from Table 2.7 to the frequency range set by Vestas it can be concluded that all the design natural frequencies are within this range.

2.6 Measurement equipment

In order to measure the natural frequency at the four installed monopiles, accelerometers are installed on these monopiles. These accelerometers monitor the dynamic behaviour of the monopiles. These accelerometers are installed at three levels inside the tower: LAT +18m, LAT +39m and LAT +78m.

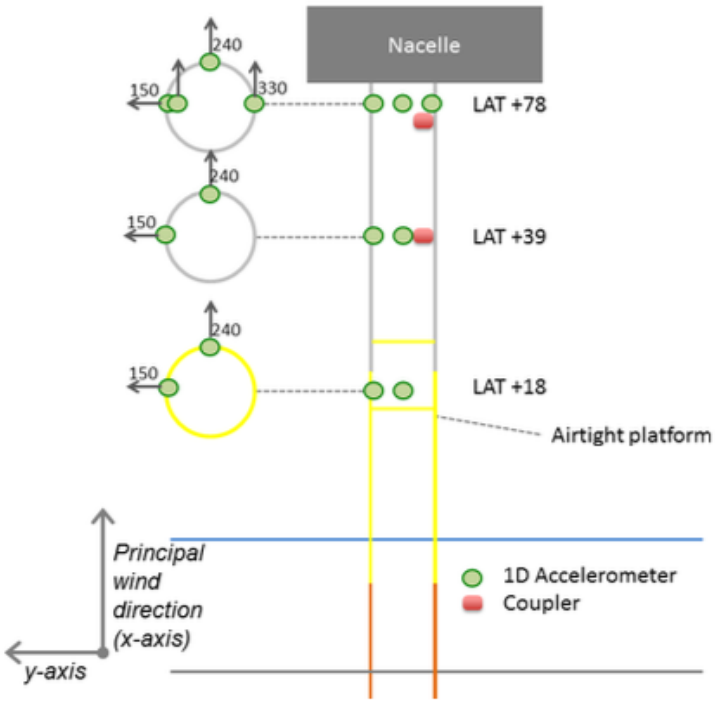

Figure 2.13: *Overview accelerometers tower*

In Figure 2.13 a schematic overview of the locations of the accelerometers are installed is given. A total of eight accelerometers have been installed inside the tower:

- A set of two accelerometers is installed at LAT +18m this the bottom of the tower just above the foundation. This accelerometer measures the bending movement of the tower.
- A second set of two accelerometers is installed at LAT +39m this is halfway the tower. This accelerometer measures the bending movement of the tower.
- A final set of four accelerometers is installed at LAT +78m this is at the top of the tower. There are two accelerometers to measure the bending movement of the tower and two accelerometers to measure the torsional movements.

3 | Identified natural frequency

In this chapter the influences on the identified first natural frequencies are discussed. First the research method is discussed. Secondly an elaborate explanation of the identification of the first natural frequencies done by Zensor is given. After this the results of the research are discussed and evaluated.

3.1 Method

As discussed in chapter 1, the objective of this research is to get a better understanding of the different influences on the first natural frequency of the monitored wind turbines at the Eneco Luchterduinen wind farm. In this part of the research the natural frequencies are identified from measured accelerations. The measurement of these accelerations is done by the accelerometers discussed in chapter 2. In this research only the first bending natural frequency is considered. In order to get a good understanding of the influences on the first natural frequency also the metocean conditions and scada information is obtained (waveheight, waterlevel, windspeed and rotor RPM). The wave height, water level and the wind speed are measured from the offshore high voltage platform (OHVS).

In this research four different factors that might influence the first natural frequency are considered:

- Water level
- Wave height
- Wind speed
- Rotor RPM

The water level and wave height are considered because earlier studies suggest that they influence the first natural frequency of an offshore wind turbine [22]. The wind speed and rotor RPM are directly dependent to each other, the wind speed is the driver for rotation of the rotor. Also the loads induced in the 1P and 3P frequency range are directly dependent to the rotor RPM. As is discussed in Chapter 1, coincidence of the first natural frequency and the excitations in the 1P and 3P frequency range should be avoided.

In order to get a good understanding of the influences of these factors a large pool of data points is needed. This data pool must consist of as many different environmental conditions as possible. Therefore the month November 2016 is considered in this research. In this month there were several calm days, several normal days and most importantly several stormy days. During these stormy days high waves, water levels and wind speeds are reached.

First the influences of the water levels, wave heights, wind speeds and rotor RPM are considered. This will be done by comparing the identified first natural frequencies at different water levels, wave heights, wind speeds and rotor RPM. Also time series will be analyzed in order to check for correlations in time between these outside influences and the identified first natural frequencies.

Another factor that might influence the first natural frequency of the wind turbines is the backfilling of the scour holes. As discussed in chapter 2, two of the monitored turbines are not protected against scour (turbine 30 and 42). During high wave conditions these scour holes might be partly refilled with soil [29]. High waves might disturb the seabed and deposit soil in the scour holes of wind turbine 30 and 42. Since the depth of the scour holes around wind turbine 30 and 42 are not measured simultaneous with the accelerations no solid conclusion can be made about the presence of backfill. But a suggestion about the presence and the possible sensitivity of backfill on the first natural frequency can be made. This is done by comparing the identified first natural frequencies of the scour protected and unprotected wind turbines during three different time spans.

- Just before high wave conditions where fully developed scour is expected
- During high wave conditions where backfilling is expected to occur
- Just after high wave conditions where the backfilled material is removed again

An evaluation on the presence of backfilling and possible influences of backfilling can be found in sections 3.3.3 and 3.4.

3.2 Identification of the first natural frequency

The monitoring campaign discussed in chapter 2 is designed by Zensor. Zensor is a company specialized in analyzing the dynamic behaviour of structures. Zenzor provides a dashboard where all results of the monitoring system can be found. One of the parameters that can be found in this dashboard is the identified first natural frequencies of the wind turbines. The natural frequencies of the wind turbines are determined with an operational modal analyses (OMA). Using the operational modal analysis means the input (forces/displacements) are unknown, therefore an output only identification model needs to be used. An output only model identifies the first natural frequency from for instance accelerations of the wind turbine. The outputs, in this case, the accelerations are transformed to the frequency domain. The natural frequencies are determined using a modal identification program which operates in the frequency domain. In this study a least squares complex frequency (LSCF) analysis is used [30].

3.2.1 LSCF

Transfer function model

In the LSCF the measured frequency response function (FRF) is compared to a modelled transfer function. The measured frequency response function is determined by transferring the accelerations to the frequency domain with a fast fourier transformation (FFT). From this modelled transfer function the eigenfrequencies and the mode shapes are determined. In this case a common denominator transfer function is used.

$$\hat{H}_k(\omega) = \frac{N_k(\omega)}{d(\omega)} \tag{3.1}$$

In Equation 3.1, $\hat{H}_k(\omega)$ is the modelled transfer function, depending on two unknown polynomials. The output polynomial is $N_k(\omega)$, $d(\omega)$ the input polynomial and k is the number of outputs. These outputs are the accelerations obtained by accelerometers placed on the wind turbine, see chapter 2. In the case of an output only system the input polynomial is expected to be white noise. The unknown output and input polynomials can be rewritten as:

$$N_k(\omega) = \sum_{j=0}^{n} \Omega_j(\omega) B_{kj} \tag{3.2}$$

and

$$d(\omega) = \sum_{j=0}^{n} \Omega_j(\omega) A_j \tag{3.3}$$

Where A_j and B_{kj} are the parameters to be estimated. $\Omega_j(\omega)$ is the polynomial basis function. And n is the order of the polynomial. The coefficients of these parameters are put in a column vector $\theta = [\beta_1, ..., \beta_k, \alpha]$.

$$\beta_k = \begin{bmatrix} B_{k0} \\ B_{k1} \\ \vdots \\ B_{kn} \end{bmatrix}, \alpha = \begin{bmatrix} A_{k0} \\ A_{k1} \\ \vdots \\ A_{kn} \end{bmatrix} \tag{3.4}$$

In this case a discrete time domain model is used, when using a discrete time domain model the polynomial basis for $\Omega_j(\omega)$ is given by $\Omega_j(\omega) = exp(-i\omega T_s j)$. Where T_s is the sampling period.

Linearizing the parameters

The estimates of the transfer function coefficients can be obtained by minimizing the non-linear least squares cost function (NLS). The minimization is done with respect to θ. θ is the a row vector of the estimated parameter K_j and B_{kj}.

$$l_{NLS}(\theta) = \sum_{k=1}^{N_o} \sum_{f=1}^{N_f} |\epsilon(\omega_f, \theta)|^2 \tag{3.5}$$

Where N_o is the number of outputs and N_f is the number of sampling frequencies and ω_f is the sampling frequency. The weighed error in the non-linear cost function is defined as:

$$\epsilon_k^{NLS} = W_k(\omega_f) \left(\frac{N_k(\omega_f, \beta_k)}{d(\omega_f, \alpha)} - H_k(\omega_f) \right) \tag{3.6}$$

The weight function used in this equation penalizes the noisy frequency response functions and makes sure the frequency response functions that have a large variance have a small contribution.

$$W_k(\omega_f) = \frac{1}{\sqrt{var(H_k(\omega_f))}} \tag{3.7}$$

Where $H_k(\omega_f)$ is the frequency response function obtained from the measurements. The non-linear least square function can be estimated by a linear least square function.

$$\epsilon_k^{LS}(\omega_f, \theta) = \epsilon_k^{NLS}(\omega_f, \theta) d(\omega_f, \theta) \tag{3.8}$$

$$\epsilon_k^{LS}(\omega_f, \theta) = W_k(\omega_f)(N_k(\omega_f, \beta_k) - d(\omega_f, \alpha) H_k(\omega_f)) \tag{3.9}$$

$$\epsilon_k^{LS}(\omega_f, \theta) = W_k(\omega_f) \sum_{j=0}^{n} (\Omega_j(\omega_f)\beta_{kj} - \Omega_j(\omega_f) A_j H_k(\omega_f)) \tag{3.10}$$

Since these equations are linear they can be formulated in matrix equations.

$$\epsilon_k^{LS}(\theta) = \begin{bmatrix} \epsilon_k^{LS}(\omega_1, \theta) \\ \vdots \\ \epsilon_k^{LS}(\omega_{N_f}, \theta) \end{bmatrix} = [X_k Y_k] \begin{bmatrix} \beta_k \\ \alpha \end{bmatrix} \tag{3.11}$$

Where,

$$X_k = \begin{bmatrix} W_k(\omega_1)[\Omega_0(\omega_1), \Omega_1(\omega_1), ..., \Omega_n(\omega_1)] \\ \vdots \\ W_k(\omega_1)[\Omega_0(\omega_{N_f}), \Omega_1(\omega_{N_f}), ..., \Omega_n(\omega_{N_f})] \end{bmatrix} \tag{3.12}$$

and

$$Y_k = \begin{bmatrix} -W_k(\omega_1)[\Omega_0(\omega_1)H_k(\omega_1), \Omega_1(\omega_1)H_k(\omega_1), ..., \Omega_n(\omega_1)H_k(\omega_1)] \\ \vdots \\ -W_k(\omega_1)[\Omega_0(\omega_{N_f})H_k(\omega_{N_f}, \Omega_1(\omega_{N_f})H_k(\omega_{N_f}, ..., \Omega_n(\omega_{N_f})H_k(\omega_{N_f}] \end{bmatrix} \tag{3.13}$$

The weighted linear least square estimates are found by:

$$l_{LS}(\theta) = \sum_{k=1}^{N_o} \sum_{f=1}^{N_f} |\epsilon_k^{LS}(\omega_f, \theta)|^2 \tag{3.14}$$

$$l_{LS}(\theta) = \sum_{k=1}^{N_o} [\beta_k^T \alpha^T] \begin{bmatrix} R_k & S_k \\ S_k^T & T_k \end{bmatrix} \begin{bmatrix} \beta_k \\ \alpha \end{bmatrix} \tag{3.15}$$

R_k, S_k, T_k are the reduced normal equations, $R_k = Re(X_k^H X_k)$, $S_k = Re(X_k^H Y_k)$ and $T_k = Re(Y_k^H Y_k)$. The reduced normal equations represent the minimum of the least squares error where all possible derivatives are zero, this is also the minimum of the cost function. The derivatives of the cost function are:

$$\frac{\delta}{\delta \beta_k} l_{LS}(\theta) = 2(R_k \beta_k + S_k \alpha) = 0 \tag{3.16}$$

$$\frac{\delta}{\delta \alpha} l_{LS}(\theta) = 2 \left(\sum_{k=1}^{N_o} (S_k^T \beta_k + T_k \alpha) \right) = 0 \tag{3.17}$$

By substitution of Equation $\beta_k = -R_k^{-1} S_k \alpha$ into Equation 3.17 the following equation is obtained.

$$\left[2 \sum_{k=1}^{N_o} (T_k - S_k^T R_k^{-1} S_k) \right] \alpha = M\alpha = 0 \tag{3.18}$$

Equation 3.16 and 3.17 are called the normal equations, these are usually formulated in matrix form.

$$2 \begin{bmatrix} R_1 & 0 & \cdots & S_1 \\ 0 & R_2 & \cdots & S_2 \\ \vdots & \vdots & \ddots & \vdots \\ S_1^T & S_2^T & \cdots & \sum_{k=1}^{N_o} T_k \end{bmatrix} \begin{bmatrix} \beta_1 \\ \beta_2 \\ \vdots \\ \beta_{N_o N_i} \\ \alpha \end{bmatrix} = 0 \tag{3.19}$$

Solving the reduced normal equations

In order to eliminate the trivial solution and remove the parameter redundancy a constraint has to be imposed. This is done by assuming that one of them is constant to a non zero value. For instance the last coefficient of α is constrained to 1. Then the reduced normal equations are:

$$Ax = b \tag{3.20}$$

Where,

$$A(nxn) = M(1:n, 1:n) \tag{3.21}$$

and

$$b(n, 1) = M(1:n, n+1) \tag{3.22}$$

Then the least squares estimate of α is:

$$\hat{\alpha}_{LS} = \begin{bmatrix} x \\ 1 \end{bmatrix} \tag{3.23}$$

where x is obtained from $x = A^{-1}b$ once $\hat{\alpha}_{LS}$ from $\beta_k = -R_k^{-1} S_k \alpha$ can be used to derive all the coefficients of $\hat{\beta}_k$. When all the coefficients are known the poles of the obtained denominator of the transfer function can be obtained.

Stabilization chart

In a modal analysis a stabilization chart is an important tool in order to separate the mathematical poles to the physical poles of the system. The physical poles can be found at the characteristic frequencies of the system while a mathematical pole mainly describes the presence of noise from the measurements. A stabilization chart is obtained by repeating the LSCF for increasing model order. The stable poles of the denominator of the transfer will have a negative real part in the laplace domain. The more frequent a pole occurs in the different orders of the polynomial the more stable the pole is expected to be. The obtained poles are the natural frequencies of the system. A disadvantage of using an operational modal analysis and an stabilization chart is that excitation frequencies can be observed as natural frequencies of the wind turbines. This happens when an excitation frequency has a stable physical pole and is close to a natural frequency of the wind turbine. Another downside of doing an operational modal analysis is that when the natural frequencies are very close to excitation frequencies no stable pole is found. In figure 3.1 an example of a stabilization chart can be found where the dots indicate the poles that are found by algorithm.

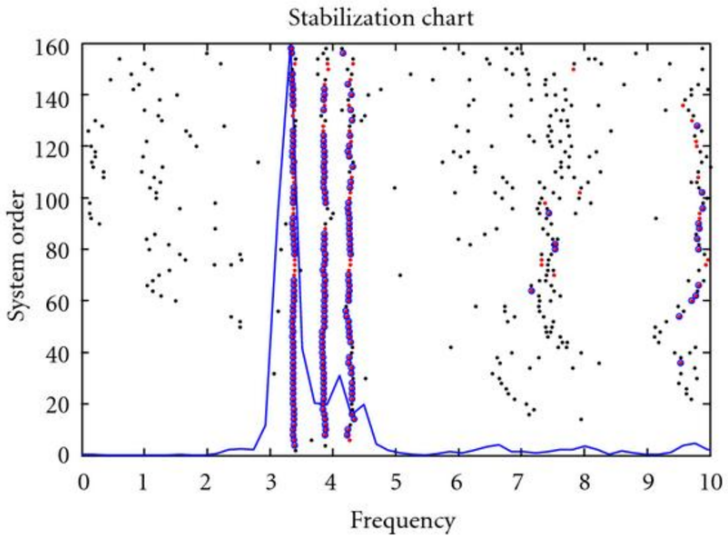

Figure 3.1: *Example of a stabilization chart [5]*

3.3 Results of the monitoring campaign

In this section all the obtained measurements are discussed. In section 3.4 all the influences and effects on the first natural frequency of the wind turbine are evaluated. First the different environmental influences are discussed. Subsequently the influence of backfill on the first natural frequency is discussed. In the last part of this section the measured natural frequencies are compared to the design natural frequencies and the differences between the design and measured natural frequencies are discussed. The environmental conditions are all measured from one point, the measurement equipment is installed on the OHVS (offshore high voltage platform). All the processed data is from the month November 2016. All the measurement data obtained from Zenzor is loaded into Matlab in order to do the analyses of the wind turbines.

3.3.1 Wind speed and rotor RPM

First the effects of the wind speed and the rotor RPM on the first natural frequency are discussed. The wind has different influences. It is not only the driver for the rotation of the rotor, but excitation due to turbulent wind could also be of influence see Figure 1.4. With higher wind speeds a higher rotor RPM is expected. Subsequently with a higher wind speed and rotor RPM a higher thrust is expected. This thrust can be found as a force in horizontal direction at hub height. The thrust becomes larger until the rotor is at rated rotor RPM. When the rotational speed is at rated RPM the blades start to

pitch and the horizontal force on the nacelle becomes smaller [31]. A change in thrust might result in a change of the first natural frequency since the soil stiffness is non linear and determined by the non linear p-y curve[21].

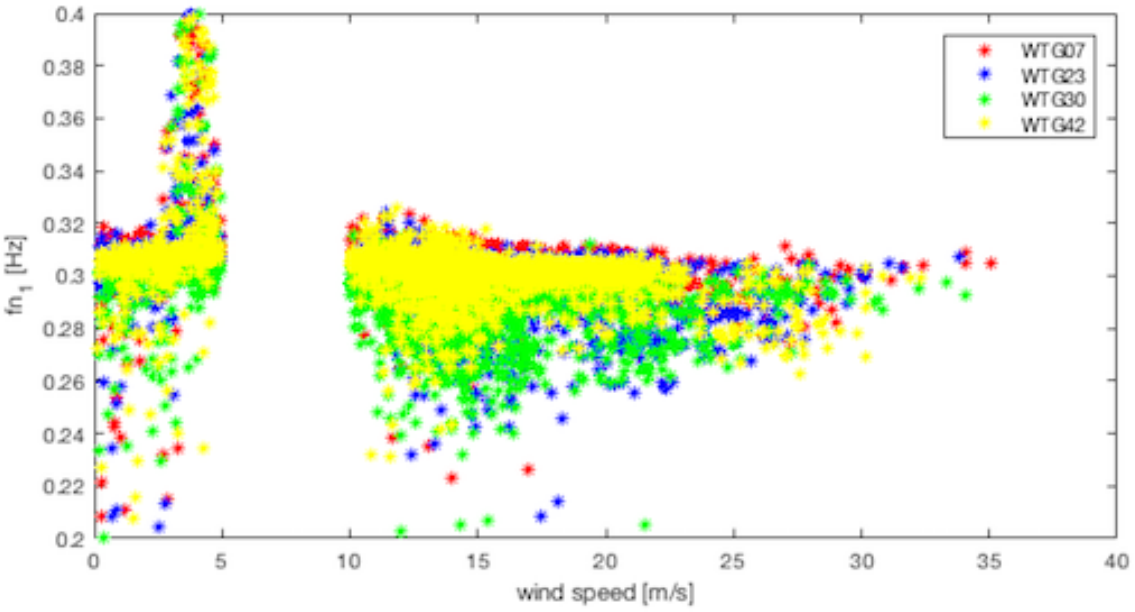

Figure 3.2: *The identified first natural frequency for different wind speeds*

In Figure 3.2 a scatter plot of the first natural frequency for different wind speeds is shown. The scatter found just below a wind speed of 5 m/s is due to the 3P frequency excitation of the rotor. This can also be found in Figure 3.6. From Figure 3.6 it can be concluded the first natural frequencies which are highly scattered and higher than expected occur at a rotor speed of 8 RPM. The 3P frequency of the wind turbines at this rotor RPM is 0.4 [Hz].
When the 3P excitations and the first natural frequency are close to each other the two poles in the frequency spectrum might merge and look as one pole in the peak picking algorithm. The poles of these frequencies are not deleted by the peak picking algorithm since they seem to have a stable pole, see section 3.2.1. However these frequencies are not the natural frequencies of the system. But they are a merger of an excitation frequency and the first natural frequency.

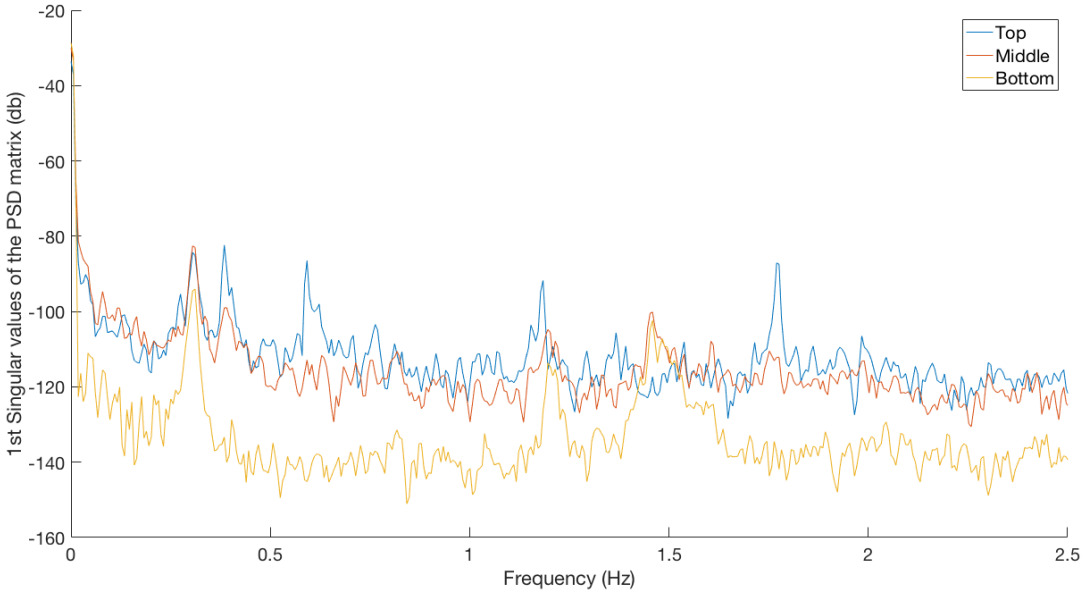

Figure 3.3: *Example of the power spectral density of the accelerometers at wind turbine 42 at a rotor RPM of 8 [RPM] and a wind speed of 4.7 [m/s]*

An example of this can be found in Figure 3.3. In the Figure the power spectral density of the three groups of accelerometers can be found. The accelerometers are located at hub height (top), the middle of the wind turbine tower (middle) and at interface height (bottom). The rotor RPM of wind turbine 42 at this time is 8 [RPM], the wind speed is 4.7 [m/s] and the identified first natural frequency by the peak picking algorithm is 0.369 [Hz]. In Figure 3.3 it is obvious to see there are two peaks just before 0.5 [Hz] the first peak is at 0.305 [Hz] and the second peak is at 0.402 [Hz]. The first peak at 0.305 [Hz] is the first natural frequency of the wind turbine and the second peak (0.402 [Hz]) is the 3P excitation frequency. However the peak picking algorithm identifies a first natural frequency of 0.369 [Hz]. This error in peak picking algorithm is expected to occur more often when the wind turbine rotor RPM is around 8 [RPM].

The missing data between 5 and 10 m/s (Figure 3.2) can also be ascribed to errors in the identification algorithm or due to coincidence with ambient excitations. When the frequency of ambient excitation coincides with first natural frequency of the wind turbine no stable pole can be found in the stabilization chart, section 3.2.1. When no stable pole is found the data point is not saved as a natural frequency of the wind turbine.

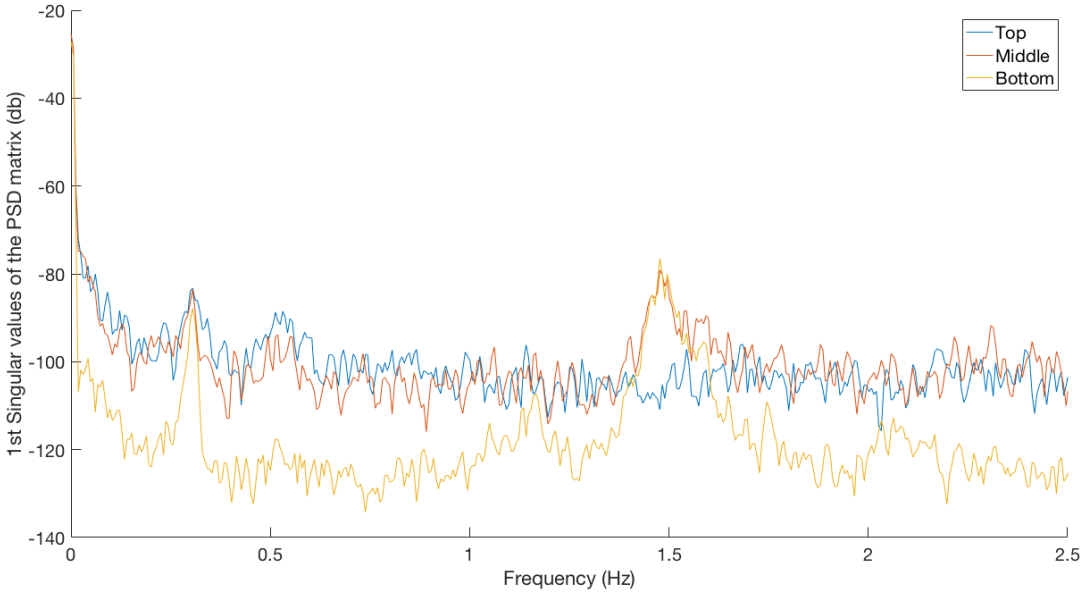

Figure 3.4: *Example of the power spectral density of the accelerometers at wind turbine 42 at a rotor RPM of 11[RPM] and a wind speed of 6.9 [m/s]*

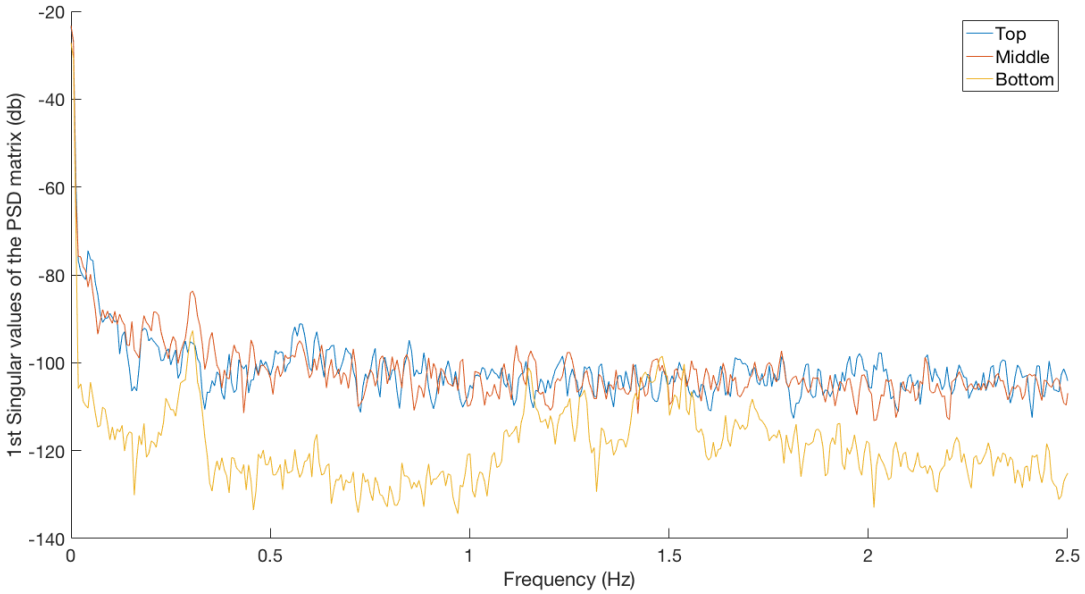

Figure 3.5: *Example of the power spectral density of the accelerometers at wind turbine 42 at a rotor RPM of 13[RPM] and a wind speed of 8.8 [m/s]*

In Figures 3.4 and 3.5 examples of situations where the identification algorithm leads to errors can be found. In both situations the peak picking algorithm did not identify the first natural frequency. In Figure 3.4 the rotor RPM was 11 RPM at a wind speed of 6.9 [m/s] and in Figure 3.5 the rotor RPM was 13 and at a wind speed of 8.8 [m/s]. In both figures it can be found that there is no coincidence with ambient excitations. The reason that the first natural frequency is not identified is unclear. For both cases the first natural frequency was identified manually at 0.305 [Hz]

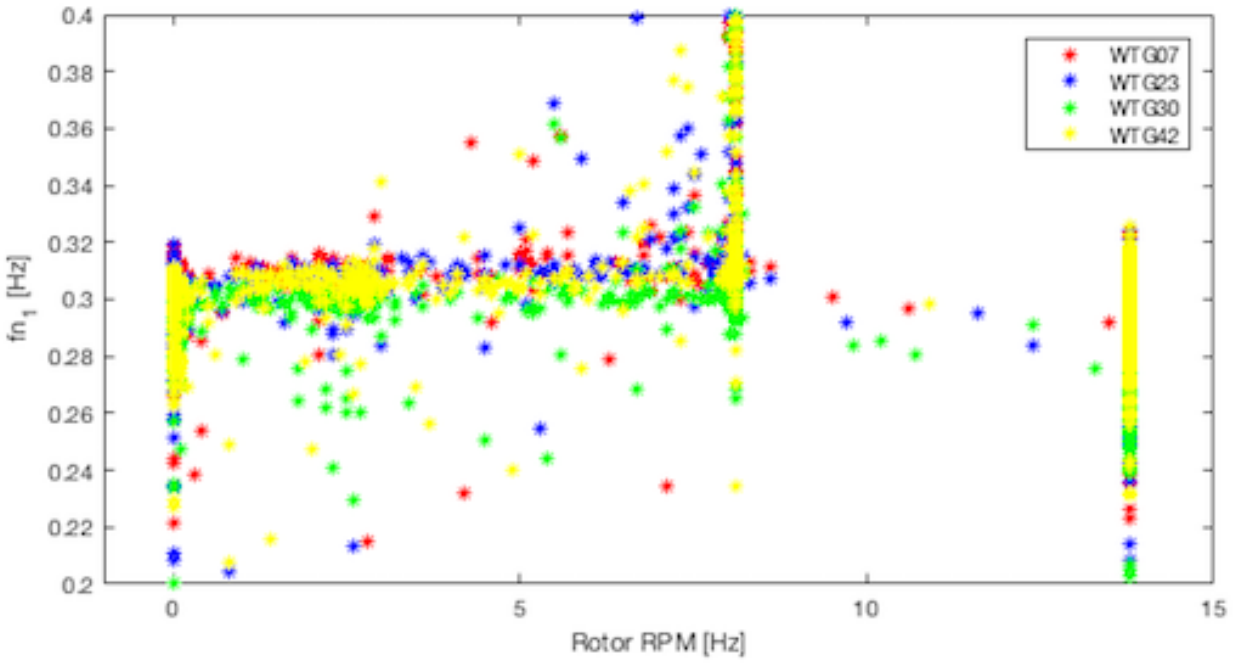

Figure 3.6: *The identified first natural frequency for different rotational rotor speeds*

In Figure 3.6 three peaks with highly scattered natural frequencies can be found. These peaks are at a rotational speed of 0, 8 and 13.78 RPM. The highly scattered natural frequencies at 0 RPM are due to wave induced loads, since at a rotor RPM of 0 RPM there is no 1P and 3P frequency. The wave induced loads have an excitation frequency between 0.11 and 0.33 [Hz][32].

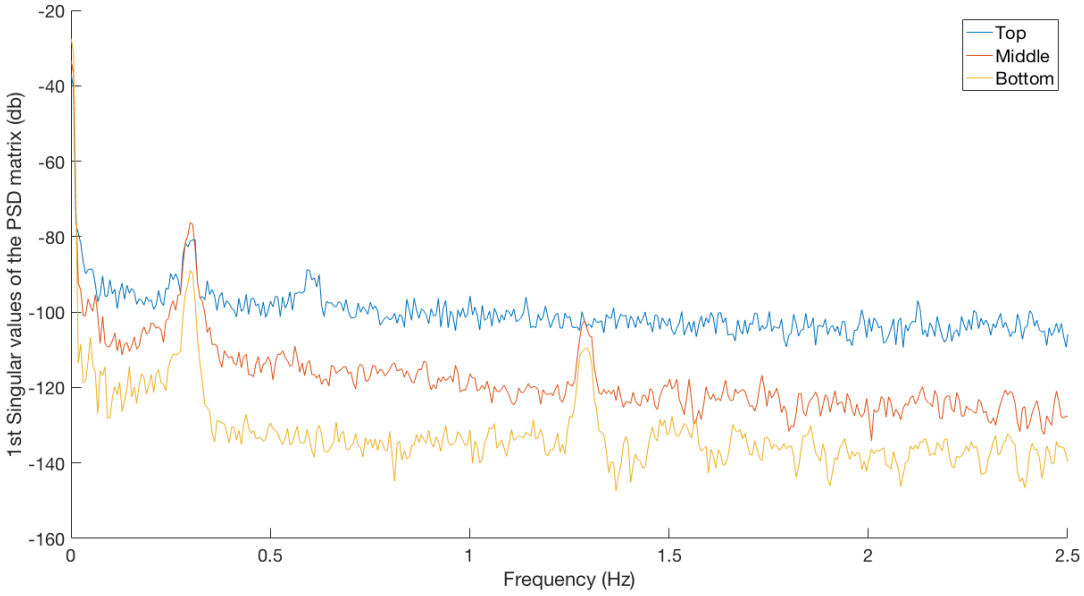

Figure 3.7: *Example of the power spectral density of the accelerometers at wind turbine 42 at a rotor RPM of 0[RPM] and a wind speed of 1.3 [m/s]*

In Figure 3.7 an example of the spectral density spectrum where this error occurs can be found. In Figure 3.7 rotor RPM was 0 RPM and the wind speed was 1.3 [m/s]. The identified natural frequency was 0.244 [Hz] while the manually identified natural frequency is at 0.305 [Hz]. Therefore it is expected that the peak picking algorithm identifies the small peak just before the peak of the first natural frequency as the the first natural frequency.

The peak at 8 RPM is due to the 3P excitation frequency of the wind turbine, which is explained before. At a rotational speed of 8 RPM the 3P frequency is 0.4 [Hz], Figure 3.3. The last observed peak in Figure 3.6 is at rated rotor RPM of 13.78 RPM. When the rotor RPM is 13.78 the natural frequency is close to the 1P frequency of the wind turbine. The 1P frequency at a rotor RPM of 13.78 is 0.23 [Hz]. Near this peak the same phenomenon as at the peak near 8 RPM might happen. The merging of the first natural frequency and an excitation frequency which look as one stable pole in the peak picking algorithm 3.2.1. This can be observed in Figure 3.8. The identification algorithm identifies the first natural frequency at 0.229 [Hz] while the manually identified first natural frequency is at 0.299 [Hz].

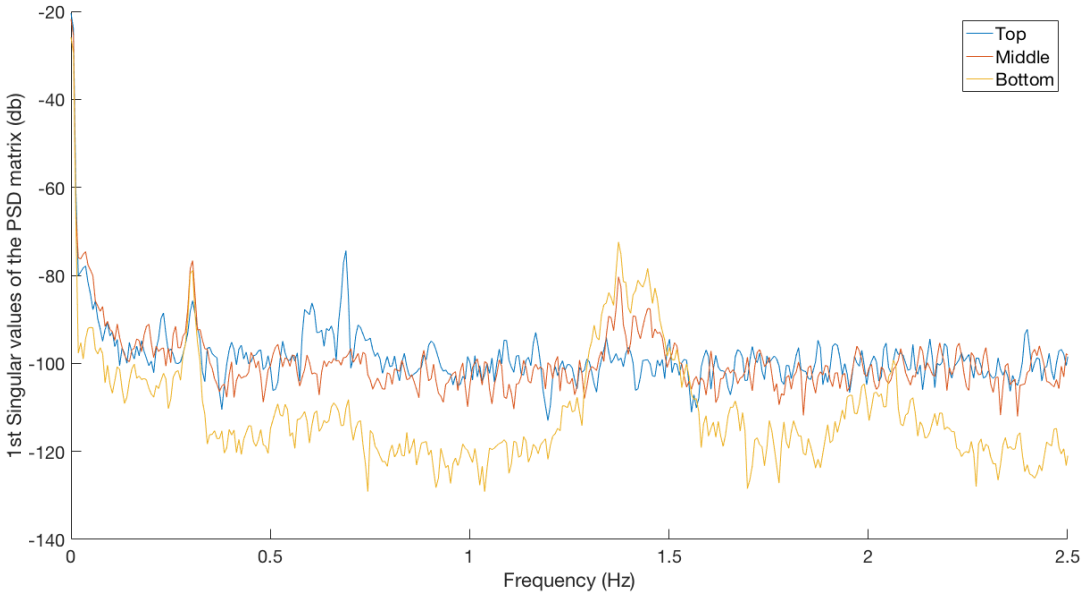

Figure 3.8: *Example of the power spectral density of the accelerometers at wind turbine 42 at a rotor RPM of 13.8[RPM] and a wind speed of 14 [m/s]*

The scatter due to the coincidence of these excitation frequencies with the natural frequency is also visible in Figure 3.6. The lack of data between 8 and 13.8 [RPM] has the same reason as the lack of data between a wind speed of 5 and 10 [m/s] in Figure 3.6: an error in the identification algorithm.

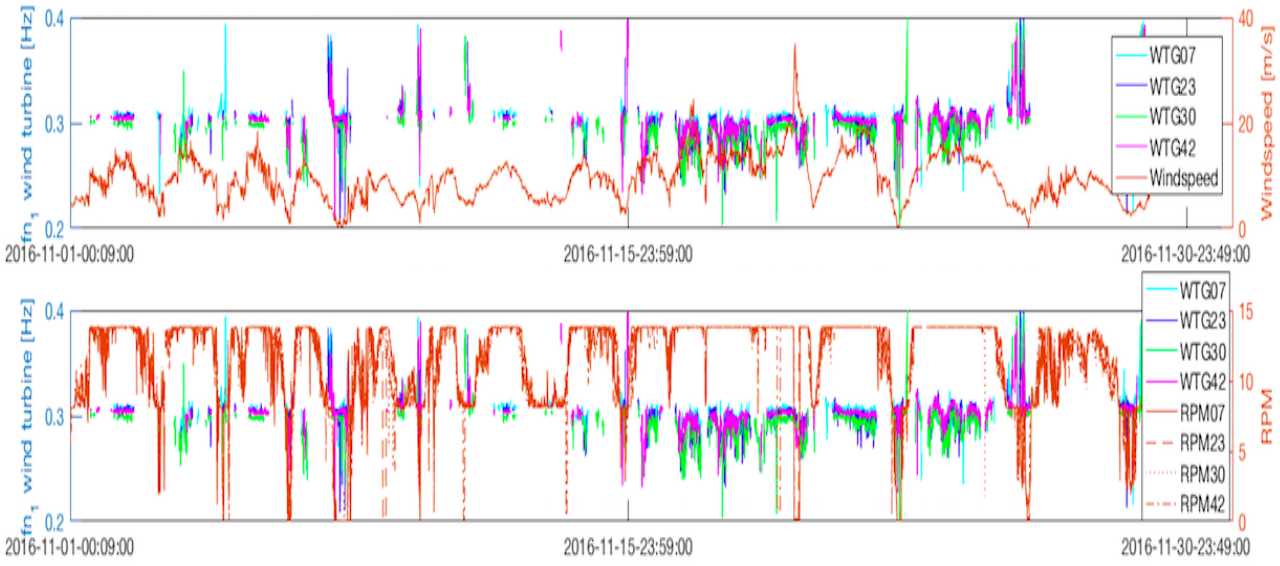

Figure 3.9: *The identified first natural frequency and wind speed/RPM over time*

From the timeseries in Figure 3.9 no obvious correlations between the wind speed and the identified natural frequency in time can be found. This is the same for the correlation between the rotor RPM and the first natural frequency.

Manually identified first natural frequencies

As is discussed in this section many identified first natural frequencies that are identified by Zenzor have an identification error. Also the first natural frequencies between 8 and 13.8 RPM are not identified at all. Therefore from this data no solid conclusion can be drawn. In order to get a solid conclusion the high frequency data from the accelerometers were requested. From these high frequency data the first natural frequencies of all four wind turbines were identified. This identification was done by hand in order to be sure no identification errors were made. The data points were chosen randomly for different conditions (wind speed, rotor RPM, wave height and water level). In total 140 first natural frequencies per wind turbine are identified by hand from a pool of 4320 data points per wind turbine.

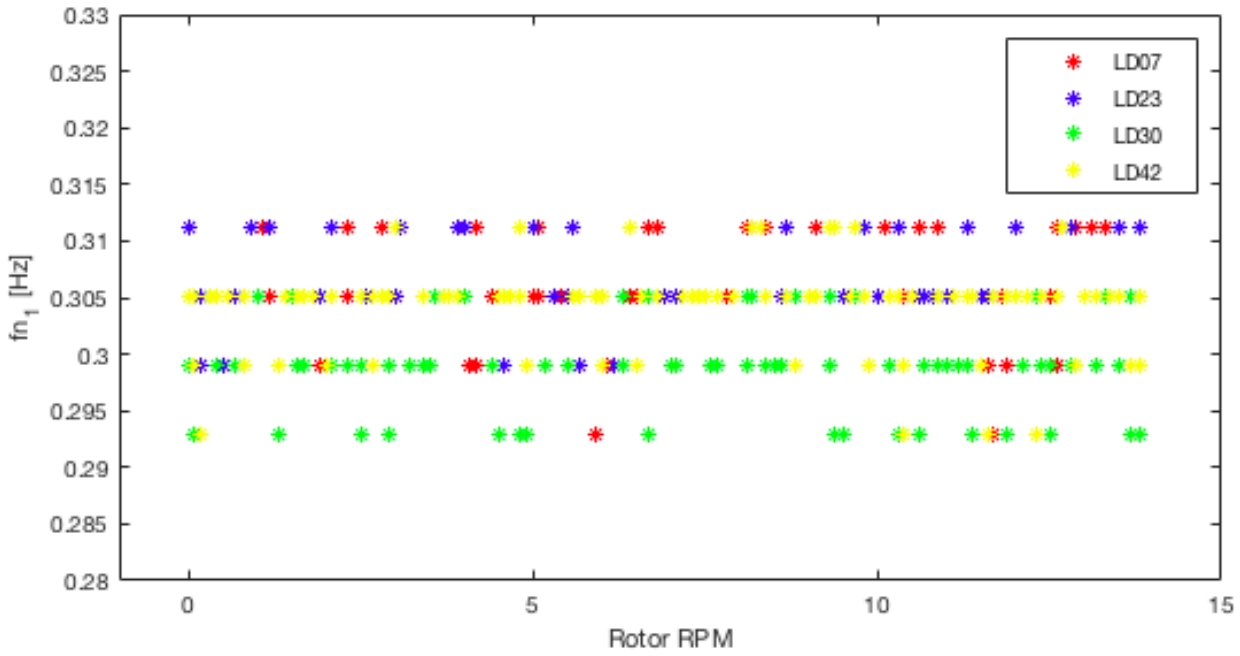

Figure 3.10: *Manually identified first natural frequencies at different rotational rotor speeds*

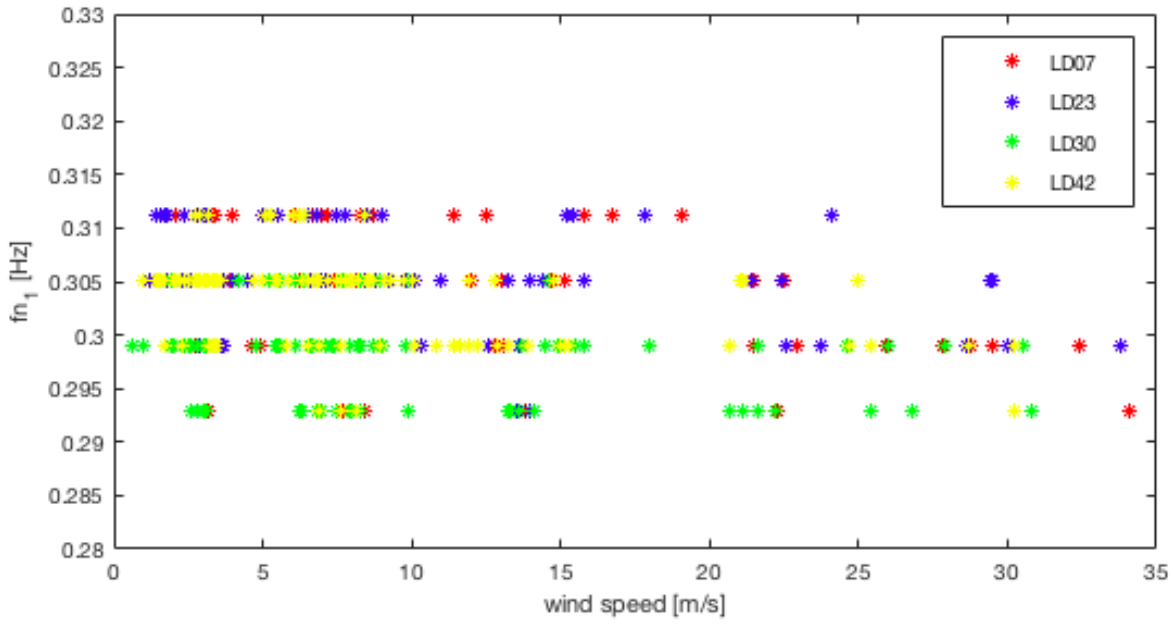

Figure 3.11: *Manually identified first natural frequencies at different wind speeds*

From Figures 3.10 and 3.11 it can be found that the scatter due to identification errors is mitigated. Also there is no data missing between a rotor RPM of 8 and 13.8 [RPM]. From Figure 3.10 it can be observed that first natural frequency remain constant at different rotor speeds. This is the case for all four wind turbines. In Figure 3.11 it can be found that at very high wind speeds the first natural frequency is slightly lower. It can be observed from Figures 3.10 and 3.11 that the resolution is coarse. This is due to sampling rate of the accelerometers, the accelerometers installed on the monitored wind turbines have a sampling rate of 50[Hz]. A higher sampling rate would lead to a less coarse resolution.

3.3.2 Water level

In this section the influence of the water level on the first natural frequencies of the wind turbines is discussed. The water level is measured as a value above the lowest astronomical tide. The influences of the water level are observed during one month (November 2016) with different wind and wave conditions. This is done in order to see maximum correlation with the first natural frequency at different moments in time. The water level can influence the first natural frequency due to hydrodynamic damping, contained mass inside the monopile and hydrodynamic added mass outside of the monopile.

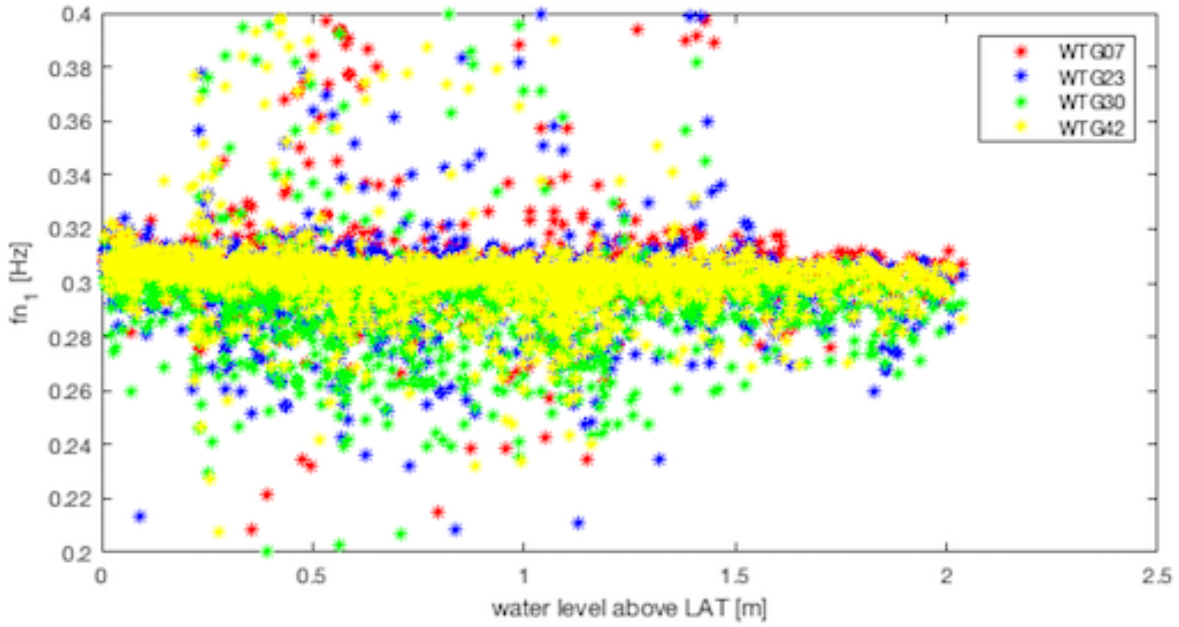

Figure 3.12: *The identified first natural frequency at different water levels*

From Figure 3.12 it can be found that the water level has an influence on the first natural frequencies of the wind turbines. There is a reduction of the first natural frequency at a higher water level. This was expected. The scattering found in Figure 3.12 is due to the coincidence of excitation frequencies with the first natural frequencies of the wind turbines. This is discussed in section 3.3.1.

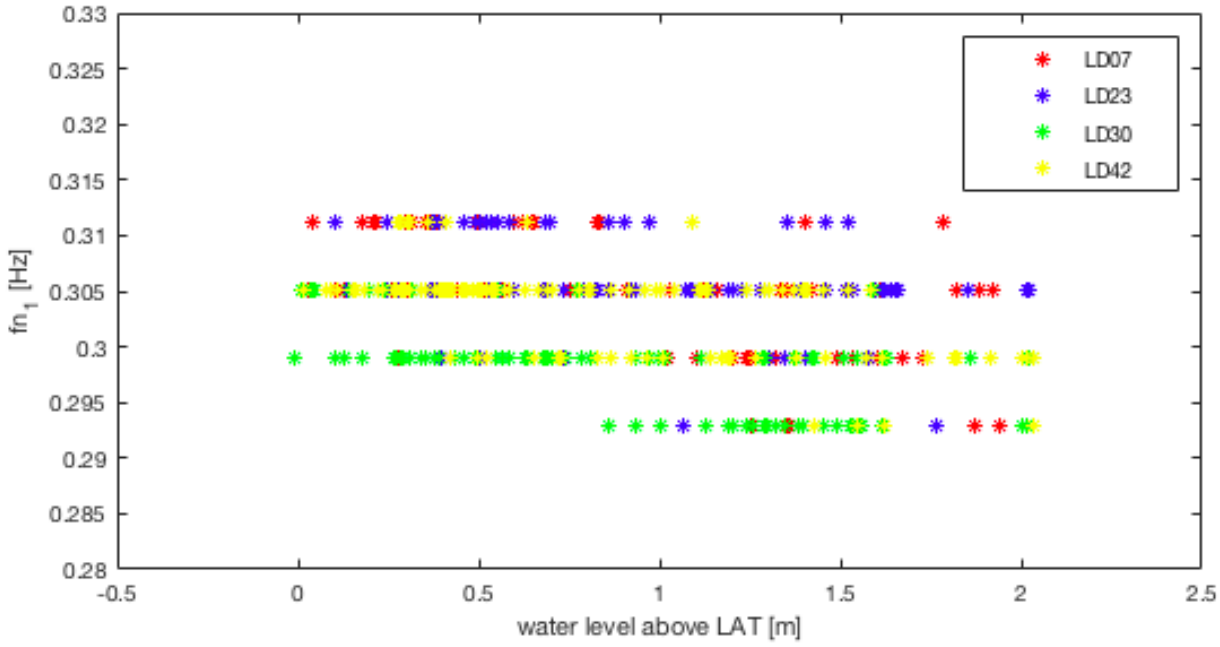

Figure 3.13: *Manually identified first natural frequencies at different water levels above LAT*

The same can be observed for the data set with the manually identified first natural frequencies, Figure 3.13. In order to make the difference in first natural frequencies more obvious two bins are formed. The first bin contains all the data points where the water level is lower than 0.3 meter above lowest average tide (LAT). The second bin contains all the data points where the water level is higher than 1.8 meter above lowest astronomical tide.

Wind turbine	<0.3 m above LAT	>1.8 m above LAT	difference
WTG 07	0.306 Hz	0.301 Hz	1.5 %
WTG 23	0.306 Hz	0.303 Hz	1.1 %
WTG 30	0.302 Hz	0.297 Hz	1.7 %
WTG 42	0.305 Hz	0.299 Hz	2.0 %

Table 3.1: *Difference in identified first natural frequency for high and low water levels above lowest astronomical tide*

In table 3.1 the difference in identified first natural frequency for high and low water levels can be found. The difference ranges between 1 and 2 %.

More evidence for correlation between the water level and the first natural frequency can be found in a time series plot of the first natural frequency over time and the water level over time.

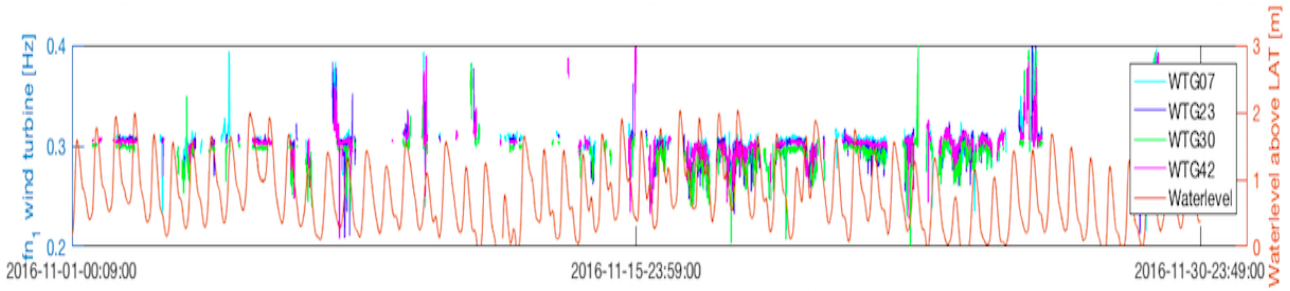

Figure 3.14: *The identified first natural frequency and water level over time*

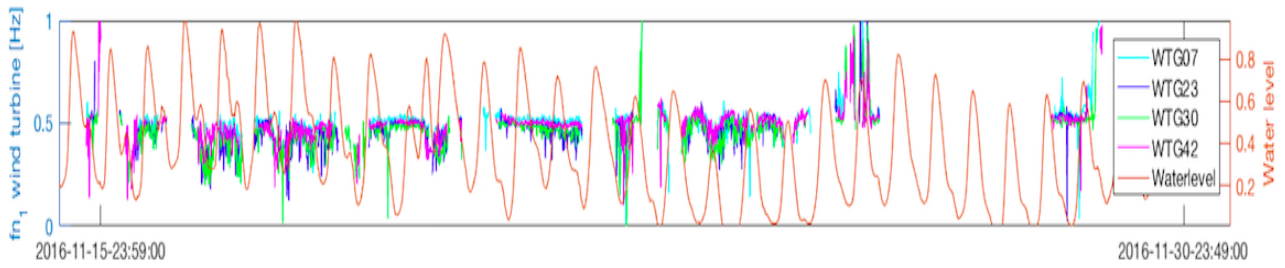

Figure 3.15: *The identified first natural frequency and water level over time when normalized (zoomed in)*

In the time series in Figures 3.14 and 3.15 all the measurements of the water level and first natural frequency for the monopiles in the month November 2016 are represented. It is clear that the water level and the first natural frequency are highly correlated. When the tide is low the natural frequency is high and when the tide is high the natural frequency is low. This is in correspondence with earlier research [22].

3.3.3 Waves

The last environmental influence that is observed are the wave conditions. The wave conditions are expected to influence the natural frequency in form of backfilling of the scour hole at the unprotected wind turbines, see Appendix A. In other words significant differences between the wind turbines without scour protection and with scour protection are expected.

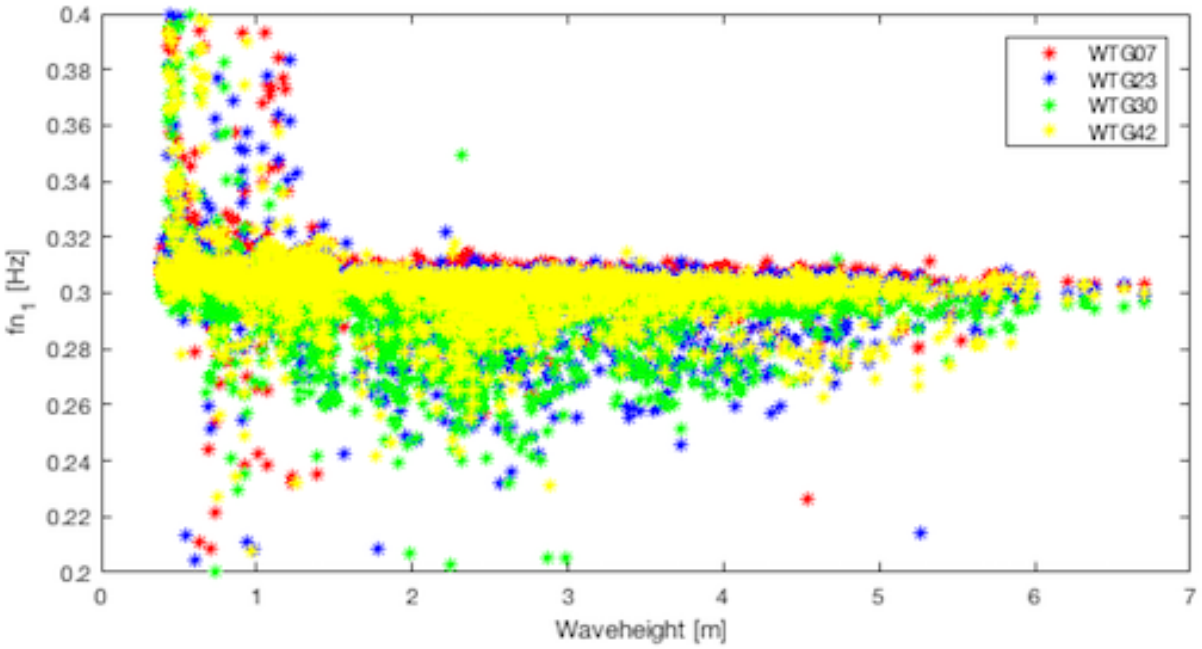

Figure 3.16: *The identified first natural frequency for different wave heights*

In Figures 3.16 an decrease in natural frequency can be found: the higher the waves the lower the first natural frequency. Again as discussed in the previous sections the areas with high scatter can be ascribed to coincidence of the natural frequency with excitation frequencies or can be due to identification errors. Furthermore from Figure 3.16 no obvious difference between the scour protected (turbine 7 and 23) and unprotected (turbine 30 and 42) wind turbines can be found

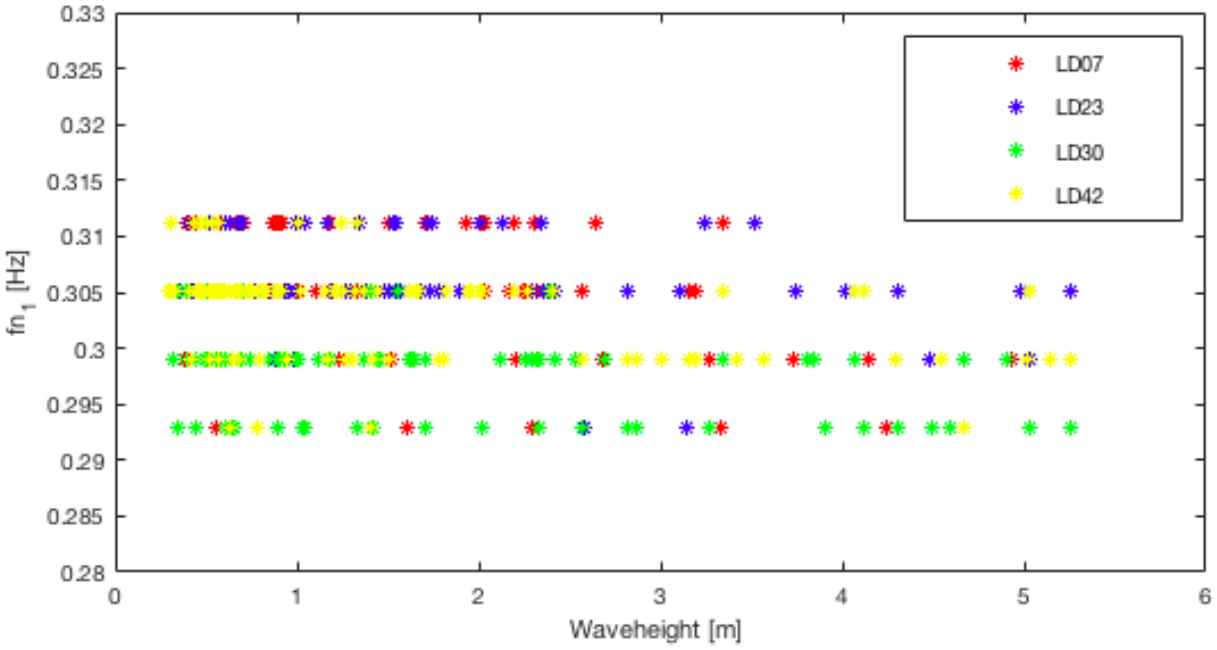

Figure 3.17: *Manually identified first natural frequencies at wave heights*

From the data set with the manually identified first natural frequencies different observations can be made, see Figure 3.17. In Figure 3.16 the first natural frequency seems to decrease slightly for high wave conditions. While in Figure 3.17 no decrease in first natural frequency can be found. What can be derived from both Figure 3.16 and Figure 3.17 is that there is no difference in behaviour of the

identified first natural frequency between wind turbine 07 and 23 (protected against scour) and wind turbine 30 and 42 (not protected against scour).

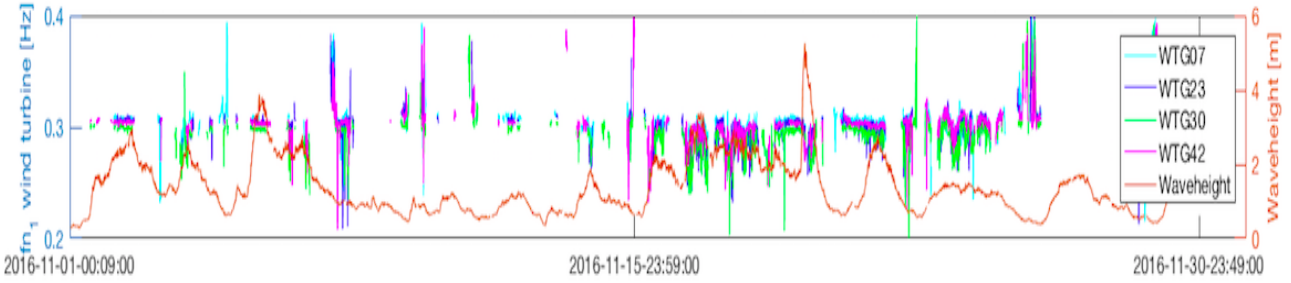

Figure 3.18: *The identified first natural frequency and wave height over time*

In Figure 3.18 no correlation in time between the wave height and the measured first natural frequency can be found. Again in Figure 3.18 no significant difference between the monopiles with scour protection and without scour protection can be observed.

3.3.4 Other influences

In the previous section only three environmental influences (wind speed, water level above LAT and wave height) are discussed, there are some other environmental influences on the natural frequency of the wind turbines. These influences are analyzed extensively. One of these influences is the air and water temperature. On the one hand from this study the conclusion can be drawn that the effect of the air temperature on the first natural frequency is extremely limited and negligible. However on the other hand earlier study states that the influence of the water temperature has a significant influence [22]. There was found that higher seawater temperature gives a lower first natural frequency, this is due to a lower stiffness of the steel at higher temperatures[22]. However the measured data in this research is only from the month November 2016 and no large change in seawater temperature was found during this month [32]. Also the effect of marine growth in the form of added mass or reduced wall thickness due to corrosion could effect the first natural frequency of the wind turbines. But since the reviewed period only consists of one month the effect of the change in marine growth and corrosion are expected to be negligible.

3.4 Evaluation

3.4.1 Evaluation environmental conditions

From the previous sections, it can be concluded that the water level has an effect on the first natural frequencies of the wind turbines. It must be noted that the wind turbines at the Eneco Luchterduinen wind farm have large holes in the monopile. These holes in the monopiles are the unused export cable entry points. Therefore the water level inside the monopile is the same as the sea water level. As a result the effect of the water level could be ascribed to the contained mass in the monopile of the wind turbine. Not only does the contained mass have an effect on the first natural frequency of the wind turbines but also the added mass of the water outside of the monopile. The hydraulic added mass is the mass of the water that is moved by the vibrations of the structure. Both the hydraulic added mass and the contained mass are added to the total mass of the wind turbine. From the equations in chapter 2 it can be found that a higher total mass leads to lower natural frequency.
Hydrodynamic damping could also influence the first natural frequency of the wind turbine [33]. This hydrodynamic damping results from wave radiation and viscous damping due to hydrodynamic drag and was expected to be low. Earlier researches confirmed that the hydrodynamic damping of a wind turbine is very low. The hydrodynamical damping is in order of 0.07 to 0.23% [33] of the critical damping of the first bending natural frequency.

$$f_d = f_{ud} * \sqrt{1 - \zeta^2} \tag{3.24}$$

Where f_d is the damped first natural frequency, f_{ud} is the first undamped natural frequency and ζ is the damping. Since in Equation 3.24 the damping is quadratic the effect of the hydrodynamic damping on the first natural frequency is very low. From the measurements it can be concluded that the influence of the hydrodynamic damping is negligible but the influence of the water level does have a significant effect on the natural frequency, table 3.1. This means the higher water level the lower the natural frequency.

The next environmental influence that is evaluated is the wind speed. It was expected the wind speed would have an effect on the soil stiffness of the wind turbines. The thrust and the axial force in the rotor shaft are different for each wind speed.

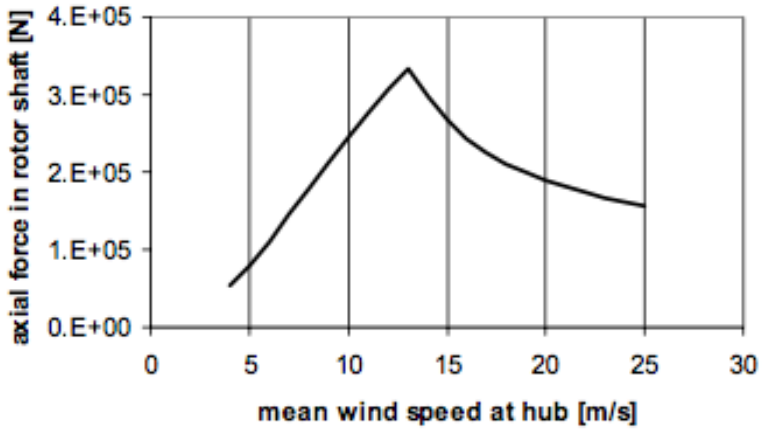

Figure 3.19: *An example of the axial rotor shaft force [6]*

In Figure 3.19 an example of the axial force in the rotor shaft of a pitch controlled wind turbine can be found. The axial force in the rotor shaft becomes larger when the wind speed increases until a maximum force is reached. The largest axial force is measured just before the blades of the rotor start to pitch. The rotor blades start to pitch when rated rotor RPM is reached. The different pitch angle of the blades ensure the rotor RPM does not exceed the rated RPM. As the pitch of the blades increases the axial force on the rotor shaft decreases. The displacement of the monopile foundation in the soil is directly dependent on the horizontal rotor shaft force. A higher force gives a larger displacement. As discussed in chapter 2 the soil stiffness is not linear. The effect of this non-linear soil behaviour is that a larger displacement leads to a smaller horizontal soil-stiffness [21]. When the soil-stiffness is smaller a lower first natural frequency is expected. However from Figure 3.2 no conclusion about a change in the first natural frequency can be drawn since much of the data in operating conditions are missing or contaminated. And in Figure 3.11 where the first natural frequencies of the wind turbines are manually identified no change in natural frequency during operating conditions can be found. Therefore it is expected that the effect of the changing thrust is negligible. In Figure 3.11 it can be found that the first natural frequencies of the wind turbines decrease slightly when the wind speed is higher than 25 [m/s]. This change can not be ascribed to a change in thrust. Because 25 [m/s] is the cut out wind speed. Therefore the wind turbine is not operating and the axial rotor force is low. This small decrease in the first natural frequency can be ascribed to other environmental conditions such as high water levels.

The third environmental condition that is evaluated in this research are the waves. The influences of the waves on the first natural frequency as shown in Figure 3.17 contradict what has been shown in Figure 3.16. The decrease in first natural frequency observed in Figure 3.16 cannot be found in Figure 3.17. Therefore no solid conclusion on the effect of the height of the waves on the first natural frequency can be made. But it can be concluded that high waves occur only during high wind and

high water level conditions. From Figure 3.20 and 3.21 it is clear that the wind speed and wave height are correlated, the correlation between the wave height and water level is also easy to observe.

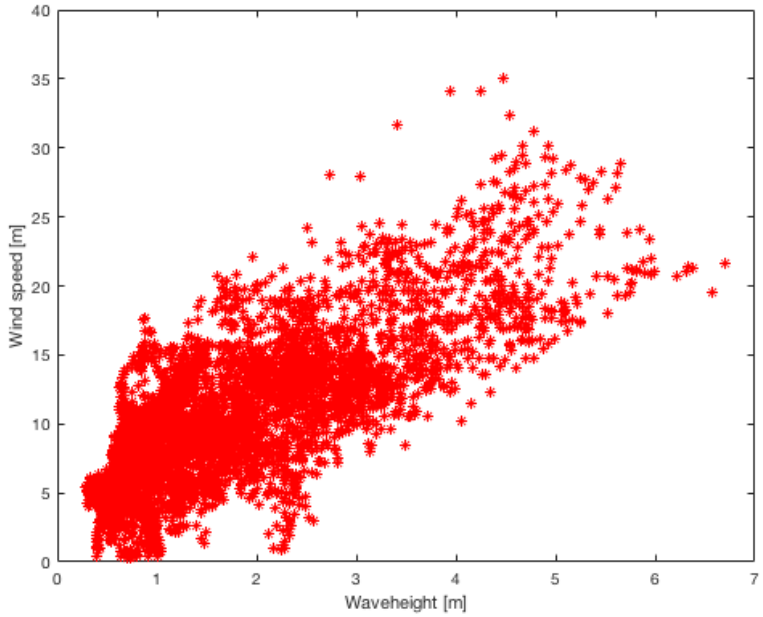

Figure 3.20: *Correlation between wind speed and wave height*

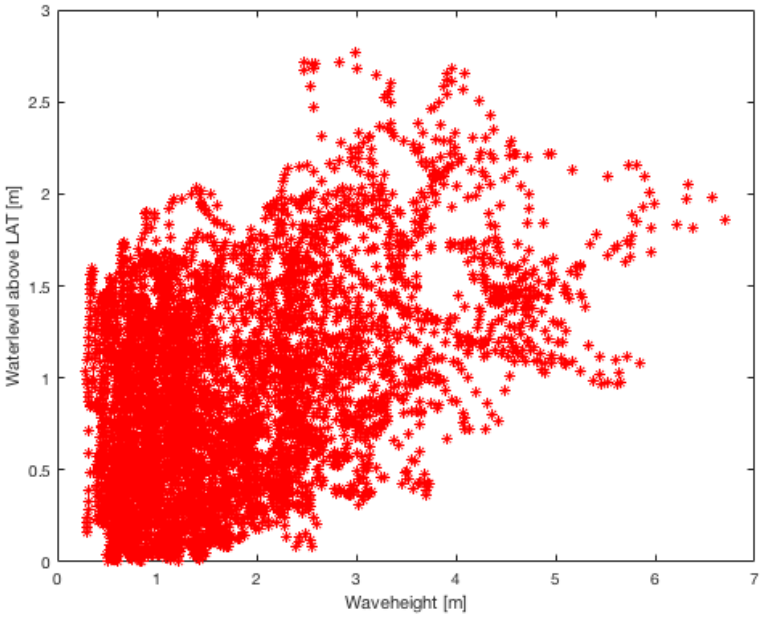

Figure 3.21: *Correlation between wind speed and water level*

Therefore it might be possible to suggest that the decrease in first natural frequency at high wave conditions in Figure 3.16 might be ascribed to other environmental effects, such as the water level height above the lowest astronomical tide.
Another important conclusion can be drawn from Figures 3.16 and 3.17, there is no significant difference in the evolution of the first natural frequency for the wind turbines with and without scour protection. The wind turbines with scour protection behave exactly the same as the wind turbines without scour protection.
The wind turbines without scour protection do not have the expected stiffening effect of a backfilled

scour pit just after high wave conditions, Figure 3.22 and 3.23. The time series in Figure 3.22 and 3.23 support that no conclusion can be made on the effect of the waves on the first natural frequency of the wind turbines. Since in Figure 3.22 we see a constant natural frequency after high wave conditions and in Figure 3.23 we see a change in the first natural frequency of the wind turbines after high wave conditions. Therefore no evidence of backfilling during high wave conditions or the removal of the backfilled soil just after high wave conditions can be found.

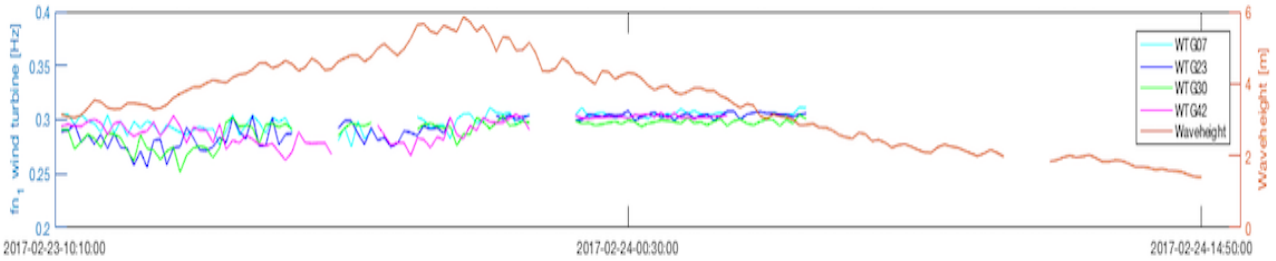

Figure 3.22: *Time series for high wave conditions day 1, natural frequencies identified by Zenzor*

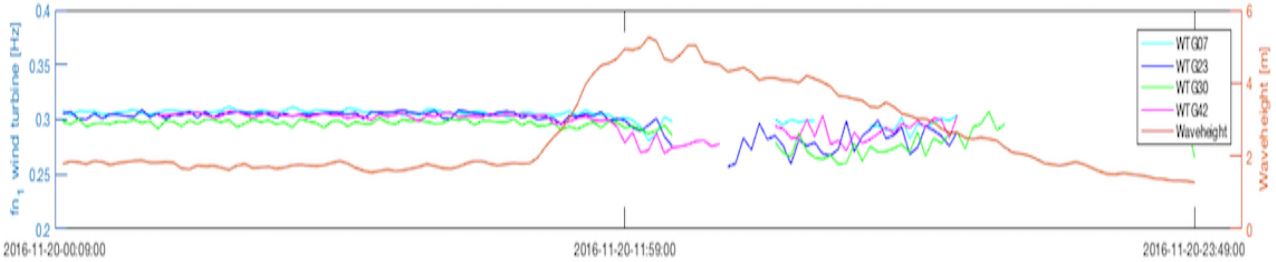

Figure 3.23: *Time series for high wave conditions day 2, natural frequencies identified by Zenzor*

The lack of stiffening just after the high wave conditions can have two main reasons. One of them is the backfilled material does not contribute to the lateral soil stiffness around the wind turbines. The reason behind this could be that the backfilled material is very loose sand and does not give lateral support to the wind turbine. Another reason could be that at high wave conditions there is very little backfill and this does not affect the lateral soil stiffness.

3.4.2 Evaluation of the design natural frequency

In the previous sections it became clear that only the water level has a noticeable effect on the first natural frequency. However when comparing the identified first natural frequencies to design natural frequencies discussed in chapter 2, it must be noted that they differ significantly. In table 3.2 the average design and measured first natural frequencies can be found.

Wind Turbine	Average natural frequency [Hz]		Difference [%]
	Design	Identified	
WTG 07	0.273	0.305	11.7
WTG 23	0.273	0.305	11.7
WTG 30	0.264	0.299	13.2
WTG 42	0.267	0.303	13.4

Table 3.2: *Designed and identified average first natural frequencies*

From table 3.2 it is clear that all the identified natural frequencies are significantly higher than the design natural frequencies. The errors between the design natural frequencies and the identified natural frequencies are of the same order as in earlier studies[25]. This error may occur due to the build up of

pore pressure in soil layers [25]. The extra pore pressure is generated by the cyclic motion of the wind turbine in the soil. This build up of pore pressure increases the lateral soil stiffness. The soil model used to model the first design natural frequencies does not take this into account. Another explanation for this error could be the incorrect modelling of the initial soil stiffness in the foundation design. Also the use of p-y curves when modelling the soil-structure interaction of large diameter monopiles might not be optimal [24].

3.5 Conclusion

In this chapter different environmental effects on the first natural frequencies are investigated. The first natural frequencies are identified from accelerometer data. The environmental effects on these identified first natural frequencies are compared to expectations of the environmental effects on the first natural frequencies.

The first natural frequencies of offshore wind turbines are affected by the environmental conditions. High water levels decrease the natural frequency due to added and contained mass. While wind conditions did not significantly affect the first natural frequencies. No solid conclusion can be made about the effect of different wave conditions, since the observations made when considering the first natural frequencies identified by Zenzor and when the first natural frequency is identified manually contradict each other. Also the wave conditions are highly correlated with high wind and high water level conditions. No significant difference in first natural frequency of wind turbines with and without scour protection is found in this research. For this reason no conclusion can be made on the occurrence of backfill after high wave conditions. Therefore from this research it can be concluded that the natural frequency of the wind turbines is only sensitive to the water level and no sensitivity to other environmental influences was observed in this research.

The next conclusion that can be drawn is that the identified first natural frequencies of the wind turbines are significantly higher than the designed first natural frequencies. Therefore it is expected that the soil stiffness has a large influence on the first natural frequency. In order to get more accurate design natural frequencies it is suggested to increase the soil stiffness during the design phase. Earlier research suggest a large increase in soil stiffness, this increase in soil stiffness during the design phase would be achieved by a soil stiffness multiplication factor [24], [25]. The soil stiffness multiplication factor multiplies the total soil stiffness. Those researches both suggest different soil-stiffness multiplication factors in order to get a more accurate model. This research will make a suggestion about the soil multiplication factor in chapter 4.

4 | Modelled natural frequency

In this chapter the influences on the modelled first natural frequencies are discussed. First the research method is discussed, secondly an elaborate explanation of the computer model used in this research is given. Then the results from the computer model will be discussed and evaluated.

4.1 Method

In chapter 3 the sensitivity of environmental influences on the identified first natural frequencies are discussed. In order to give a better suggestion about the sensitivities of these influences, these influences are also investigated in a computer model. In this chapter the influences of the water level, scour depth, soil stiffness and backfill of scour holes in a computer model are investigated. All these influences are investigated separately. This is done in order to mitigate the effect of other factors. For example when investigating the effect of different water levels on the first natural frequencies, the scour depth, the amount of backfill and the soil stiffness remain constant. The natural frequencies of the investigated wind turbines (7, 23, 30 and 42) are determined with a computer model this computer model is built following the guidelines from the wind turbine designers.

The computer model will consist of two parts: the wind turbine model and the pile-soil interaction model.

The model of the wind turbine consist of two main components, the tower of the wind turbine with the rotor nacelle assembly on top and the monopile with the added masses. The wind turbine model will be developed in MATLAB. The model of the wind turbine will be a 1D model the wind turbine is simplified as a Euler-Bernoulli beam model.

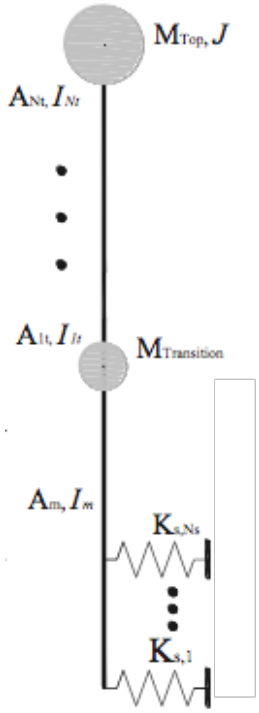

Figure 4.1: *Schematic view of the intended 1D model*

In Figure 4.1 a schematic view of the model can be found. The 1D Euler-Bernoulli beam finite element model will consist of multiple elements and the mass of the rotor nacelle assembly and other appurtenances will be modelled as lumped masses.

The second part of the computer model will be the pile soil interaction model. Pile-soil interaction will be simulated by independent Winkler Springs, see Figure 4.1. The soil stiffness of these springs will be determined using the p-y curve of the soil layers. For a more elaborate explanation about the computer model see section 4.2.

After the computer model is built first the influence of the water level will be investigated. The water level is varied from lowest astronomical tide to highest astronomical tide. Then the effect of scour around monopile 30 and 42 is discussed the scour depth is varied from zero meters to the maximum expected scour depth. After this is done the effect of backfilling of the scour holes at location 30 and 42 is discussed. And finally the modelled first natural frequencies are compared to the identified first natural frequencies. This is done in order to get an insight into the sensitivity of the soil stiffness on the modelled first natural frequency.

4.2 Computer Model

In this section the computer model is explained that was used to determine the first natural frequencies of the offshore wind turbines in this research. The computer model used consists of two main components. The first component is the 1D Euler-Bernoulli beam. This model used to describe the offshore wind turbine. The second component is the pile-soil interaction model. The pile-soil interaction model describes the lateral soil stiffness and the scour that is present at wind turbine 30 and 42.

4.2.1 Euler-Bernoulli beam model

In this research there is chosen to use a 1D Euler-Bernoulli beam model instead of a more elaborate model. The Euler-Bernoulli beam model is chosen because of its simplicity. One of the downsides of the Euler-Bernoulli beam model when comparing it to for instance the Timochenko model is that the Euler-Bernoulli model disregards shear. But for slender structures such as an offshore wind turbine and since only the first natural frequency of the wind turbines is considered the Euler-Bernoulli beam model will be sufficient [34]. In this research the Euler-Bernoulli beam model is modelled in MATLAB.

In this research only the first natural frequency of the offshore wind turbines is evaluated. As discussed in chapter 2, when determining the first natural frequency of a system the mass and the stiffness matrix are needed.

4.2.2 Mass and Stiffness Matrix

The 1D finite element model used in this research consists of many elements each of these elements have a mass and a stiffness matrix. In order to compute the mass and the stiffness matrix of each element first the shape functions are considered. The shape functions of each element are dependent on the geometry of the system and the boundary conditions for each element.

$$\begin{aligned} N_1 &= \frac{1}{L^3}\left(2x^3 - 3x^2L + 3L\right) \\ N_2 &= \frac{1}{L^3}\left(x^3L - 2x^2L^2 + xL^3\right) \\ N_3 &= \frac{1}{L^3}\left(-2x^3 + 3x^2L\right) \\ N_4 &= \frac{1}{L^3}\left(x^3L - x^2L^2\right) \end{aligned} \tag{4.1}$$

In Equation 4.1 the shape functions of one single element can be found. In Equation 4.1, L is the length of the element and x is the displacement. When the shape functions of each element are determined the Euler-Lagrange equations are considered[35], Equation 4.2.

$$L \equiv T - V \tag{4.2}$$

In Equation 4.2 L is the Lagrangian, T is the kinetic energy and V is the potential energy of the element. When considering the kinetic energy the mass matrix of the element can be derived and when considering the potential energy the stiffness matrix of the element can be derived. A more elaborate discussion about the construction mass and stiffness matrices can be found in Appendix B.

$$\mathbf{M} = \frac{\rho A l}{420} \begin{bmatrix} 156 & 22l & 54 & -13l \\ 22l & 4l^2 & 13l & -3l^2 \\ 54 & 13l & 156 & -22l \\ -13l & -3l^2 & -22l & 4l^2 \end{bmatrix} \tag{4.3}$$

In Equation 4.3 the mass matrix of one single element of the system can be found. In order to compute the total mass matrix of the system, the element mass matrices are into a system matrix. The mass matrix only consists of information of the wind turbine tower and monopile and not the mass of the rotor nacelle assembly and other appurtenances. The masses of these appurtenances are added as lumped masses on the nodes of the elements corresponding to geometry of the wind turbine. This is the same as the original wind turbine foundation designers did, their guidelines are followed [36].

Item	Elevation(LAT)[m]	Mass [kg]	I[$kg * m^2$]
Nacelle	80.22		-
Rotor	80.80		-
Unspecified mass 1	78.5		-
Unspecified mass 2	72.054		-
Unspecified mass 3	40.15		-
Unspecified mass 4	17.35		-
External platform	16.5		-
Airtight platform	16.1		-

Table 4.1: *Added masses*

$$\mathbf{K} = \frac{EI}{l^3} \begin{bmatrix} 12 & 6l & -12 & 6l \\ 6l & 4l^2 & -6l & 2l^2 \\ -12l & -6l & 12 & -6l \\ 6l & 2l^2 & -6l & 4l^2 \end{bmatrix} \tag{4.4}$$

In Equation 4.4 the stiffness matrix of one single element of the system can be found. The stiffness matrices are also combined into one matrix in order to compute the system stiffness matrix. In the stiffness matrix the soil stiffness is not yet considered.

4.2.3 Soil-Structure interaction

The second main part of the computer model is the pile-soil interaction model. The soil-structure interaction model is made according to the same guidelines as the wind turbine designers did [36]. The lateral soil stiffness is modelled as horizontal springs on the nodes of the monopile. The stiffness of these springs are obtained from the p-y curves of the different soil layers.

Winkler springs

There are different options to model the soil stiffness [4], this research uses the Winkler spring model. The Winkler spring model is the most accurate model after the total finite element model [4]. Another reason to the use the Winkler spring model is that the original wind turbine foundation designers also used the Winkler spring model to describe the soil-structure interaction.

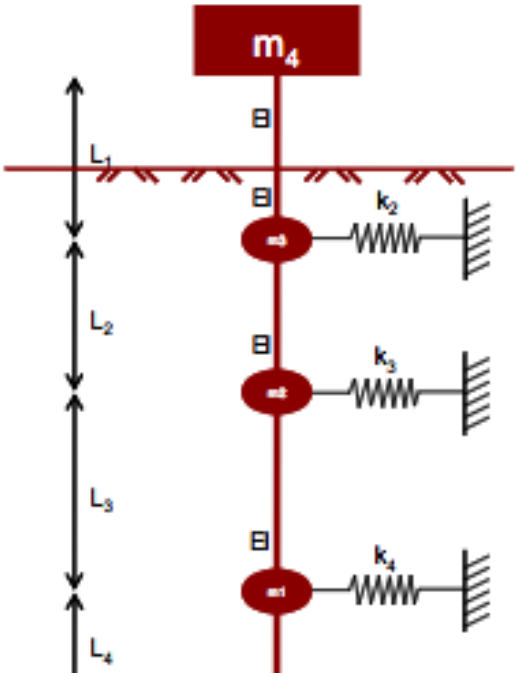

Figure 4.2: *Schematic example of the Winkler spring model [7]*

In Figure 4.2 an schematic example of the soil-structure model used in this research can be found. The soil is modelled as horizontal springs. These horizontal springs are called the Winkler springs. The stiffness of these springs is obtained from the p-y curves. A more elaborate explanation of this p-y curves will be given in the next section. Each of these springs connect to one of the nodes of the monopile foundation. The stiffness of these springs determined with the p-y curves are added into the stiffness matrix of each element of the corresponding element.

Lateral soil stiffness

It is most common to determine the soil stiffness of each soil layer from the p-y curves of the soil [21]. The use of p-y curves is common practice in offshore environments.

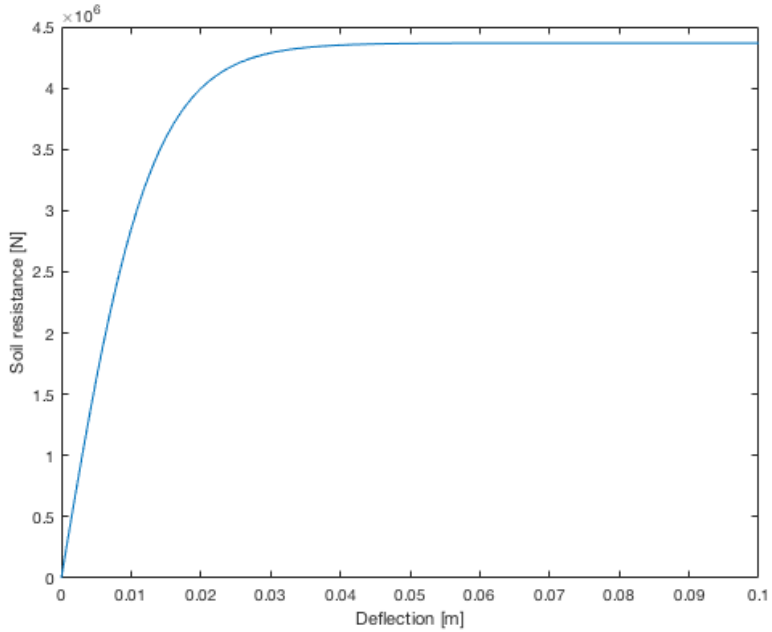

Figure 4.3: *P-y curve for the sand layer at 8.5 m depth at the location of wind turbine 07*

In Figure 4.3 the p-y curve for the sand layer at a depth of 8.5 m below the seabed at monopile location EL07 can be found. The stiffness of the soil is calculated by $k = \frac{p}{y}$. It is obvious that the soil stiffness is non-linear. However for very small deflections the soil stiffness is linear, this part of the p-y curves is called the linear part. This linear part is used to model the soil stiffness in the computer model. This linear part is also used by the designers of the wind turbines for the natural frequency analyses [36].

Construction of the p-y curves

In order to get the soil stiffness of each soil layer the p-y curve of each soil layer needs to be constructed. In this research two different construction methods are used. The first construction method is for soil layers containing sand. The second construction method is for soil layers containing clay. These p-y curves are constructed following the API, DNV and wind turbine foundation designers guideline [37][8][36]. The information that is needed to construct these p-y curves is obtained from cone penetration tests. These cone penetration tests are conducted before designing the Eneco Luchterduinen offshore wind farm. Data obtained from cone penetration tests have been processed to obtain design soil profiles.

P-y curve sand

When constructing the p-y curves of sand, first the diameter of the pile, the specific gravity of the material (sand or clay) and the angle of internal friction need to be determined. For sand the second step is the determination of coefficients C_1, C_2, C_3 and the initial modulus of subgrade reaction k. These are dependent on the angle of internal friction. The parameters can be obtained from Figure 4.4 and 4.5.

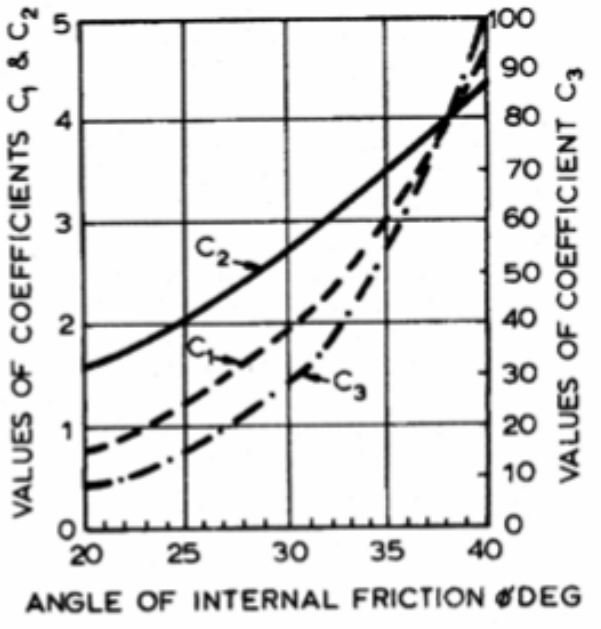

Figure 4.4: *Coefficients dependent on internal friction angle [8]*

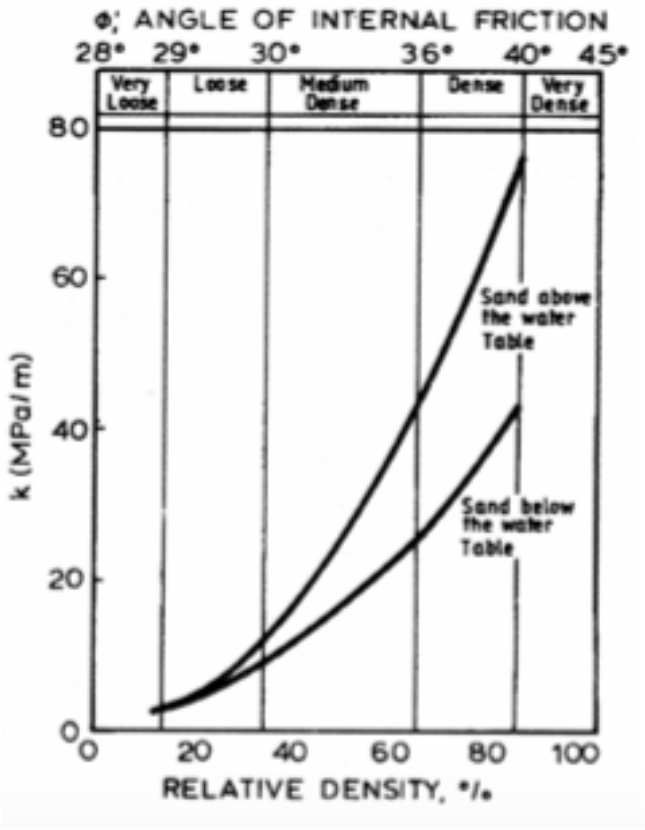

Figure 4.5: *Initial modulus of subgrade dependent on the angle of internal friction [8]*

After obtaining these parameters the p-y curves can be constructed. First the ultimate soil resistance is calculated.

$$p_u = \begin{cases} (C_1 X + C_2 D)\,\gamma X \\ C_3 D \gamma X \end{cases} \tag{4.5}$$

In equation 4.5 the ultimate soil resistance of the sand layer can be found. The ultimate soil resistance is dependent on the monopile diameter D, the specific gravity of the soil γ and the depth below the soil surface X[8]. The lowest value for the ultimate soil resistance p_u from equation 4.5 is chosen for the following calculations.

$$p = A p_u tanh\left(\frac{kX}{Ap_u} y\right) \tag{4.6}$$

With equation 4.6 the unit soil resistance for the soil layer containing sand can be found. In equation 4.6 A is a constant, this constant accounts for static or cyclic loading. In this case we only consider cyclic load and therefore $A = 0.9$[8]. And y is the lateral deflection of the monopile at the depth of each soil layer (X). An example for a p-y curve in a sandy soil layer can be found in Figure 4.3.

P-y curve clay

Next the construction of the p-y curves for soil layers consisting of clay is discussed. When constructing the p-y curves for soil layers consisting of clay first the effective vertical stress is calculated [36].

$$\sigma = \gamma X \tag{4.7}$$

In equation 4.7, γ is the specific gravity of the soil, X is the depth of the soil layer below the seabed and σ is the effective vertical stress. After the effective vertical stress is considered the undrained shear strength is obtained from the cone penetration tests. The p-y curves for clay have two calculation methods. The first method is for soil layers containing clay with a undrained shear strength larger

than $96kPa$ (stiff clay) and the second for an undrained shear strength smaller than $96kPa$ (soft clay)[36].

Method 1 (stiff clay)
With the information from equation 4.7 and the concerning undrained shear strength (cu) the ultimate soil resistance can be calculated.

$$p_u = \begin{cases} 2cuD + \sigma D + 2.83cuX \\ 11cuD \end{cases} \tag{4.8}$$

The ultimate bearing capacity (p_u) is the lowest value from equation 4.8. This value depends on the pile diameter D and the depth below the seabed X. When the ultimate bearing capacity is calculated the p-y curve can be constructed with equation 4.9.

$$p = 0.5p_u \left(\frac{y}{y_c}\right)^{\frac{1}{2}} \tag{4.9}$$

In equation 4.9, y_c is the deflection where the bearing capacity is half the ultimate bearing capacity. $y_c = \epsilon_{50}D$, where ϵ_{50} is the strain which occurs at one-half of the maximum stress in laboratory undrained compression tests [38].

Method 2 (soft clay)

$$p_u = \begin{cases} 3cu + \sigma + 0.5cu\frac{X}{D} \\ 9cu \end{cases} \tag{4.10}$$

The ultimate bearing capacity p_u is the lowest value from equation 4.10. Again this value depends on the pile diameter D and the depth below the seabed X. When the ultimate bearing capacity is calculated the p-y curve can be constructed with equation 4.11.

$$p = 0.5p_u \left(\frac{y}{y_c}\right)^{\frac{1}{3}} \tag{4.11}$$

In equation 4.11, y_c is the deflection where the bearing capacity is half the ultimate bearing capacity. $y_c = 2.5\epsilon_{50}D$, where ϵ is the strain which occurs at one-half of the maximum stress in laboratory undrained compression test [38].

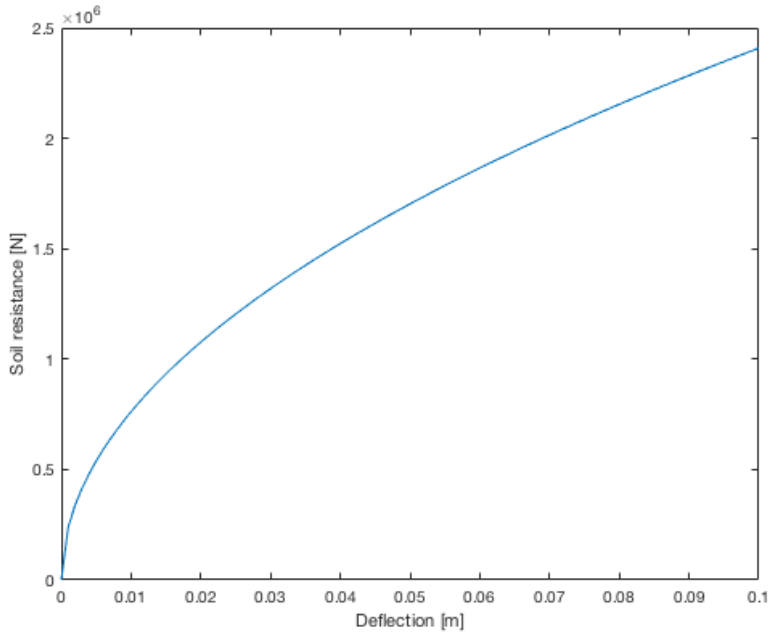

Figure 4.6: *P-y curve for the clay layer at 17 m depth at the location of wind turbine 42*

In Figure 4.6 the p-y curve of the clay layer 17 m below the seabed and an undrained shear strength above $96kPa$ at wind turbine location 42 can be found. Again only the linear part of the p-y curve is used. This is at the point where $y = 0.1 * y_c$[21].

Updating the p-y curves for scour

As discussed in previous chapters at the Eneco Luchterduinen offshore wind farm there are two wind turbines which are not protected against scour. The wind turbines that are not protected against scour are wind turbine 30 and 42. In Chapter 2, it is discussed that the presence of scour might change the soil stiffness around these monopiles and more information about the effects of scour can be found in Appendix A.

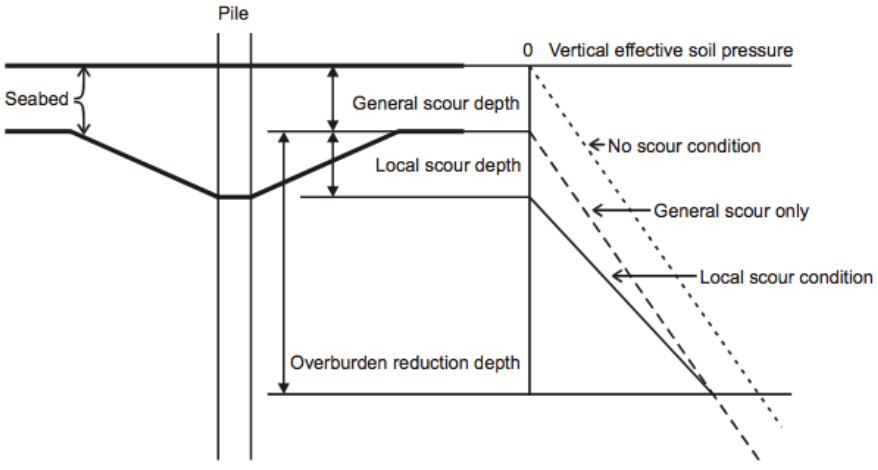

Figure 4.7: *Schematic overview of local and global scour [9]*

From 4.7 it can be found that scour reduces soil stiffness around the pile because of the absence of soil in the scour hole. Also the reduction of soil pressure leads to less soil stiffness around the monopile foundation. This is also clear when evaluating equations 4.5 and 4.10. Therefore when scour occurs at the wind turbines which are not protected against scour the soil structure interaction at these locations

will change.

The model used in this research follows the same guidelines when modelling the influences of scour as the wind turbine foundation designers did [36]. The soil that is removed due to scour will not give any lateral soil stiffness to the monopile foundation. This means the Winkler springs that were simulating this soil resistance are removed, Figure 4.8.

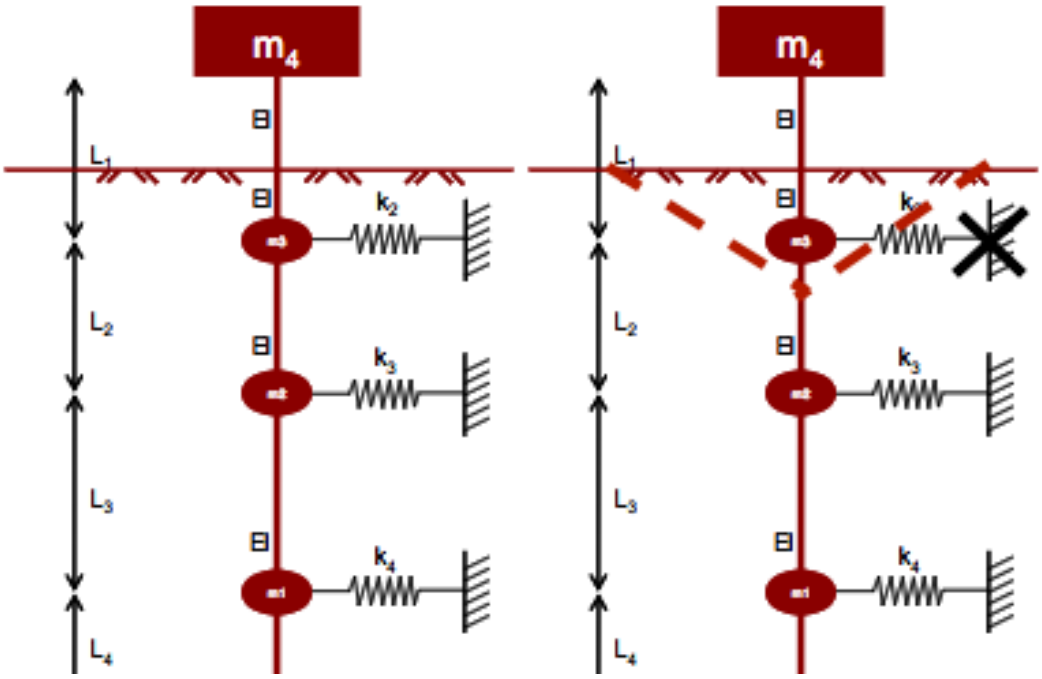

(a) *Schematic example of the model without scour*

(b) *Schematic example of the model with scour*

Figure 4.8: *Schematic Winkler model*

Also the p-y curves for the underlying soil layers are updated. The depth below seabed (X) in equations 4.5, 4.5, 4.7, 4.10 and 4.11 is changed. The new depth below the seabed is the original depth minus the depth of the scour hole $X_{scour} = X - scourdepth$.

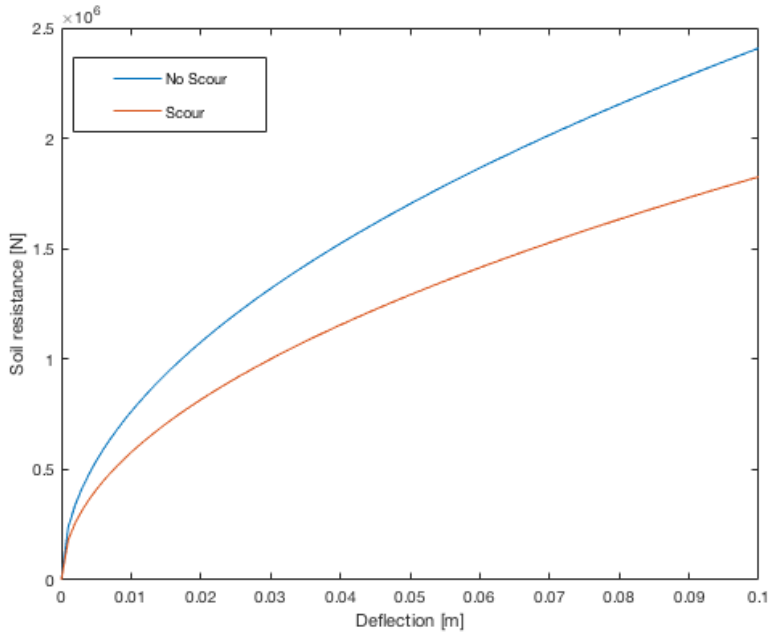

Figure 4.9: *Original and updated p-y curve for the clay layer at 17 m depth below seabed at wind turbine location 42*

In Figure 4.9 the red line is the updated p-y curve for the clay layer at original depth below seabed of 17 m. In this case the maximum expected scour depth is taken in to account. This scour depth is 1.3 times the diameter (6.5 meter) as is discussed in Chapter 2.

4.2.4 Added and contained mass

Next to the mass of the monopile, wind turbine tower, the mass appurtenances and the mass of the rotor nacelle assembly the model also takes into account the added and contained mass. The contained mass is the mass of the sea water and soil contained inside the monopile. The seawater inside the monopile changes at the same rate as the tidal level due to large holes in the bottom of the monopile. The added and contained mass are evaluated in the same manner as the designers of the wind turbines did [36]

$$m_{contained} = \frac{\rho \pi D^2}{4} l \tag{4.12}$$

Where ρ is the specific gravity of the seawater/soil, D is the diameter of the monopile and l is the length of each element. The contained mass of each element is calculated and added to the mass matrix of each submerged element.
Next to the contained mass the wind turbine is also subject to added hydrodynamic mass. This is the mass of the seawater that is moved due to vibrations of the wind turbine.

$$m_{added} = \frac{\rho c_a \pi D^2}{4} l \tag{4.13}$$

The added hydrodynamic mass for each submerged element is calculated with equation 4.13. The added mass is dependent on the specific gravity of the seawater ρ, the diameter of the monopile D, the length of the element l and the added mass coefficient c_a. The added mass coefficient for offshore monopiles is determined in earlier researches [39]. The added mass of each submerged element is added to the mass matrix in the same manner as the contained mass.

4.2.5 Validate model

A validation of this model is needed in order to use it in further research. This model is validated against the computer model used by the wind turbine and foundation designers (Ramboll) [40].

First the natural frequency of the wind turbine without the monopile foundation is compared to the design values. When calculating the natural frequency of the wind turbine tower without the monopile foundation the node of the wind turbine model at interface height is clamped. In a clamped node nodal displacements are zero.

	asbuilt data	current model	Difference
Ramboll model	- [Hz]	- [Hz]	0.69%
Vestas model	- [Hz]	- [Hz]	2.52%

Table 4.2: *Comparison tower only first natural frequency*

In Table 4.2 the natural frequencies of the different computer models can be found. The difference in first natural frequency when comparing it to the Vestas[40] model was expected since very little is known about this model. It is unknown which analysis tool was used. For instance Vestas did use a different method to lump the mass of the rotor nacelle assembly. Consequently, it is more important for this research to compare the computer model to the model described in the design report by Ramboll [36]. Since the computer model used in this research is built by the guidelines supplied in the design report. When comparing the computer model used in this research to the Ramboll computer model it can be found that the difference is very small. A possible reason for this small difference is Ramboll used different element sizes in their computer model. But since the Ramboll model is used to design the monopile foundations. The computer model used in this research for the wind turbine tower without the monopile foundation is expected to be sufficiently accurate.

After validating the model for the wind turbine tower without the monopile foundation, the total model needs to be validated. As is done in the design report the computer model will be validated in three environmental regimes. These regimes are a stiff, median and soft regimen and are described in Chapter 2.

Wind turbine	current model	Ramboll model	Difference
WTG07	0.278 [Hz]	0.278 [Hz]	0%
WTG23	0.278 [Hz]	0.278 [Hz]	0%
WTG30	0.291 [Hz]	0.289 [Hz]	0.69%
WTG42	0.294 [Hz]	0.291 [Hz]	0.68%

Table 4.3: *Comparison first natural frequency stiff regime*

Wind turbine	current model	Ramboll model	Difference
WTG07	0.274 [Hz]	0.273 [Hz]	0.36%
WTG23	0.275 [Hz]	0.273 [Hz]	0.73%
WTG30	0.266 [Hz]	0.264 [Hz]	0.75%
WTG42	0.268 [Hz]	0.267 [Hz]	0.37%

Table 4.4: *Comparison first natural frequency median regime*

Wind turbine	current model	Ramboll model	Difference
WTG07	0.273 [Hz]	0.271 [Hz]	0.74%
WTG23	0.274 [Hz]	0.272 [Hz]	0.74%
WTG30	0.265 [Hz]	0.263 [Hz]	0.75%
WTG42	0.267 [Hz]	0.266 [Hz]	0.38%

Table 4.5: *Comparison first natural frequency soft regime*

As is clear form tables 4.3, 4.4 and 4.5 the model never exceeds the 1% accuracy. It's also clear from the above tables that the model is less accurate in softer regimes. This can be explained because the

model does not take into account the effect of corrosion or the effect of marine growth. These factors are left out of the model because of a lack of information about these factors in the design reports [36]. This model only takes into account the water level, the soil conditions and the scour depth (WTG30 and WTG42). The next obvious thing to note is that the accuracy is lower at monopiles without scour protection. A reason for the larger inaccuracy is the estimation of the presence of sandwaves. The design data of the Eneco Luchterduinen wind farm give no solid conclusion about the presence of sandwaves [38]. Therefore an estimation is made about the presence of sandwaves at wind turbine location 30 and 42. A maximum sand wave of 1 m is expected at location 30 and and location 42 [38]. This estimation is made from the figures in the design reports.

Since the inaccuracy of the model is never larger than 1.0%, Ramboll states that the inaccuracy with respect to the Vestas model should be lower than 2%[36]. Therefore the computer model is expected to be sufficiently accurate.

4.2.6 Updated soil model

Updated scour model

In this section the scour model used by this research is discussed. This is different from the scour model used by the wind turbine foundation designers. The scour model used by wind turbine designers (Ramboll) does not take the effect of the sloped scour hole into account.

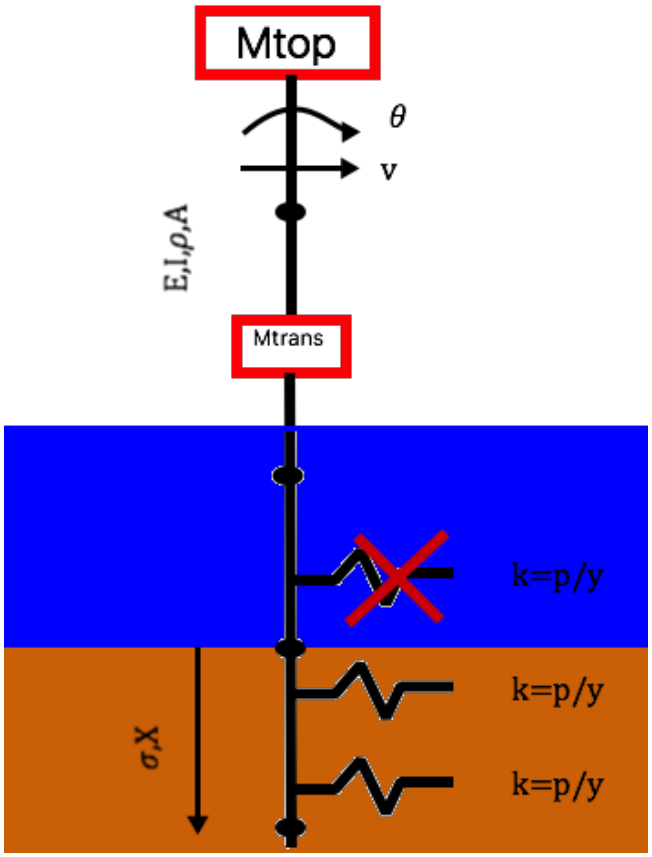

Figure 4.10: *Schematic view of scour in Ramboll model*

In Figure 4.10 the scour model used by the wind turbine foundation designers can be found. In this scour model the scour is modelled as if there is no slope in the scour hole and therefore this slope does not add any overburden pressure to the soil layers below the scour hole. However this representation of the scour is not physically correct. In the real world the scour hole has a slope.

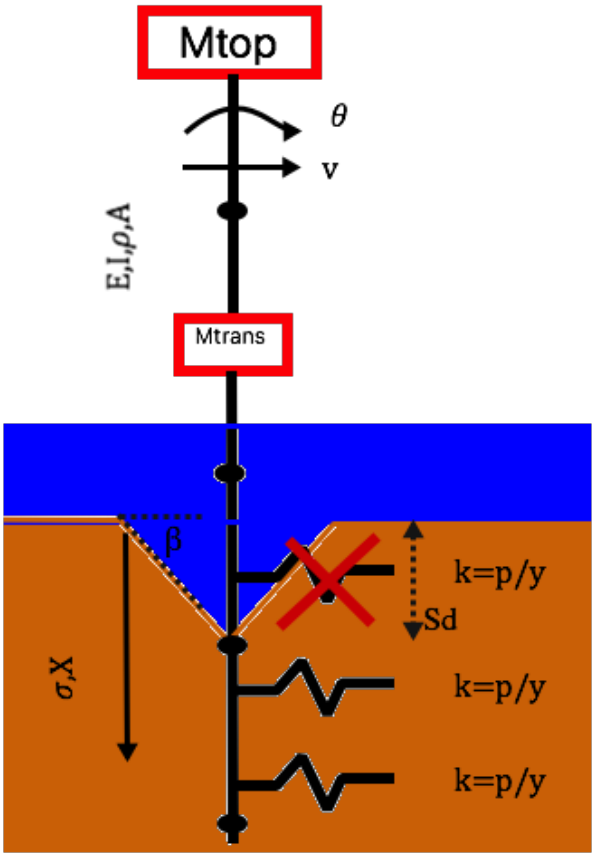

Figure 4.11: *Schematic view of sloped scour hole*

In Figure 4.11 a schematic view of the scour model used in this research can be found. The scour hole is sloped. The sloped scour hole gives extra vertical stress to the under laying soil layers [41].

$$\Delta\sigma = \gamma X tan(\beta) \frac{\frac{S_d}{tan(\beta)}}{sqrt((\frac{S_d}{tan(\beta)})^2 + X^2)} \tag{4.14}$$

With Equation 4.14 the effective vertical stress ($\Delta\sigma$) added by the sloped hole can be calculated. In Equation 4.14, X is the depth below the original sea bed, γ is the specific gravity of the soil, S_d is the depth of the scour hole and β is the slope of the scour hole. The slope of the scour hole is expected to be 10 degrees[38]. The effective vertical stress generated by the scour hole $\Delta\sigma$ is added to the effective vertical stress calculated with Equation 4.7.

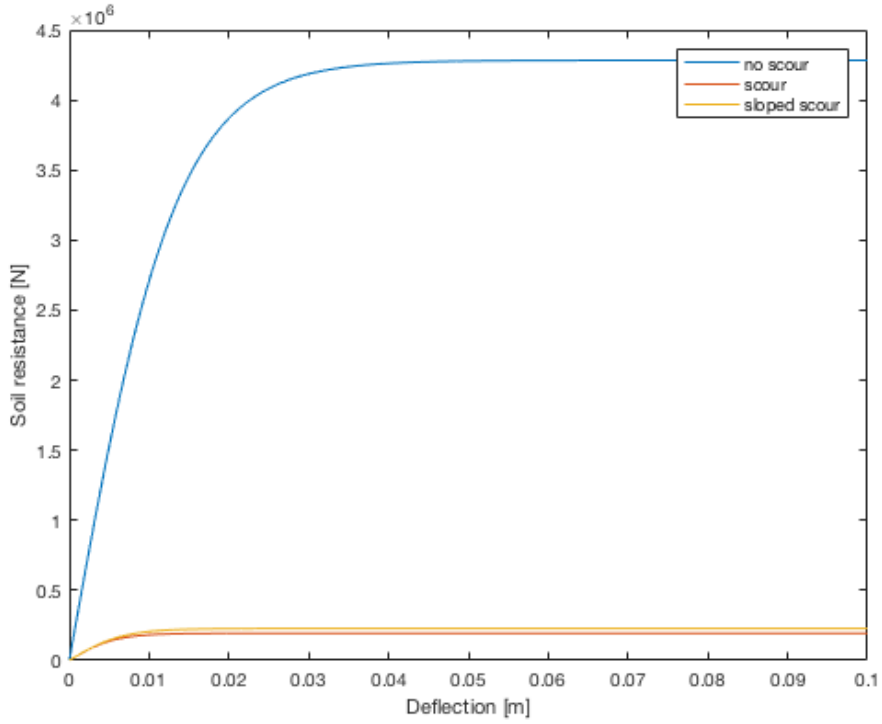

Figure 4.12: *P-y curves for the sandy soil layer on a depth of 7 meters at monopile 42*

In Figure 4.12 the p-y curves of the sandy soil layer at a depth of 7 meters at monopile 30 can be found. As can be observed when there is no scour the soil is the stiffest and when the model does not take the sloped scour hole into account the soil resistance is the lowest. A slight increase in soil stiffness/resistance is obtained by adding the vertical stress induced by the sloped scour hole. Therefore also the first natural frequencies calculated by the model differ slightly, see table 4.6.

Wind turbine	flat scour model	updated scour model	difference
WTG07	0.273 [Hz]	0.273 [Hz]	0%
WTG23	0.274 [Hz]	0.274 [Hz]	0%
WTG30	0.266 [Hz]	0.268 [Hz]	0.75%
WTG42	0.267 [Hz]	0.269 [Hz]	0.75%

Table 4.6: *Comparison the scour model with the sloped scour hole and the flat scour hole in the softest regime*

As can be found in table 4.6 at wind turbine number 7 and 23 there is no difference since these wind turbines are protected against scour. And a small increase in first natural frequency can be found at wind turbine 30 and 42.

Axial effects on the first natural frequency

In the computer model used in this research the monopile foundation is modelled as a 1D Euler-Bernoulli model. The use of a 1D model for slender structures is expected to sufficient [34], but since the monopile foundations get ever larger diameters the skin friction might give extra soil stiffness.

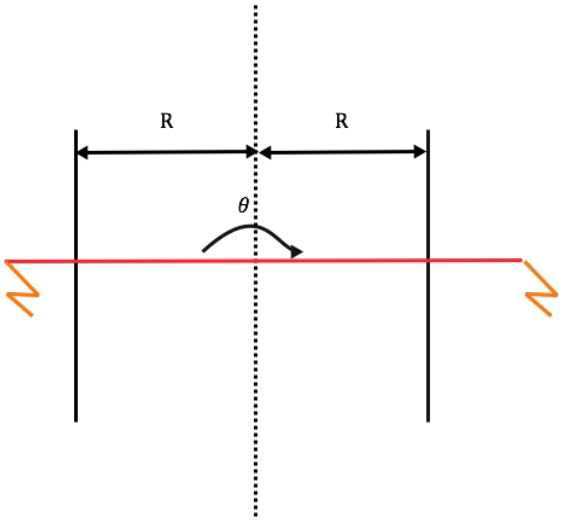

Figure 4.13: *Schematic view of the effect of skin friction*

In Figure 4.13 a schematic view of the monopile can be found. When the wind turbine is operating the monopile in the earth is subjected to small rotations, due to these small rotations and the skin friction an opposed moment is generated. This moment could be seen as extra lateral soil stiffness. The stiffness of the springs in Figure 4.13 can be determined with the linear part of the t-z curves, see Equation 4.15.

$$t = \frac{z * G_0}{R} \tag{4.15}$$

In Equation 4.15, z is the axial displacement, R the radius of the monopile and G_0 is the initial shear stiffness calculated with Equation 4.16

$$G_0 = \frac{m(\sigma_a * \sigma_v)^{\frac{1}{2}}}{2(1+v)} \tag{4.16}$$

$$m = 1000 * tan(\phi) \tag{4.17}$$

In Equation 4.16, σ_a is the reference pressure σ_v the effective vertical stress and ϕ is the angle of friction of the soil. The extra resistance these springs give are added to the rotational part of the stiffness matrix of the system and is calculated with Equation 4.18.

$$k_{skin} = 2 * 0.5D * t \tag{4.18}$$

where k_{skin} is the stiffness, D is the diameter and t is the rotational stiffness.

Wind turbine	without skin friction	with skin friction	difference
WTG07	0.273 [Hz]	0.273 [Hz]	0%
WTG23	0.274 [Hz]	0.275 [Hz]	0.33%
WTG30	0.268 [Hz]	0.269 [Hz]	0.33%
WTG42	0.269 [Hz]	0.269 [Hz]	0%

Table 4.7: *Comparison with and without skin friction*

As can be found from table 4.7 there is a very small difference for wind turbine 23 and 42.

4.3 Results

In this section the first natural frequencies obtained by the computer model are discussed. First the natural frequency at different water levels is discussed. Then different scour and backfill conditions are evaluated for wind turbine 30 and 42 (not protected against scour). And finally the sensitivity of the soil stiffness on the first natural frequency is discussed.

4.3.1 Water level

The water level is expected to influence the first natural frequency of all the wind turbines. This can also be found in the analyses from the identified first natural frequencies, Chapter 3. The natural frequencies calculated by the model are expected to be lower for higher water levels.

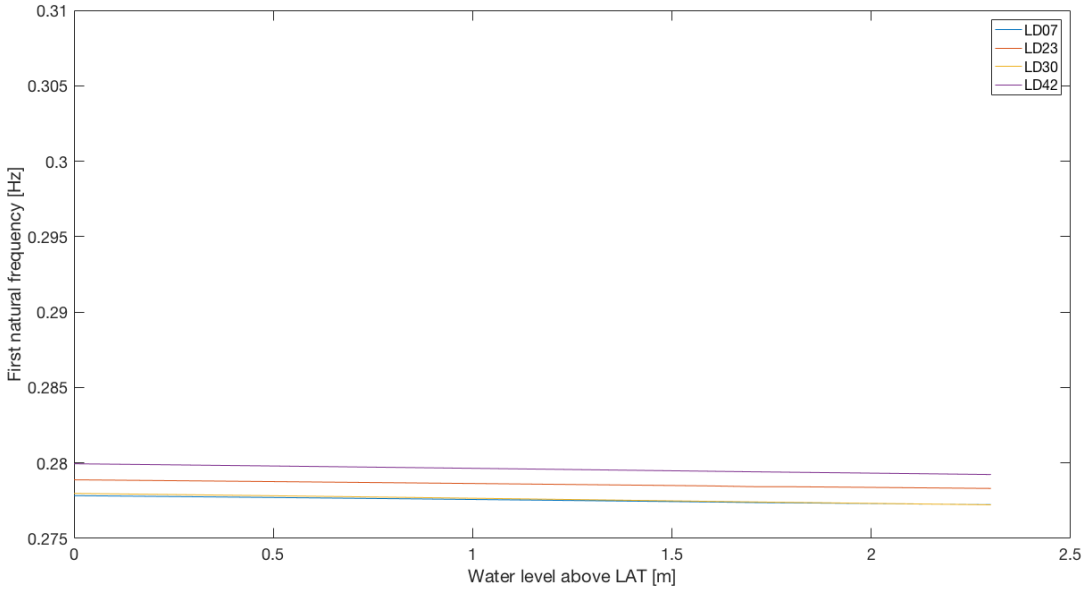

Figure 4.14: *First natural frequencies obtained from the model for different water levels*

In Figure 4.14 the first natural frequencies for all the wind turbines at different water levels can be found. The amount of scour at wind turbine 30 and 42 is constant for all water levels. Also the amount of backfill is constant. And the soil model is set to the stiffest scenario. The stiffest scenario is chosen because this the scenario that has the least unknown parameters effecting the first natural frequency (corrosion, marine growth and the presence of sandwaves). The water level is varied from 0 m above the lowest astronomical tide (LAT) to 2.3 m above the lowest astronomical tide. 2.3 m above lowest astronomical tide is the highest tide measured in the month November 2016. In Figure 4.14 it can be seen that for higher water levels there is a lower natural frequency. This is as expected since the added and contained mass is higher, section 4.2.

Wind turbine	Water level 0 m above LAT	Water level 2.3 m above LAT	difference
WTG07	0.278 [Hz]	0.274 [Hz]	1.4%
WTG23	0.278 [Hz]	0.275 [Hz]	1.1%
WTG30	0.277 [Hz]	0.274 [Hz]	1.1%
WTG42	0.279 [Hz]	0.276 [Hz]	1.1%

Table 4.8: *Comparison first natural frequencies obtained from the model for high and low water level*

In table 4.8 the difference in first natural frequency between high and low water level can be found. The difference in natural frequency ranges between 1.1 and 1.4 %.

4.3.2 Scour depth and backfill

In this section the effect of scour and backfill of the scour hole on the first natural frequencies of wind turbine 30 and 42 is discussed. First the effect of scour on the first natural frequencies is discussed. The scour is modelled according to section 4.2. From earlier research a change in first natural frequency of 8 % between no scour and fully developed scour is expected [23].

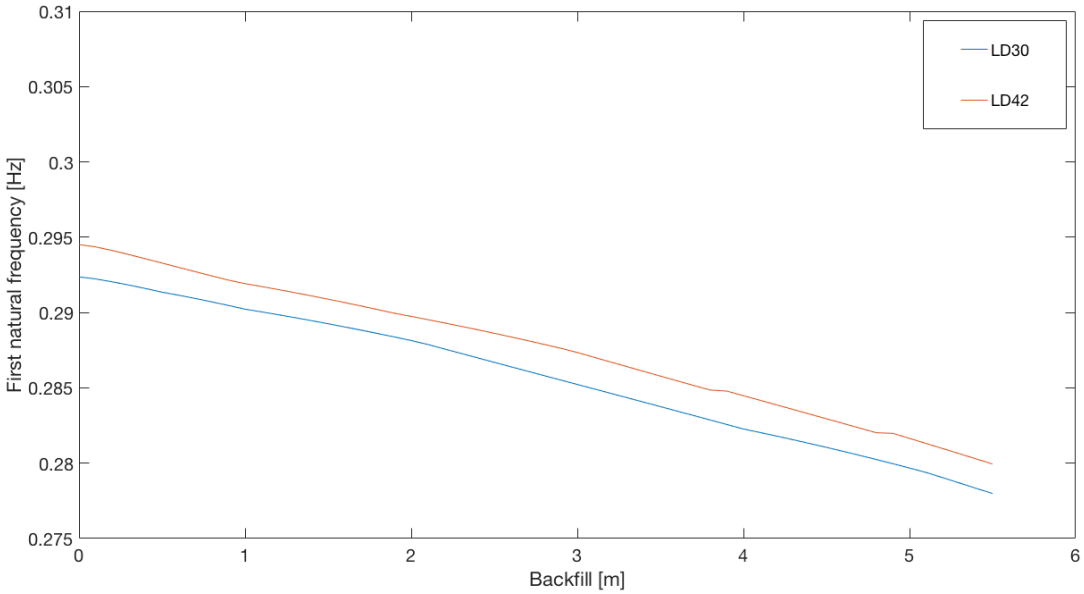

Figure 4.15: *First natural frequencies obtained from the model for different scour depths*

In Figure 4.15 the first natural frequencies obtained by the model for wind turbine 30 and 42 can be found. In the model while the scour depths vary between 0 and 5.5 m. 5.5 m of scour is the measured amount of scour at wind turbine 30 and 42 [42]. The water level and the amount of backfill in the scour hole remains constant. Again the stiffest soil scenario is used while varying the scour depth. From Figure 4.15 it can be found the first natural frequency changes significantly. The deeper the scour hole the lower the first natural frequency.

Wind turbine	0 m scour	5.5 m scour	difference
WTG30	0.291 [Hz]	0.277 [Hz]	5.1%
WTG42	0.294 [Hz]	0.279 [Hz]	5.4%

Table 4.9: *Comparison first natural frequencies obtained from the model for maximum and minimal scour*

In table 4.9 the difference in first natural frequency between fully developed scour and no scour can be found. The difference ranges between 5.1 and 5.4 %. This difference is slightly lower than expected. This difference between the literature and the results obtained by the model could be due to difference in fully developed scour depth. In earlier researches a scour depth of 1.3 D was found while at the Eneco Luchterduinen a scour depth of 1 D was found. Therefore a smaller decrease in first natural frequency is logical.

Now the effect of backfill of the scour hole will be discussed. The backfilled material in the scour hole will not give any lateral stiffness to the wind turbine foundation, since this material is expected to be loose [43]. The backfilled material will only increase the overburden pressure on the under laying soil and increase the soil stiffness of these layers slightly. Therefore it is expected that the backfilled material will slightly influence the first natural frequencies of the wind turbines. While the amount of backfill around wind turbines 30 and 42 is varied from 0 to 5.5 m, the water level and the scour depth remain constant.

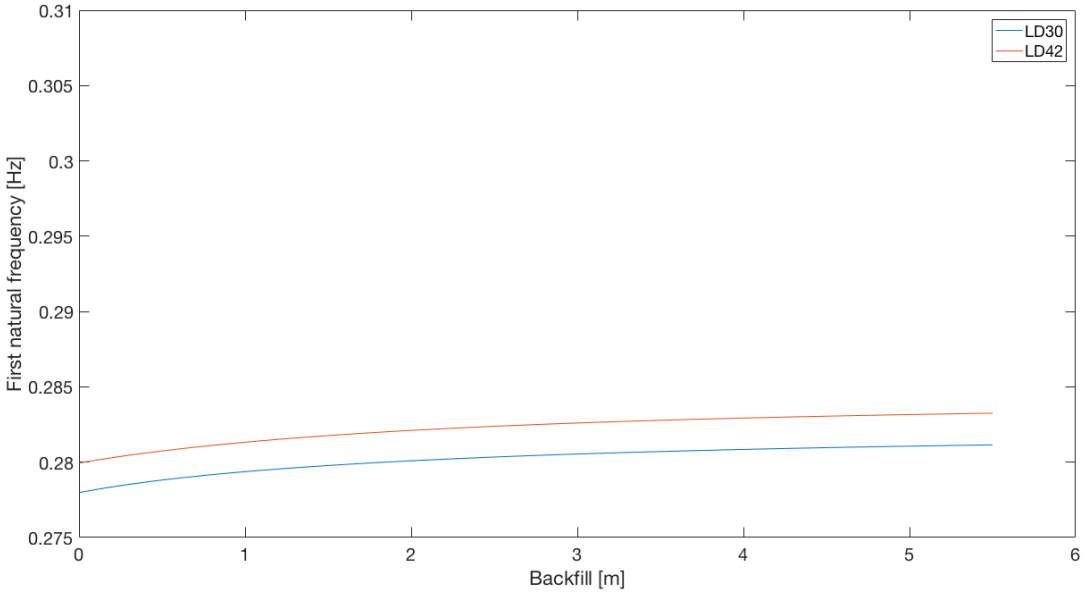

Figure 4.16: *First natural frequencies obtained from the model for different amounts of backfill*

From Figure 4.16 it can be concluded that the first natural frequencies changes for different amounts of backfill. Therefore the extra overburden pressure of the backfilled soil gives extra soil stiffness to under laying soil layers. However it is not expected to reach maximum backfill during storm conditions [44]. Therefore in table 4.10 the maximal expected backfill is 1 m.

Wind turbine	0 m backfill	1 m backfill	difference
WTG30	0.277 [Hz]	0.279 [Hz]	0.33%
WTG42	0.279 [Hz]	0.281 [Hz]	0.33%

Table 4.10: *Comparison first natural frequencies obtained from the model for no backfill and 1 m of backfill*

In table 4.10 it can be found that the effect of 1 m of backfill is very small only 0.33 %.

4.3.3 Soil stiffness

The last parameter that is varied in the model is the soil stiffness. From Chapter 3 it can be concluded that the first natural frequencies of the wind turbines are between the 11.7 and 13.4 % higher, table 3.2. This change in first natural frequency is expected to be due to stiffening of the soil or consequent errors in the soil stiffness model. Earlier studies have suggested a soil multiplication factor could be a solution to this problem [25], [24]. Therefore this research also does a suggestion about this soil multiplication factor. The soil multiplication factor simply multiplies the total soil stiffness.

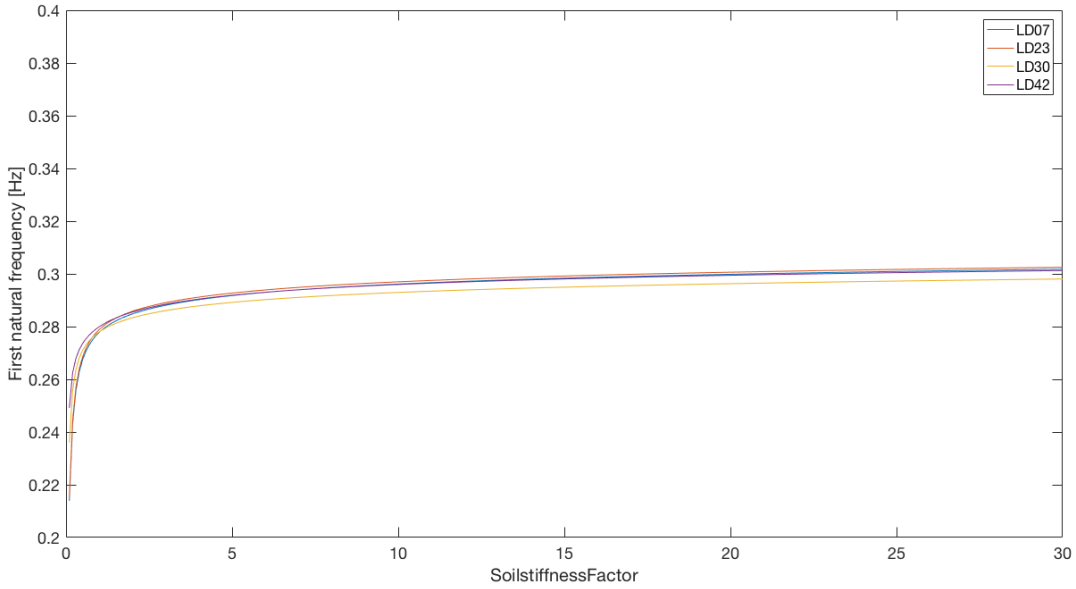

Figure 4.17: *First natural frequencies obtained from the model for different soil multiplication factors*

In Figure 4.17 it can be found that higher soil multiplication factors results in higher first natural frequencies of all wind turbines. It can also be observed that the first natural frequency moves to a maximum. This maximum would be reached when the soil stiffness reaches infinity and then it would be as if the monopile was clamped at the seabed. The clamped first natural frequency of all wind turbines is approximately 0.321 [Hz]. In Figure 4.17 it can also be observed that the first natural frequencies obtained from the computer model are less sensitive for soil stiffness for stiffer soils. In a more accurate model the first natural frequency obtained by the model would only differ 2 % from the identified first natural frequency. The wind turbine foundation designers state that a difference of 2% is acceptable [36].

Wind turbine	Identified first natural frequency	Soil multiplication 20	difference
WTG07	0.305 [Hz]	0.299 [Hz]	2.0%
WTG23	0.305 [Hz]	0.300 [Hz]	1.7%
WTG30	0.299 [Hz]	0.296 [Hz]	1.0%
WTG42	0.303 [Hz]	0.299 [Hz]	1.3%

Table 4.11: *Comparison identified first natural frequency and first natural frequency obtained by the model at multiplication factor 20*

From table 4.11 it can be found that the multiplication factor in order to have an acceptable error needs to be at least 20.

4.4 Conclusion

In this chapter the computer model used in this research is explained. And the effect of the water level, scour depth, the amount of backfill and soil stiffness on the first natural frequency is evaluated.

The first natural frequency of the wind turbines is dependent on the water level around the monopile. This is due to the effect of the contained and added mass as discussed in section 4.2. The decrease in first natural frequency is in the same order of magnitude as found from the identified first natural frequencies, chapter 3. In chapter 5 a more elaborate discussion about the differences between the identified first natural frequencies and the first natural frequencies obtained from the computer model can be found.
From this computer model it can be concluded that the effect of scour is large. And the first natural

frequency of an offshore wind turbine is sensitive to scour. The effect of scour is smaller than found in earlier researches [23]. However this difference can be ascribed to a difference in relative scour depth. The effect of the extra overburden pressure due to the backfilled material is very small for 1m of backfill. Therefore the sensitivity of the first natural frequency is low. And might not be noticeable in full scale tests.
From the computer model it can be concluded that the first natural frequency is highly sensitive for a change in soil stiffness and a large increase in soil stiffness during the design phase of the wind turbines is suggested. The large increase of the soil stiffness implies over conservative designs. This research finds that the soil should be modelled approximately twenty times stiffer in order to achieve a first natural frequency obtained by the computer model that is similar to the identified first natural frequency.

5 | Identified vs modelled natural frequency

In this research the sensitivities of different influences on the first natural frequencies are discussed. In Chapter 3 the effect of the waves, water level wind speed, rotor RPM and the soil on the identified first natural frequencies are investigated. In Chapter 4 the first natural frequencies obtained from a computer model are discussed. In this Chapter the differences between the identified first natural frequencies and the first natural frequencies obtained from the computer model are discussed. An explanation for these differences might lead to a better understanding on the sensitivities of influences on the first natural frequencies of offshore wind turbines. A better understanding on the sensitivities of these influences on the first natural frequency enables designers to make more accurate computer models. Subsequently, with more accurate computer models the design of offshore wind turbines in the future might be more cost effective, which will lead to a lower levelized cost of energy, see Chapter 1 and will give investors a larger incentive to invest in offshore wind farms. Ultimately these larger investments might help to reach the renewable energy goals set by the Dutch government [18].

In this chapter first the difference between the identified and modelled first natural frequencies for different water levels are discussed. Then the sensitivities of soil effects are discussed.

5.1 Water level

In this section the influence of the water level on the first natural frequency is discussed. In Chapter 3 was found that the water level has an identifiable effect on the first natural frequency. This effect is in the form of added and contained hydraulic mass. In Table 5.1 the results of the research of the water level above the lowest astronomical tide (LAT) are found.

Wind turbine	<0.3 m above LAT	>1.8 m above LAT	difference
WTG 07	0.306 Hz	0.301 Hz	1.5 %
WTG 23	0.306 Hz	0.303 Hz	1.1 %
WTG 30	0.302 Hz	0.297 Hz	1.7 %
WTG 42	0.305 Hz	0.299 Hz	2.0 %

Table 5.1: *Difference in identified first natural frequency for high and low water levels above lowest astronomical tide*

The identified first natural frequencies for all wind turbines decrease slightly, between 1.1 and 2.0 %. In Table 5.2 the differences in first natural frequencies obtained from the model can be found.

Wind turbine	Water level 0 m above LAT	Water level 2.3 m above LAT	difference
WTG07	0.278 [Hz]	0.274 [Hz]	1.4%
WTG23	0.278 [Hz]	0.275 [Hz]	1.1%
WTG30	0.277 [Hz]	0.274 [Hz]	1.1%
WTG42	0.279 [Hz]	0.276 [Hz]	1.1%

Table 5.2: *Comparison first natural frequencies obtained from the model for high and low water level*

The first natural frequencies of all wind turbines obtained from the computer model also decrease slightly, between 1.1 and 1.4%. The computer model gives a smaller decrease in first natural frequency for high water level than the difference between the bins for high and low water level. However these differences are very small.

5.2 Soil effects

In this section the effects of scour, backfilling of the scour hole and the soil stiffness on the identified and the first natural frequencies obtained by the computer model are compared.

5.2.1 Scour and backfill

From the computer model it can be found that different scour conditions have a large effect on the first natural frequencies of wind turbines which do not have scour protection. The scour depth measured at wind turbine 30 and 42 was 5.5 m [42]. The obtained natural frequencies from the computer model for 0 m and 5.5 m of scour can be found in Table 5.3.

Wind turbine	0 m scour	5.5 m scour	difference
WTG30	0.291 [Hz]	0.277 [Hz]	5.1%
WTG42	0.294 [Hz]	0.279 [Hz]	5.4%

Table 5.3: *Comparison first natural frequencies obtained from the model for maximum and minimal scour*

Also a small effect of backfilling of the scour hole on the first natural frequency was found from the computer model, see Table 5.4.

Wind turbine	0 m backfill	1 m backfill	difference
WTG30	0.277 [Hz]	0.279 [Hz]	0.33%
WTG42	0.279 [Hz]	0.281 [Hz]	0.33%

Table 5.4: *Comparison first natural frequencies obtained from the model for no backfill and 1 m of backfill*

However none of these effects were found when looking to the identified first natural frequencies. The identified first natural frequencies for the wind turbines without scour protection changed in the same manner for different conditions as the identified first natural frequencies for the wind turbines with scour protection did. A possible reason that no effect was observed is that the scour hole around wind turbine 30 and 42 (not protected against scour) is constant during the whole month of November 2016. A possible reason that no effect of backfill is observed during high wave conditions is the effect is too small to observe. From the computer model it can be found that for 1 m of backfill only gives an increase in first natural frequency of 0.33 %. This change in first natural frequency is already limited and it is unknown if this amount of backfill is reached.

5.2.2 Soil stiffness

In Chapter 3 it can be found that the identified first natural frequencies differ a lot from the design natural frequencies discussed in Chapter 2, see Table 5.5.

Wind Turbine	Average natural frequency [Hz]		Difference [%]
	Design	Identified	
WTG 07	0.273	0.305	11.7
WTG 23	0.273	0.305	11.7
WTG 30	0.264	0.299	13.2
WTG 42	0.267	0.303	13.4

Table 5.5: *Designed and identified average first natural frequencies*

This large difference between the design natural frequencies and the identified first natural frequency is found in other studies [25], [24]. One of the reasons for this large difference might be the build op soil pressure in the soil layers [25]. When the pore pressure is higher the lateral soil stiffness is higher. And from Chapter 2 it can be found that a higher lateral soil stiffness gives a higher first natural frequency. Another reason for the difference between the identified first natural frequency and the

design first natural frequency might be the use of p-y curves. In the oil and gas industry p-y curves are commonly used to determine the lateral soil stiffness. However the oil and gas industry uses piles with smaller diameters. Therefore the p-y curve method is developed for long and flexible piles [24]. And the use of p-y curves for large diameter piles used in the offshore wind energy industry might not be optimal. Both studies suggest the use of soil multiplication factor [25],[24]. This soil multiplication factor multiplies the total soil stiffness. In this research a suggestion for a soil multiplication for the wind turbines at the Eneco Luchterduinen wind farm was made, Chapter 4. It was found that in order to obtain an accuracy of 2 % in the computer model a soil multiplication factor of at least 20 is needed, Table 5.6.

Wind turbine	Identified first natural frequency	Soil multiplication 20	difference
WTG07	0.305 [Hz]	0.299 [Hz]	2.0%
WTG23	0.305 [Hz]	0.300 [Hz]	1.7%
WTG30	0.299 [Hz]	0.296 [Hz]	1.0%
WTG42	0.303 [Hz]	0.299 [Hz]	1.3%

Table 5.6: *Comparison identified first natural frequency and first natural frequency obtained by the model at multiplication factor 20*

The second eigenmode and soil stiffness

This research only considers the first natural frequency which is an important design parameter. Since the 1P and 3P frequencies of the wind turbines are close to the first natural frequency. But to get a better understanding of lateral soil stiffness around large diameter monopile foundations it might be more useful to take a look at the shape of the second bending mode of the wind turbines. Since the second mode shapes of the wind turbines are more sensitive to the soil stiffness, see Figure 5.1. The mode shapes can be calculated with the formulas found in Chapter 2. And from the ratio between the modal displacements obtained by computer model at the three sensor heights and the ratio between modal displacements in the frequency spectrum it might be possible to make a more accurate suggestion about the soil stiffness multiplication factor. It is important to notice that this modal displacements are not the real displacements of the wind turbine. These displacements only describe the second mode shape of the wind turbine in the model. But the ratio between the displacements from the model is the same as in the real world.

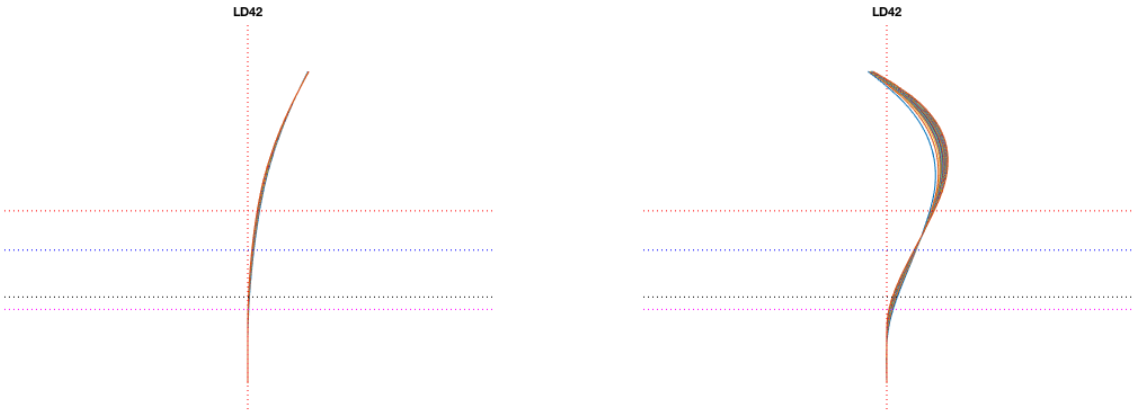

(a) *first bending mode shape* ***(b)*** *Second bending mode shape*

Figure 5.1: *Mode shapes for different soil multiplication factor for wind turbine 42*

In Figure 5.1a and 5.1b the mode shapes for soil stiffness multiplication factors from 1 to 30 can be found for wind turbine 42. In this Figures the red line dotted is the interface height, the blue dotted line is the water level, the black dotted line the original level of the seabed and the purple dotted line represents the level of the seabed adjusted for scour. In both Figures the blue line indicates the mode

shape of with multiplication factor 1. From Figure 5.1a it is clear that shape of the first bending mode barely changes.

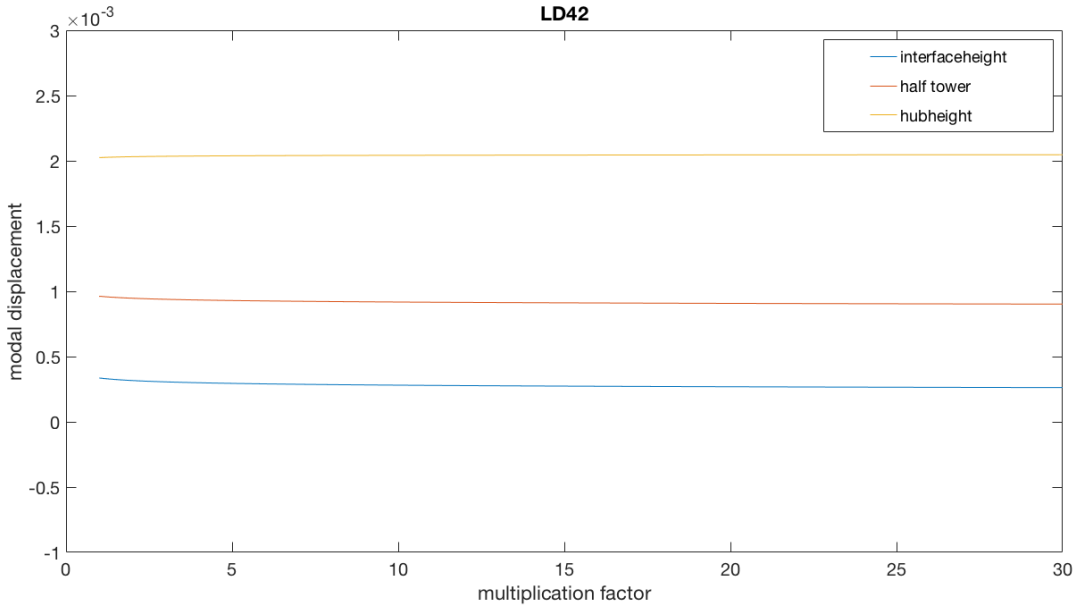

Figure 5.2: *The modal displacements of the first bending mode from the computer for the three sensor heights at different soil stiffness multiplication factors at wind turbine 42*

From Figure 5.2 the same observation can be made as from Figure 5.1a the modal shape of the first bending mode barely changes for different soil multiplication factors. Therefore also the ratio between modal displacements changes barely. While the shape of the second bending mode changes a lot more, see Figure 5.1b and 5.3.

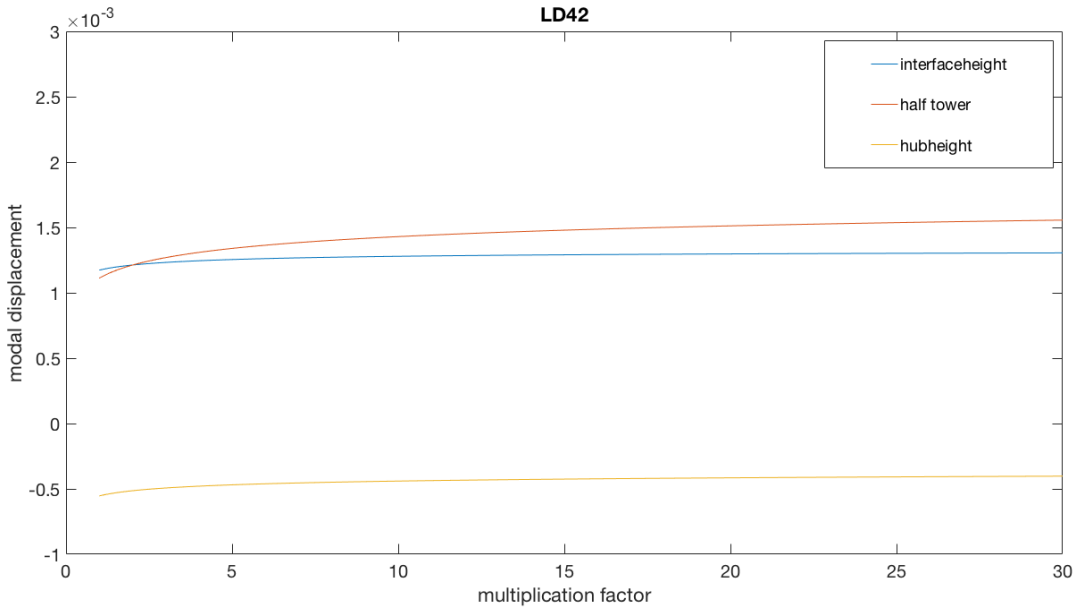

Figure 5.3: *The modal displacements of the second bending mode from the computer for the three sensor heights at different soil stiffness multiplication factors at wind turbine 42*

In Figure 5.3 it can be found that the modal displacement change with different amounts for larger soil stiffness multiplication factors, this changes also the ratio's between these displacements. The ratio between the modal displacements might be an indicator for the soil multiplication factor. It might be possible to link the ratio of the modal displacements to the ratio of the difference in power density for

the three different sensor heights obtained from offshore measurements. However it must be noted that the modal displacements obtained from the computer model are undamped. And that the computer model does not take any loading into account. Therefore a link between these two ratio's can only be a suggestion.

In Figures 5.4, 5.5 and 5.6 the power spectral density of wind turbine 42 at three different rotor RPM's can be found.

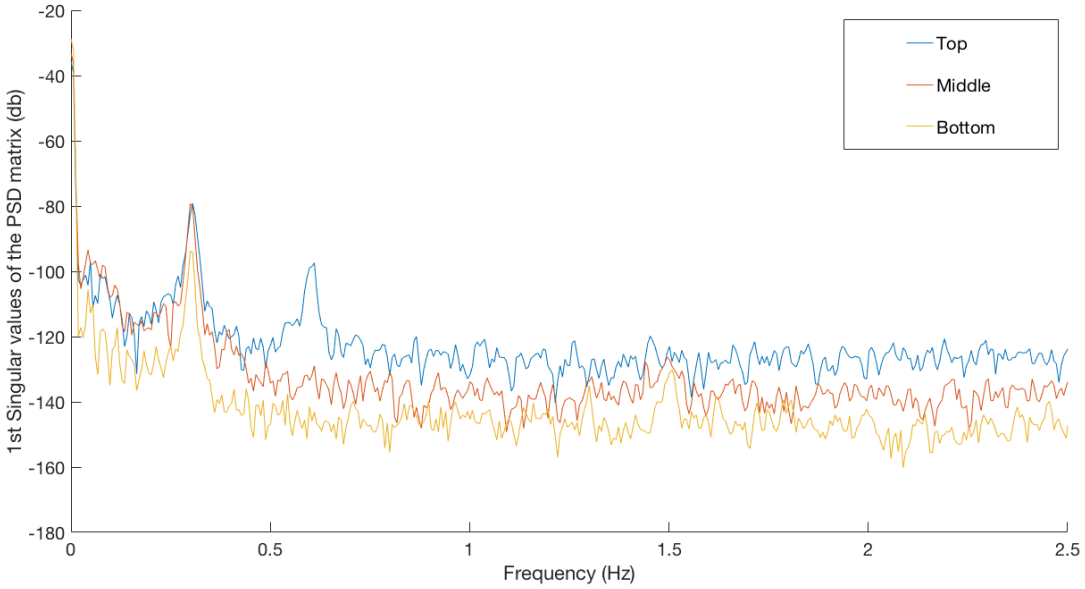

Figure 5.4: *The power spectral density of wind turbine 42 at a rotor RPM of 0 RPM, second natural frequency 1.45 [Hz]*

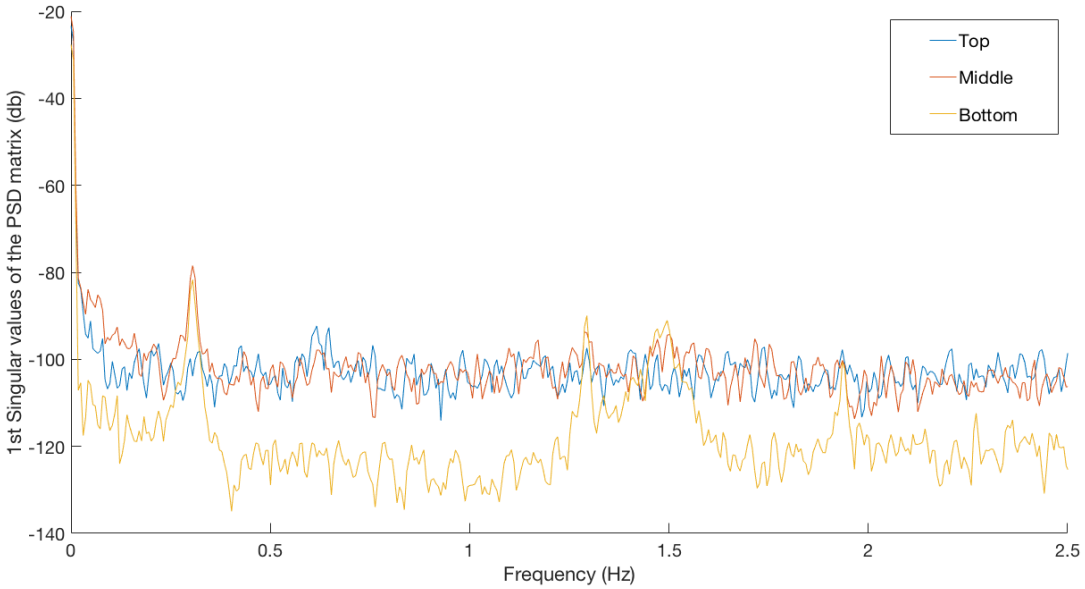

Figure 5.5: *The power spectral density of wind turbine 42 at a rotor RPM of 12.7 RPM, second natural frequency 1.45 [Hz]*

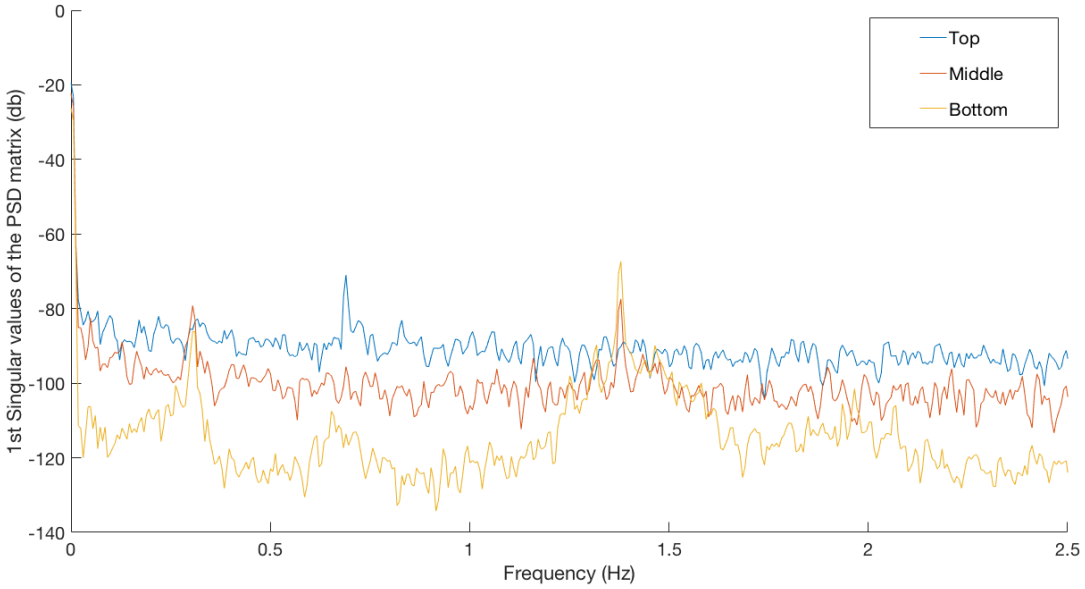

Figure 5.6: *The power spectral density of wind turbine 42 at a rotor RPM of 13.8 RPM, second natural frequency 1.45 [Hz]*

In Figure 5.4 it is possible to see the sensor at half of the tower (middle) has the largest power density at the second natural frequency (approximately 1.45 [Hz]). While in Figure 5.5 the power densities for the sensors at hub height (bottom) and half of the tower (middle) have the same power density and in Figure 5.6 the bottom sensor has the largest power density at second natural frequency (approximately 1.45 [Hz]). Since the ratio between the spectral densities change for different rotor RPM's this ratio cannot be linked to a soil multiplication factor. It must be noted that the spectral densities in Figures 5.4, 5.5 and 5.6 use a db scale and the ratio's cannot directly be calculated. But a change of sensor with the largest power density denotes a clear change in ratio.

5.3 Conclusion

In this chapter the sensitivities of different influences on the identified first natural frequencies are compared to the sensitivities of these influences on the first natural frequencies obtained by the computer model.

It can be concluded that the first natural frequencies of the wind turbines in the Eneco Luchterduinen wind farm are sensitive to a change in water level. This is found from both the identified first natural frequencies and the first natural frequencies obtained from the computer model. The differences found from the computer model for high and low water level are comparable to the differences found in the identified first natural frequencies. Therefore it can be concluded that the effect of the water level is modelled accurately enough in the present computer models.
No identifiable effect of backfill on the first natural frequencies of the wind turbines without scour protection (wind turbine 30 and 42) was found from the identified first natural frequencies. A small effect for one meter of backfill on the first natural frequency was found in the computer model. This effect might not be noticeable in identified first natural frequencies of wind turbine 30 and 42 because the resolution of the identified first natural frequencies is to coarse. A higher resolution can be obtained by using accelerometers with a higher sampling rate. This research can conclude that the effect of backfill is small and it is not needed to incorporate this effect in computer models at this time.
In Chapter 3 was found that the identified first natural frequencies differ significantly from the design natural frequencies. From this it can be concluded that at the modelling of the soil-structure interaction is inaccurate. In order to obtain first natural frequencies from the computer model which are similar to the identified first natural frequencies a soil stiffness multiplication factor of approximately twenty

is needed.

6 | Conclusion & Recommendations

In this chapter the conclusions that can be drawn from this research are discussed also suggestions for further research are given.

6.1 Conclusion

The objective of this thesis as stated in the Chapter 1:

Get a better insight into the sensitivities of different influences on the first natural frequency of the wind turbines in the Eneco Luchterduinen wind farm.

From this study it can be concluded that the first natural frequencies of the offshore wind turbines in the Eneco Luchterduinen wind farm are sensitive to a change in water level. An increase in water level resulted in an decrease in first natural frequency. While wind and wave conditions did not significantly affect the identified first natural frequencies. In this study no identifiable effect of backfilling on the first natural frequency was found and therefore no conclusion on the presence of backfill can be given. It was found that the identified first natural frequencies are significantly higher than the design first natural frequencies.

From the computer model was found that the first natural frequency of the wind turbines discussed in this research are sensitive for a change in water level also marginal sensitivity for one meter of backfill of the scour hole was found. Only small changes were found for different amounts of backfill in Chapter 4. In the computer model only the effect of the mass of the backfilled material was taken into account. The mass added by the backfilled material resulted in a higher overburden pressure and consequently a higher lateral soil stiffness in under laying soil layers. From the computer model it can be concluded that the first natural frequency of wind turbines without scour protection are highly sensitive to a change in scour depth. The deeper the scour hole around the lower the first natural frequency of the wind turbines.

From both the identified first natural frequencies and the first natural frequencies obtained from the computer model was found that a higher water level leads to a lower first natural frequency. This effect was found in earlier researches including a model to solve this influence [39]. This confirms that this solution is accurate enough for the wind turbines in the Eneco Luchterduinen wind farm.
A small effect of one meter of backfill on the first natural frequency of wind turbines without scour protection was found from the computer model, while no effect was found from the identified first natural frequencies. Therefore it is expected that the effect of backfill on the first natural frequencies of wind turbines without scour protection is limited.
As stated earlier in this chapter, it was found that the identified first natural frequencies of all four wind turbines differed a lot from the first natural frequencies in the design. All the identified first natural frequencies were higher than expected in the design phase. The expected reason for this difference in first natural frequencies is a higher soil stiffness. The computer model confirmed that the first natural frequencies of the wind turbines were highly dependent on the lateral soil stiffness, a higher lateral soil stiffness results in a higher natural frequency. An option to achieve similar identified first natural frequencies and first natural frequencies obtained from the computer model is multiplication of the lateral soil stiffness in the computer model. This multiplication is done by the soil stiffness multiplication factor. This research suggests a soil multiplication factor of approximately 20 for the wind turbines in the Eneco Luchterduinen wind farm.

To summarize the first natural frequency of the offshore wind turbines in the Eneco Luchterduinen wind farm are sensitive to effects of the water level. This can be concluded from both the identified and the natural frequency obtained from the computer model. This study finds that identified first natural

frequencies are significantly higher than the design first natural frequencies. A possible reason for this difference is that the soil-structure interaction model currently used by the wind turbine foundation designers is inaccurate. An option to achieve similar first natural frequencies from the computer model and the real world is the use of a soil stiffness multiplication factor. In this research no effect of backfilling of the scour hole can be found from the offshore measurements also no conclusion can be made on the presence of backfill.

6.2 Recommendations

In this research no conclusion is reached on the effect of backfill on the first natural frequency. In order to make a conclusion on this topic further research is suggested in respect of effect of backfill. In such a research constant monitoring of the scour hole would be necessary. The monitoring of the scour hole is needed in order to determine the amount of backfill in the scour hole. Also the soil density of the backfilled material should be investigated. Because at this moment it is unknown if the backfilled material supports the monopile in lateral direction.

This research also suggests a more elaborate investigation on the second mode shapes of the wind turbines. The different soil effects might have a larger influence on this mode shape. Since the displacements of the second mode are larger near the seabed.

Only the first natural frequencies are considered in this research and it is found that the lateral soil stiffness is highly underestimated. In further research it would be interesting to check if a correct estimation of the soil stiffness would create the possibility of the use of monopile foundations with less penetration depth. In order to check this not only the first natural frequency should be considered but also the ultimate limit states described in the DNV codes [8].

Bibliography

[1] Entrance. Renewable Energy In The Netherlands. Technical report, Entrance, 2016.

[2] Noordzeeloket. Route Kaart Wind Op Zee. https://www.noordzeeloket.nl/en/Images/Routekaart_Wind%20op%20Zee_20170109_5243.pdf, April 2017. [Online; accessed 3-April-2017].

[3] Andrew R. Henderson. Offshore wind in Europe. Walking the tighttrope to success. *Refocus*, 3(2):14–17, 2015.

[4] Ir. M.B.Zaaijer. Design Methods for Offshore Wind Turbines at Exposed Sites. Technical report, TU Delft, 2002.

[5] https://www.researchgate.net/profile/Piotr_Omenzetter/publication/258385656/figure/fig8/AS:307382669332515@1450297147511/Typical-stabilization-chart-showing-stable-mode png, september 2017. [Online; accessed 15-spetember-2017].

[6] D. J. Cerda Salzmann and J. Van Der Tempel. 1 aerodynamic damping in the design of support sturctures for offshore wind turbines.

[7] May May, Eui-kyu Yang, and Myoung Mo Kim. Natural Frequency Calculation of a Pile-Soil System in Dry Sand Under an Earthquake Loading. 2010.

[8] Det Norske Veritas. Design of Offshore Wind Turbine Structures. Technical report, DNV, 2014.

[9] M. B. Zaaijer and J Van Der Tempel. Scour protection: a necessity or a waste of money? *Proceedings of the 43 IEA Topixal Expert Meeting*, pages 43–51, 2004.

[10] A. A. Nemeth. Modelling offshore sandwaves. Technical report, Technische uninversiteit Twente, 2003.

[11] Hwang R.R Sau, A. Interaction of trailing vortices in the wake of a wall-mounted rectangular cylinder. https://www.researchgate.net/profile/Robert_Hwang/publication/8952784/figure/fig3/AS:280338342400004@1443849277430/FIG-3-Instantaneous-streamlines-showing-the-horseshoe-vortex-formation-at-t-20-Re.png, April 2017. [Online; accessed 10-April-2017].

[12] Engineer Live. http://power1805.rssing.com/chan-18850844/all_p3.html, April 2017. [Online; accessed 11-April-2017].

[13] Tim Raaijmakers and Daniel Rudolph. Time-dependent scour development under combined current and waves conditions - Laboratory experiments with online monitoring technique. *Proc. 4th Int. Conf. Scour Erosion, ICSE, Tokyo*, pages 152–161, 2008.

[14] Deltares. https://image.slidesharecdn.com/offshorescourandscourprotectiontimraaijmakerslecture95/offshore-scour-and-scour-protection-lecture29nov2010-tu-delft-22-728.jpg?cb=1302238445, April 2017. [Online; accessed 12-April-2017].

[15] Jh Den Boon, J Sutherland, and R Whitehouse. Scour behaviour and scour protection for monopile foundations of offshore wind turbines. *... the European Wind Energy ...*, pages 1–14, 2004.

[16] http://www.brainkart.com/article/One-Dimensional-Finite-Element-Analysis--Beam-Element_5949/, september 2017. [Online; accessed 06-spetember-2017].

[17] British Petroleum. https://knoema.com/smsfgud/bp-world-reserves-of-fossil-fuels, May 2016. [Online; accessed 08-May-2017].

[18] Rijksoverheid. Wind Energie Op Zee. https://www.rijksoverheid.nl/onderwerpen/duurzame-energie/inhoud/windenergie-op-zee, April 2017. [Online; accessed 3-April-2017].

[19] European environment agency. Europe's Onshore And Offshore Wind Energy Potential. Technical report, EEA, 2009.

[20] Paul Breeze. Wind Power. *Power Generation Technologies*, 1(5):223–242, 2014.

[21] Det Norske Veritas. Design of Offshore Wind Turbine Structures. Technical report, DNV, 2013.

[22] W. Weijtjens, T. Verbelen, G. De Sitter, and C. Devriendt. Foundation structural health monitoring of an offshore wind turbine–a full-scale case study. *Structural Health Monitoring*, 15(4):389–402, 2016.

[23] M. Damgaard. *Dynamic Properties of Offshore Wind Turbine Foundations*. 2014.

[24] W G Versteijlen, F W Renting, P L C Van Der Valk, J Bongers, and K N Van Dalen. Effective soil-stiffness validation : Shaker excitation of an in-situ monopile foundation. 102(August):241–262, 2017.

[25] M Damgaard, M Bayat, L V Andersen, and L B Ibsen. Computers and Geotechnics Assessment of the dynamic behaviour of saturated soil subjected to cyclic loading from offshore monopile wind turbine foundations. *Computers and Geotechnics*, 61:116–126, 2014.

[26] van Oord. OFFSHORE WIND FARM PROJECT WTG DESIGN BASIS PART C. (14), 2013.

[27] Jordan Matthieu. Morphologic assessment of the Luchterduinen wind farm. 2012.

[28] Intertek. ENECO WIND BV DUTCH SECTOR Q10 OFFSHORE WIND FARM - METOCEAN DATA REV 2. 44(0), 2012.

[29] B M Sumer, Thor U. Petersen, Luca Locatelli, J Fredsøe, Rosaria E. Musumeci, and Enrico Foti. Backfilling of a Scour Hole around a Pile in Waves and Current. *Journal of Waterway, Port, Coastal, and Ocean Engineering*, 139(February):114, 2012.

[30] Patrick Guillaume. A poly-reference implementation of the least- squares complex frequency-domain estimator COMPLEX FREQUENCY-DOMAIN ESTIMATOR. (January), 2003.

[31] N M Bychkov, A V Dovgal, and V V Kozlov. A method to avoid negative damped low frequent tower vibrations for a floating , pitch controlled wind turbine .

[32] Radac. `http://www.radacconnect.nl/index.php/login/callback/concrete`, june 2017. [Online; accessed 28-june-2017].

[33] Laszlo Arany, S. Bhattacharya, John H G Macdonald, and S. John Hogan. Closed form solution of Eigen frequency of monopile supported offshore wind turbines in deeper waters incorporating stiffness of substructure and SSI. *Soil Dynamics and Earthquake Engineering*, 83:18–32, 2016.

[34] A. Labuschagne, N.F.J. van Rensburg, and A.J. van der Merwe. Comparison of linear beam theories. *Mathematical and Computer Modelling*, 49(1–2):20 – 30, 2009.

[35] Aerospace Dynamics Spring. Lecture # 7 Lagrange ' s Equations. 2003, 2003.

[36] Ramboll. OFFSHORE WIND FARM PROJECT WTG DESIGN REPORT - COMPUTER MODEL. 2013.

[37] American Petroleum Institute. Recommended Practice for Planning , Designing and Constructing Fixed Offshore Platforms — Working Stress Design. (December 2000), 2003.

[38] Ramboll. OFFSHORE WIND FARM PROJECT WTG & OHVS DESIGN REPORT - GEOTECHNICAL REPORT. 2013.

[39] F W Renting, K N Van Dalen, and A V Metrikine. Exact Analytical Expression For The Added Mass For O ff shore Monopile Foundations. 2016.

[40] Ramboll. OFFSHORE WIND FARM PROJECT WTG DESIGN REPORT - NATURAL FREQUENCY ANALYSIS. 2013.

[41] Cheng Lin. The Loss of Pile Axial Capacities due to Scour : Vertical Stress Distribution. (Ictim), 2017.

[42] Alan Robertson. SCOUR PROTECTION SURVEY LUCHTERDUINEN OFFSHORE WINDPARK. (June), 2016.

[43] S P H Sørensen, L B Ibsen, and P Frigaard. Experimental evaluation of backfill in scour holes around offshore monopiles. *Frontiers in Offshore Geotechnics II, ISFOG 2010 - Proceedings*, pages 617–622, 2010.

[44] B Mutlu Sumer, Thor U Petersen, Luca Locatelli, Jørgen Fredsøe, Rosaria E Musumeci, and Enrico Foti. Back filling of a Scour Hole around a Pile in Waves and Current. 139(February):9–23, 2013.

[45] J. Schachner. Scour protection: a necessity or a waste of money? *Power connections for offshore wind farms*, 2004.

[46] F. Brink. Influence of liquefaction on scour around offshore monopile foundations. pages 1–115, 2014.

[47] B. W. Melville A. J. Sutherland. Design method for local scour at bridge piers. *Journal of Hydraulic Engineering*, 114(10):1210–1226, 1988.

A | Introduction to scour

Scour is the hydro dynamical removal of sediment around the foundation of the wind turbine. This removal of sediment can effect the soil properties in the wind farm. It can also affect the soil stiffness around the monopile. In this Chapter the different sorts of scour are discussed, the effect of scour on the wind turbine and the possibilities to mitigate these effects.

A.1 Types of scour

There are two types of scour, global scour and local scour. Global scour is the overall movement of the seabed. Global scour generally occurs in places where the upper soil layer consists of loose material, this material is transported by the sea waves. This global seabed movement is also referred as sand waves, in Figure A.1 an example of these sandwaves van be found.

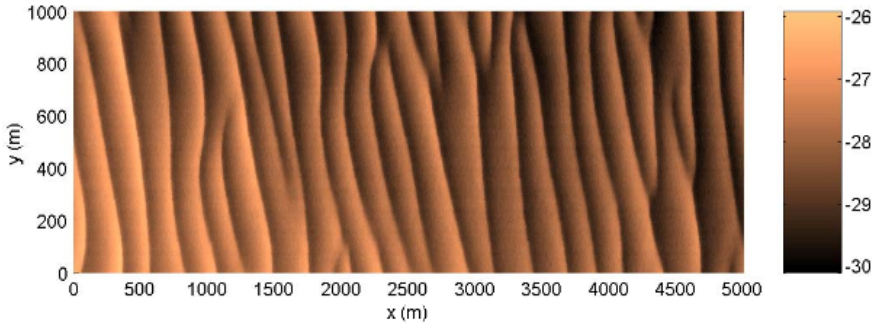

Figure A.1: *Example sand waves [10]*

The second sort of scour is local scour. Local scour can be found around offshore structures, due to the presence of an offshore structure a scour pit is created. This scour pit is often shaped like an inverted cone. The scour pit is created when a steady current encounters an offshore structure, the flow speeds up around the periphery of the structure. This increase in speed produces a "horse shoe vortex" and highly turbulent wake in the region downstream of the structure, Figure A.2.

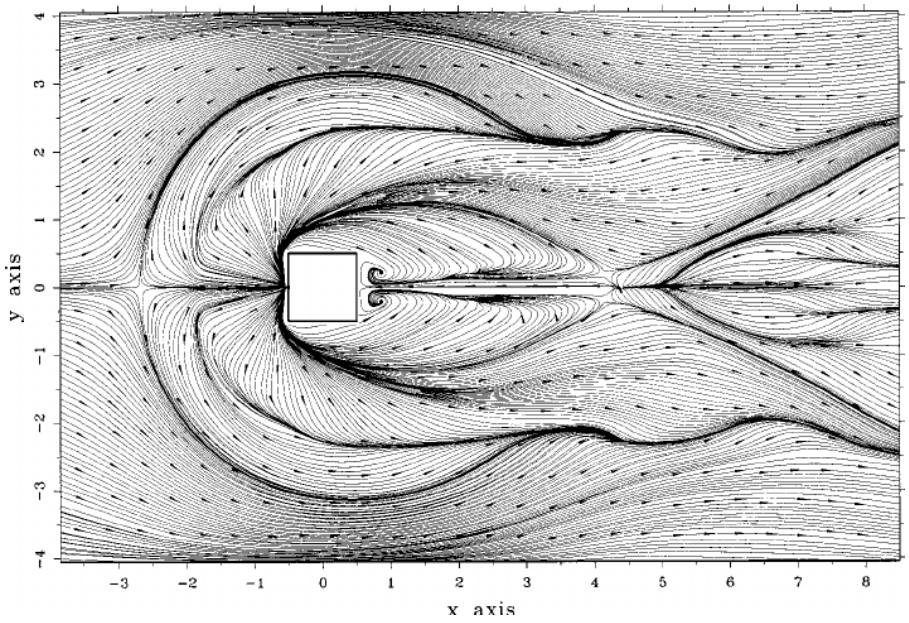

Figure A.2: *Horse shoe vortex [11]*

This horse shoe vortex is the main driver for local scour, the turbulent flow behind the structure has

a lower velocity. This lower velocity causes the floating sediment to settle again. Because of this settlement a zone of deposition is created. This zone is higher than the unscoured seabed [9].

Figure A.3: *Exmample of local scour on a beach. [9]*

In Figure A.3 an example of local scour can be found. This example is not a real offshore structure, but of a cylindrical and rectangular pole on a beach. However the scour hole in Figure A.3 resembles the scour hole of an offshore wind turbine on a monopile foundation. The shape of the scour hole around an offshore wind turbine is the same as the scour hole in Figure A.3

There are several drivers for global scour and local scour, the most common drivers are[9]:

- Currents: in rivers and estuaries
- Waves: for seas with small tidal influences
- Waves and currents: for most offshore locations
- Ship screws: vessels can cause large local velocities

In this report only offshore locations are discussed. Therefore the main scour drivers in this report will be the waves and the current.

A.2 The effects of scour

There are several effects of scour on a offshore structure. The effects of local and global scour are the same. They reduce the soil pressure around the offshore structure. The reduction of this soil pressure has an effect on the strength and stiffness of the soil. Since the strength and stiffness are directly dependent on the soil pressure and the soil pressure is dependent on the weight of the soil. A scour hole not only reduces the soil pressure around the wind turbine foundation. In the scour hole there is no soil-pile interaction at all, in the scour the mudline is lowered. Due to the lack of this interaction the soil does not provide any lateral soil stiffness. An schematic overview of global scour, local scour and the soil pressures is found in Figure A.4.

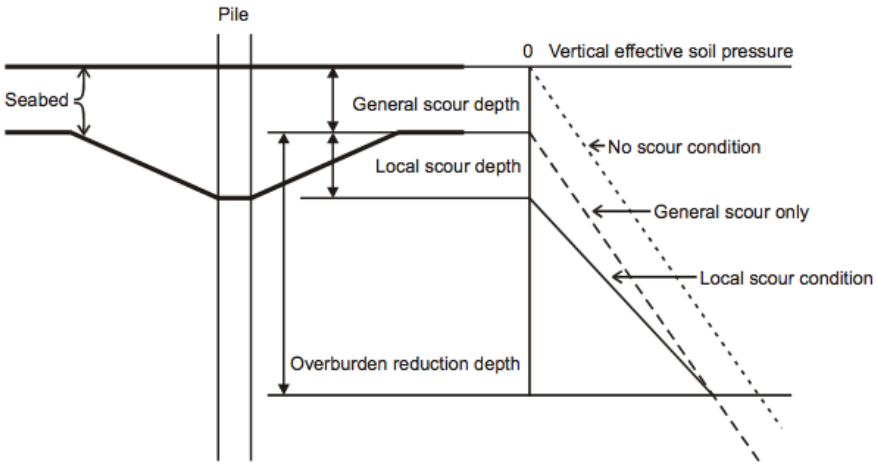

Figure A.4: *Schematic overview of local and global scour. [9]*

The consequences of scour can be reduced to three main components. The static strength and stability, more complicated design requirements and the dynamic behaviour of the offshore structure. We will only discuss the effects of scour around a monopile foundation since this the foundation type present at the Eneco Luchterduinen wind farm.

First the effect of scour on the static strength and the stability of the monopile is discussed. The presence of a local scour hole reduces the support strength around the monopile. It also increases the lever arm of the wind and waves loadings. By increasing the lever arm of the wind and wave loads the overturning moment is increased. The increase in overturning moment and the decrease in support strength may cause the need for larger monopiles. Larger monopiles consist of more steel and therefore increase the cost price of a monopile.

The second consequence of scour is complicating the design of the design of the monopile. A complication can be found in the grid connection of the wind turbine. Naturally each offshore wind turbine needs a grid connection to transport the electrical energy from the wind turbine to shore. This connection is in the form of a power cable leaving the monopile near the seabed and connecting it to an offshore high voltage platform (OHVS) or the connection point on the main land.

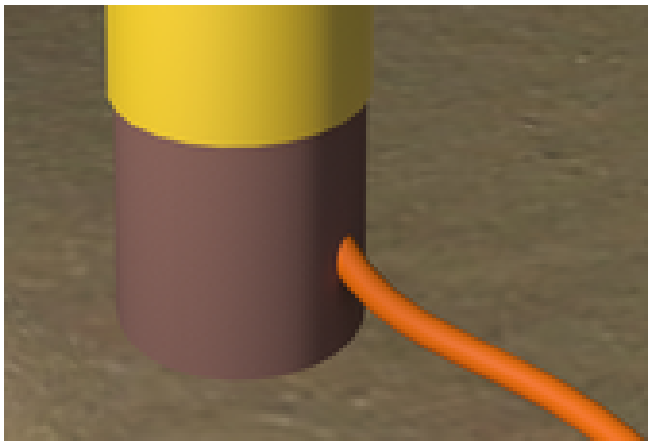

Figure A.5: *Schematic view of the monopile grid connection [12]*

When a scour hole is developed the connection cable has overcome this scour hole. This means the grid connection cable is hanging free over the scour hole. The free hanging cable can get influenced by the waves and currents. This constant movement of the cable may lead to cable failure [45].

The third consequence of scour is a change in the dynamic behaviour of the wind turbine. The most

important change in the dynamics of the wind turbine is a change in the natural frequency of the wind turbine. As discussed in Chapter 1 the first natural frequency is a very important design parameter. And the lateral soil stiffness around the monopile foundation is one of the most important parameters for the natural frequency. As stated in Chapter 2 a reduction in soil stiffness might reduce the first natural frequency. From earlier studies the reduction of the first natural frequency due to the presence of a scour hole might be as high as 8% [23]. With this reduction of the first natural frequency, the first natural frequency might come close to 1P region of the wind turbine Figure 1.4. Also the drop of the natural frequency might lead to coincide with the wave and wind excitation's. These two events might lead to resonance and compromising the structural stability of the wind turbine. To avoid this problem longer and larger monopiles might be needed. These longer and larger monopiles consist of more steal and are therefore more expensive.

A.3 Prediction of scour

A.3.1 Scour depth

As stated in section A.1 the two main drivers for scour at an offshore monopile construction are the currents and the waves. The scour depth is presented as a dimensionless parameter $\frac{S}{D}$, where S is the scour depth and D is the pile diameter.
When the monopile is placed in a steady current the dimensionless scour depth can be determined by [46]:

$$\frac{S}{D} = K_I K_\delta K_d K_s K_\alpha \tag{A.1}$$

Where K_I is the flow intensity factor,

$$K_I = \begin{cases} 2.4 & for\ \frac{U-U_a-U_{cr}}{U_{cr}} > 1 \\ 2.4\left|\frac{U-U_a-U_{cr}}{U_{cr}}\right| & for\ \frac{U-U_a-U_{cr}}{U_{cr}} \leq 1 \end{cases} \tag{A.2}$$

K_s is the shape factor for cylindrical monopiles this is 1. K_δ denotes the influence of the boundary layer thickness. The boundary layer thickness describes the thickness of the horseshoe vortex. K_d is a factor that represents the medium grain size. K_a is the alignment factor for cylindrical monopiles this is 1. U_a is the armoured peak velocity in uniform current can be found as $U_a = U_{cr}$. More information on these factors can be found in papers about steady current around piers and bridges [47].

However in offshore situations there is almost never a steady current. In offshore situations often wave induced scour is also a factor in the total scour. Therefore DNV states that the following empirical expression deduced model by tests may be used [8].

$$\frac{S}{D} = 1.3\left(1 - exp\left(-0.03\left(KC - 6\right)\right)\right) \tag{A.3}$$

Equation A.3 only holds when $KC \leq 6$, KC is the Keulegan-Carpenter number. The Keulegan-Carpenter number indicates whether a "horse shoe" vortex, as discussed in section A.1 is formed. If the the Keulegan-Carpenter is $KC < 6$ no "horse shoe" vortex is formed. If there is no "horse shoe" vortex no scour will occur. The Keulegan-Carpenter number is defined as follows,

$$KC = \frac{u_{max} T}{D} \tag{A.4}$$

Where T is the wave period, D is the monopile diameter and u_{max} is the orbital velocity at the seabed. The orbital velocity follows from the linear wave theory,

$$u_{max} = \frac{\pi H}{T sinh(kh)} \tag{A.5}$$

Where H is the wave height, h is the water depth and k is the wave number the wave number can be found by solving the dispersion equation,

$$\frac{2\pi}{T}^2 = g * k * tanh(kh) \tag{A.6}$$

In the dispersion equation g denotes the gravitational acceleration. Also when using Equation A.3 it must be taken into account that the Shields parameter must be higher than the threshold value $\theta > \theta_{cr}$. When θ exceeds θ_{cr} the live bed conditions are in place. The critical Shields parameter is 0.05 to 0.06 according to the DNV codes [8]. When Shields parameter exceeds this value seabeds erosion starts. The Shields parameter is defined by,

$$\theta = \frac{U_f^2}{g(s-1)d} \tag{A.7}$$

Where s is the specific gravity for the sediment, d is the grain diameter according to the DNV codes the grain diameter can be defined as the mediam grain diameter d_{50} [8] and U_f is the shear bed velocity and can be found from equation A.8 for steady current and from Equation A.9 for waves.

$$\frac{U_c}{U_f} = 6.4 - 2.5ln\left(\frac{2.5d}{h} + \frac{4.7v}{hU_f}\right) \tag{A.8}$$

$$U_f = \sqrt{\frac{f_w}{2}} u_{max} \tag{A.9}$$

Where v is the kinematic viscosity and f_w is the frictional coefficient given by,

$$f_w = \begin{cases} 0.04\left(\frac{a}{k_N}\right)^{-0.25} & \frac{a}{k_N} > 100 \\ 0.4\left(\frac{a}{k_N}\right)^{-0.75} & \frac{a}{k_N} < 100 \end{cases} \tag{A.10}$$

Where k_N is the seabed roughness this is equal to 2.5 the median grain diameter and a is the free stream amplitude,

$$a = \frac{u_{max}T}{2\pi} \tag{A.11}$$

A.3.2 Scour development

The depth of the scour hole is not constant in time, backfill can occur. Backfill is the refill of the scour hole. For instance in harsh wave conditions the scour hole can be less deep than for average sea conditions. The soil that is deposited during the backfill of the scour pit does not have the same soil properties as the soil which has not been effected by scour. The soil in the scour pit has less density then the soil not effected by scour [43]. The reduction of the soil density might affect the lateral soil stiffness as discussed in section A.2. The temporal evolution of the scour depth can be found from Equation A.12 [8].

$$S_t = S\left(1 - exp\left(\frac{-t}{T_1}\right)\right) \tag{A.12}$$

Where t denotes the time, S the scour depth and T_1 the timescale of the scour process. T_1 can be found from the non-dimensional time scale parameter T^*. The non-dimensional time scale parameter can be found from equation A.13.

$$T^* = \frac{\sqrt{g\,(s-1)\,d^3}}{D^2} T_1 \tag{A.13}$$

T^* is abtained from the empirical Equations A.14 and A.15.

$$T^* = \frac{1}{2000}\frac{h}{D}\theta^{-2.2} \quad \text{for steady current} \tag{A.14}$$

$$T^* = 10^{-6}\left(\frac{KC}{\theta}\right) \quad \text{for waves} \tag{A.15}$$

A.3.3 Improved scour model for Dutch coastal waters

The scour prediction model suggested by DNV is discussed in section A.3. In this model the main scour driver is the current induced scour. This model is in general valid. However for the Dutch coastal waters an updated model is created. This model is tested for monopiles in the Dutch coastal waters and has proven to be more accurate than the model suggested in the DNV design codes. The model also takes back filling into account due to storm conditions. The improved scour distinguishes between the wave induced scour and current induced scour [13].

$$S_{n+1} = S_{eq(n+1))} + \left(S_n - S_{eq(n+1))}\right) exp\left(-\frac{dt}{T_{char}}\right) \tag{A.16}$$

In Equation A.16 the improved solution to the scour development can be found. Important to note is this Equation is discretesized for time. Where S_{eq} is the equilibrium scour depth and T_{char} is the characteristic time scale. Both the equilibrium scour depth and the characteristic timescale are very site specific. The equilibrium scour depth is a measure of the monopile diameter Figure A.6. The characteristic timescale is the time the scour takes to fully develop the scour pit.

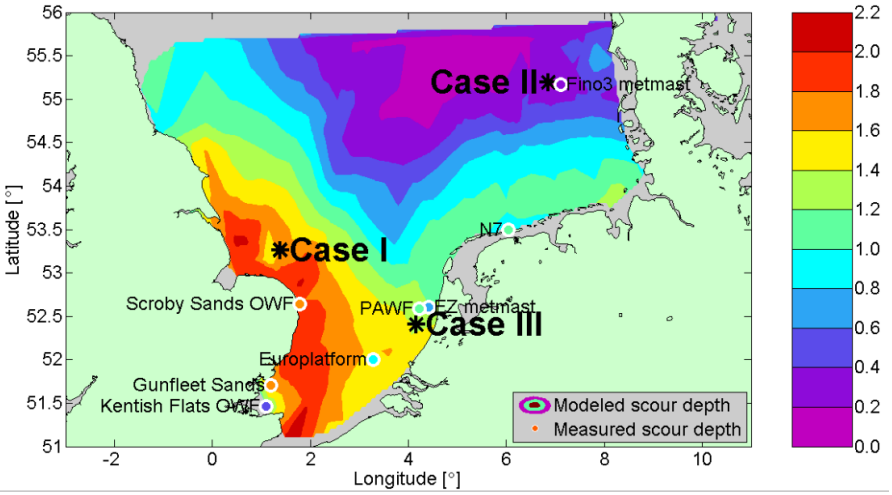

Figure A.6: *Pile dependent equilibrium scour depth [13]*

A.3.4 Lateral extension of the scour hole

For the soil stiffness around the monopile the lateral extension of the scour hole is not really important. Because for the soil stiffness around the monopile there is no difference if the soil is 3m away or just 1m. However the difference in overburden pressure due to different shapes of the scour hole effects the soil stiffness of deeper soil layers. Also the size of the scour hole is important when designing the scour protection. Because the scour protection should cover the whole scour hole otherwise the scour protection would not be efficient. More detailed information about scour protection can be found in section A.4.

$$r = \frac{D}{2} + \frac{S}{tan(\phi)} \tag{A.17}$$

In Equation A.17, r is the radius of the scour hole. The radius of the scour hole is the same as the lateral extension of the scour hole in one direction. The radius of the scour hole is measured from the center of the monopile. Also r is the radius at the original seabed level. The scour depth (S) is found from Equation A.3 and ϕ is the friction angle of the soil.

A.4 Scour protection

There are several different methods to protect the monopile from scour. Some of these scour protection options are [9]:

- Rock dumping around the monopile directly after installation
- Rock dumping in the scour hole after it has developed
- Seabed protection with geotextile and concrete matrasses
- A concrete protection wall around the monopile
- Seabed improviment by gluing the sand

The most common way to protect the monopile form scour is by the placement of rocks around the monopile. There are two different ways to protect the monopiles from scour with placement of rocks these will be discussed in this section. For both methods it is of importance that the placed rocks do not move due to currents and waves.

A.4.1 Static scour protection

Static scour protection consists of several layers of rocks. First a so called filter layer is placed on the sea floor. This filter layer is placed before installing the monopile. The monopile is hammered through this filter layer. When the monopile is in place the larger rocks are placed around the monopile.

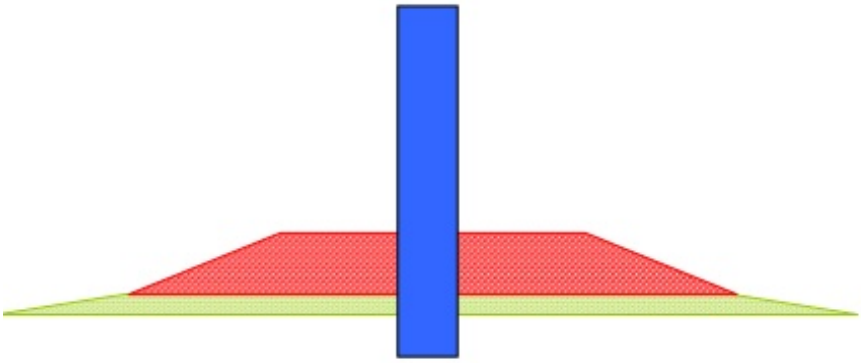

Figure A.7: *Example of static scour protection. [14]*

A disadvantage of the static scour protection is, scour is expected at the edges of the scour protection. The scour on the edges of the scour protection will degrade the scour protection. Therefore the initial diameter of the scour protection must be large enough to accommodate this degradation and still protect the monopile. In Figure A.8 an example of the degradation of the scour protection can be found.

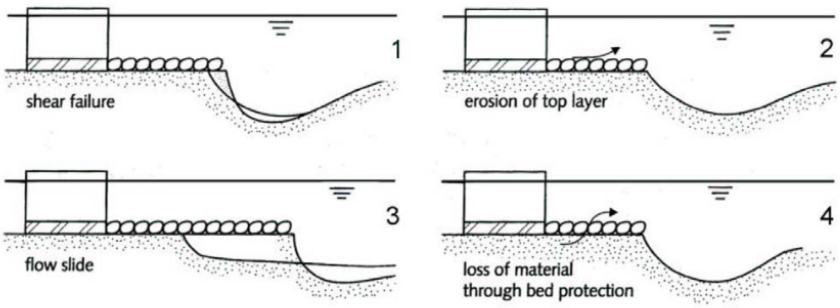

Figure A.8: *Failure of static scour protection. [9]*

The size of rocks that need to be used in the scour protection is dependent on the orbital velocity of the water near the scour protection at seabed level. The size of rocks that is stable under the design waves and currents is determined using the Shield threshold approach, Equation A.18 [15].

$$\theta_{max} = \frac{\tau_{max}}{g\,(\rho_s - \rho)\,D_{50}} \tag{A.18}$$

Where τ_{max} is the maximum bed shear stress, ρ_s is the density of the rocks and D_{50} is the median of the rock diameters. The Shields threshold approach is satisfied if Equation A.19 is satisfied. In Equation A.19 $\theta_{cr} = 0.056$ for rocks larger than 1 cm.

$$1 < \frac{\theta_{max}}{\theta_{cr}} \tag{A.19}$$

A.4.2 Dynamic scour protection

The second option to protect the wind turbine to the effects of scour is by the use of dynamic scour protection. When using dynamic scour protection first the monopile is installed the after installation of the monopile, the monopile is left undisturbed for a while. In this time a scour hole can develop this development can take several weeks. After the scour hole is fully developed the scour hole is filled with rocks.

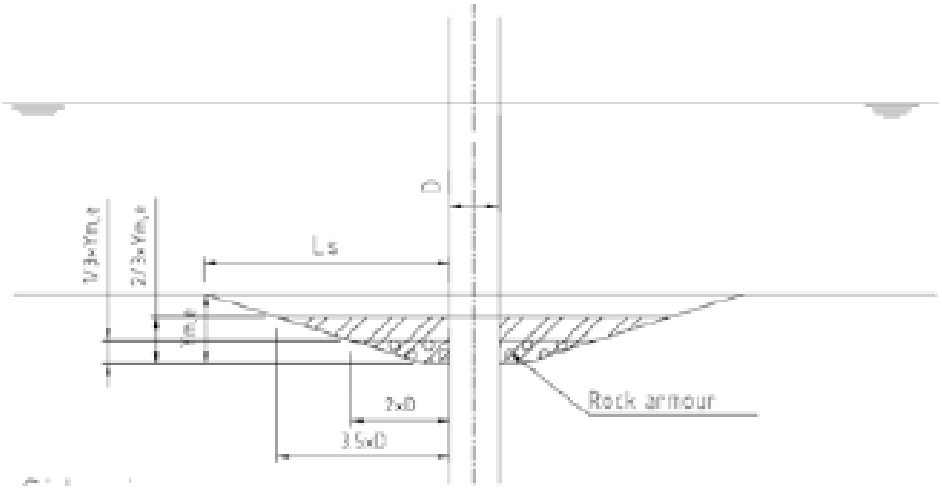

Figure A.9: *Schematic overview of dynamic scour protection [15]*

For the dynamic scour protection design a large variety of rocks is placed in the scour pit. The same criteria of rock size is present as for the static scour protection. An advantage of the dynamic scour protection is that not the whole scour pit needs to be filled. Therefore a smaller amount of rocks is needed to protect the monopile from scour. Also the dynamic scour protection cannot fail from edge scour while the static scour protection can fail due to edge scour. It must be noted that the monopile must withstand waves and currents while the scour pit is formed before fill up.

B | Mass and Stiffness Matrices

In this chapter a more elaborate explanation about the construction of the mass and stiffness matrices is given.

Geometry

A 1D finite element model consists elements and each of these elements have two nodes. Each of these two nodes can have a displacement and a rotation. Those displacements and rotations are called the nodal displacements. The elements between these nodes contain information about the material properties of the beam.

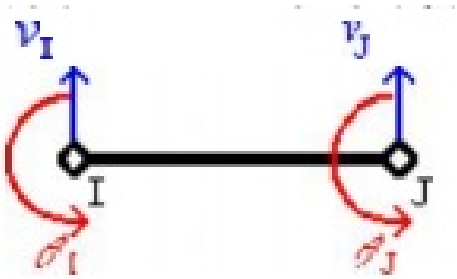

Figure B.1: *Example of the nodal displacements for 1D beam model[16]*

In Figure B.1 an example of one element of a 1D beam model can be found. This example consists of two nodes. These nodes are called I and J. The finite element model used to model the wind turbines in this research consists of many more nodes and elements. But each of these nodes have an rotation and a displacement. The nodes of two elements are connected to each other this can be observed in Figure B.2.

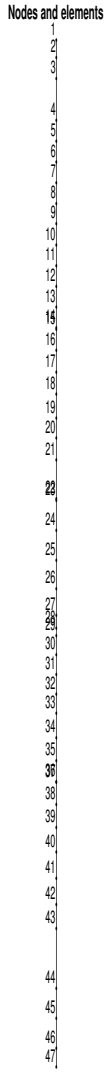

Figure B.2: *Nodes and elements of the 1D wind turbine model (EL07)*

In Figure B.2 the geometrical representation of wind turbine seven can be found. The nodes are at each place in the monopile where the diameter of the tower or the pile changes or where the wall thickness changes. In the MATLAB code the elements contain information about the wall thickness, Youngs modulus, diameter and specific gravity.

Mass and stiffness matrices

As discussed in chapter 2 in order to calculate the first natural frequency of a system the mass and stiffness matrices need to be determined. But in order to determine the mass and stiffness matrices first the shape functions of the system are obtained.

Shape functions

The shape functions of an element describe the shape of the displacements of the element. From Figure B.1 it is clear each element has four unknown displacements. Therefor the shape function is expected to be cubical, see Equation B.1.

$$w\left(x,t\right)=a_1x^3+a_2x^2+a_3x^1+a_4 \tag{B.1}$$

These shape functions must meet four boundary conditions. But first we determine that node I is at $x=0$ and node J is at $x=L$ in Figure B.1. The boundary conditions are independent of time.

$$\begin{aligned} &w\left(x=0,t\right)=v_I\\ &w\left(x=L,t\right)=v_j\\ &\frac{\delta w}{\delta x}\mid_{(x=0)}=\theta_I\\ &\frac{\delta w}{\delta x}\mid_{(x=L)}=\theta_J \end{aligned} \tag{B.2}$$

In Equation B.2 the boundary conditions are found when evaluating the boundary conditions for Equation B.2 it can be found that:

$$\begin{aligned} &w\left(x=0,t\right)=a_4\\ &w\left(x=L,t\right)=a_1L^3+a_2L^2+a_3L+a_4\\ &\frac{\delta w}{\delta x}\mid_{(x=0)}=a_3\\ &\frac{\delta w}{\delta x}\mid_{(x=L)}=3a_1L^2+2a_2L+a_3 \end{aligned} \tag{B.3}$$

When substituting Equation B.3 into Equation B.1 the displacement function is obtained.

$$w\left(x,t\right)=\left(\frac{2}{L^3}(v_I-v_J)+\frac{1}{L^2}(\theta_I+\theta_J)\right)x^3+\left(-\frac{2}{L^3}(v_I-v_J)-\frac{1}{L^2}(\theta_I+\theta_J)\right)x^2+\theta_Ix+v_I \tag{B.4}$$

In matrix form this displacement function can be described as,

$$w\left(x,t\right)=\begin{bmatrix}N_1 & N_2 & N_3 & N_4\end{bmatrix}\begin{bmatrix}v_I\\ \theta_I\\ v_J\\ \theta_J\end{bmatrix} \tag{B.5}$$

with the shape functios,

$$\begin{aligned} N_1&=\frac{1}{L^3}\left(2x^3-3x^2L+3L\right)\\ N_2&=\frac{1}{L^3}\left(x^3L-2x^2L^2+xL^3\right)\\ N_3&=\frac{1}{L^3}\left(-2x^3+3x^2L\right)\\ N_4&=\frac{1}{L^3}\left(x^3L-x^2L^2\right) \end{aligned} \tag{B.6}$$

and $v_I,\theta_I,v_J,\theta_J$ the time dependent displacements.

Mass and stiffness matrices

In order to compute the mass and stiffness matrices the Euler-Lagrange equations are considered [35].

$$L\equiv T-V \tag{B.7}$$

where L is the Lagrangian, T is the kinetic energy and V is the potential energy of the element. First the kinetic energy of the element is considered.

$$T=\frac{1}{2}\rho A\int_0^l\dot{w}(x,t)^2dx \tag{B.8}$$

where ρ is specific weight of the tower material, A is the surface of the tower and $\dot{w}$ is the time derivative of the displacement function described in Equation B.4. The displacement function is divided in the shape functions and the nodal displacements, see Equations B.6. The shape functions are only dependent on place and the nodal displacements are only dependent on time. For simplicity the shape functions are called $N(x)$ and the nodal displacements $Q(t)$.

$$T = \frac{1}{2}\dot{Q}^T(t)\left(\rho A \int_0^l N(x)N(x)^T dx\right)\dot{Q}(t) \tag{B.9}$$

from Equation B.9 it can be found the mass matrix is obtained since:

$$T = \frac{1}{2}\dot{Q}^T(t)\mathbf{M}\dot{Q}(t) \tag{B.10}$$

$$\mathbf{M} = \rho A \int_0^l N(x)N^T(x)dx \tag{B.11}$$

When evaluating Equation B.11 the mass matrix for each single element of the system can be derived. The mass matrix of each element will be in the form of matrix B.12.

$$\mathbf{M} = \frac{\rho A l}{420}\begin{bmatrix} 156 & 22l & 54 & -13l \\ 22l & 4l^2 & 13l & -3l^2 \\ 54 & 13l & 156 & -22l \\ -13l & -3l^2 & -22l & 4l^2 \end{bmatrix} \tag{B.12}$$

In order to compute the stiffness matrix the potential energy of each element is considered.

$$V = \frac{1}{2}EI \int_0^l w_{xx}^2(x,t)dx \tag{B.13}$$

where E is the Youngs modulus of the tower material and I is the mass moment of inertia. Again the displacement function is divided into the shape functions and the nodal displacements.

$$V = \frac{1}{2}Q^T(t)\left(EI \int_0^l N_{xx}(x)N_{xx}^T(x)dx\right)Q(t) \tag{B.14}$$

from Equation B.14 can be obtained since:

$$V = \frac{1}{2}Q^T(t)\mathbf{K}Q(t) \tag{B.15}$$

$$\mathbf{K} = EI \int_0^l N_{xx}(x)N_{xx}^T(x)dx \tag{B.16}$$

When evaluating Equation B.16 the stiffness matrix for each single element of the system can be derived. The stiffness matrix of each element will be in the form of matrix B.17.

$$\mathbf{K} = \frac{EI}{l^3}\begin{bmatrix} 12 & 6l & -12 & 6l \\ 6l & 4l^2 & -6l & 2l^2 \\ -12l & -6l & 12 & -6l \\ 6l & 2l^2 & -6l & 4l^2 \end{bmatrix} \tag{B.17}$$